

Dynamics and Control of Nonlinear Systems

A Thesis Submitted
in Partial Fulfillment of the Requirements
for the Degree of
Doctor of Philosophy

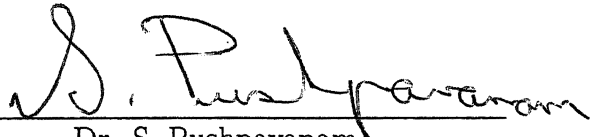
by
Rahul Konnur

to the
Department of Chemical Engineering
Indian Institute of Technology, Kanpur
April, 1997

Certificate

21/4/97

It is certified that the work contained in this thesis entitled *Dynamics and Control of Nonlinear Systems* by *Rahul Konnur* has been carried out under my supervision and that this work has not been submitted elsewhere for a degree.



Dr. S. Pushpavanam

Associate Professor
Department of Chemical Engineering
Indian Institute of Technology
Kanpur. 208 016 (India)

April, 1997

- 9 JUL 1998

~~CHE-1997-D-KON-DYN~~
CENTRAL LIBRARY
I. I. T., KANPUR

~~CHE-1997-D-KON-DYN~~ A 125675

CHE-1997-D-KON-DYN

Entered in system

Nishu
10-6-98



Synopsis

In this thesis we study the open-loop and closed-loop response of nonlinear systems. In the first part we investigate the open-loop behavior of two nonlinear reacting systems using bifurcation theory and singularity theory. In the second part we apply results from differential-geometry based nonlinear control theory to analyse the problem of synchronization of chaotic systems. A survey of the literature and the scope and motivation of the thesis are outlined in chapter 1.

In the second chapter we discuss the dynamics of a discretely forced batch reactor system. Each cycle of operation of the reactor consists of the following steps. In the first step, the reactants are charged instantaneously into the reactor and the reaction is allowed to occur in batch mode for a fixed time P . At the end of this time, the reactor contents are emptied partially and the reactor volume is made up by the addition of fresh reactant. Both the discharge of the reactor contents and the recharging of the fresh feed are assumed to occur instantaneously. The above steps are repeated in the next cycle of operation. Hence the operation of the reactor is periodic, with period P . Such an operation emulates the batch process in the limit of $P \rightarrow \infty$ and the CSTR as $P \rightarrow 0$.

We consider the reaction occurring to be the first order, exothermic and irreversible reaction $A \rightarrow B$. The reactor dynamics in the two limiting cases of forced operation, *viz.*, the batch reactor and the CSTR, are well understood. This investigation enables us to study the transition of the dynamics of this discretely forced reactor system from that of the batch reactor to the CSTR. We have used the shooting method and the

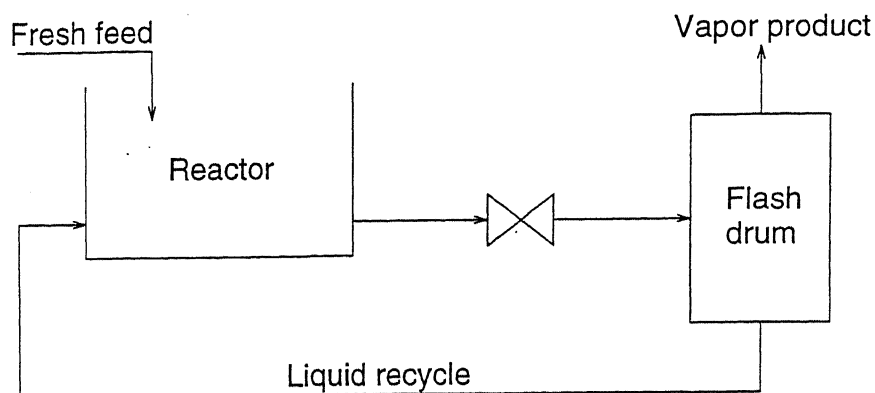


Fig. 1. Schematic diagram of the reactor-separator system with recycle.

continuation method to compute the periodic solutions and generate the bifurcation diagrams of the system respectively. Stability of the periodic solutions has been computed using Floquet theory. The stroboscopic map and the Lyapunov exponents have been used to characterize the nature of the dynamic behavior of the system. Extensive simulations indicate that the system can exhibit a wide variety of complex periodic and aperiodic behavior. These include the period doubling, intermittency and quasi-periodic routes to chaos, crisis and mixed-mode oscillations.

In chapter 3 we investigate the steady-state multiplicity behavior of a reactor-separator system with recycle (Fig. 1). We consider the reactor to be a CSTR again sustaining the first order, exothermic and irreversible reaction $A \rightarrow B$. The separator is considered to be a single stage flash. It separates the reactor effluent stream into a reactant rich liquid stream and a product rich vapor stream. The reactant rich liquid stream from the separator is recycled back to the CSTR, while the product rich vapor stream is withdrawn from the system.

We study the effect of different sets of design specifications on the steady-state behavior of the system. The objective of this work is to investigate the steady-state multiplicity features and obtain a qualitative picture of the dynamic behavior that can be expected for different design specifications of this system. The system selected is such that it permits the application of singularity theory for the determination of the steady-state multiplicity features. For the coupled system, the assumption of

vapor-liquid equilibrium separation imposes constraints on the operation of the coupled system. These constraints influence the multiplicity features of the coupled system. Application of singularity theory enables us to obtain a comprehensive picture of the steady-state multiplicity features of the system in the presence of these constraints. The bifurcation diagram is used to represent the multiplicity features of the system. It is shown that for some sets of design specifications, there can exist regions in parameter space, where there are no steady-states of the coupled system.

In the next two chapters we discuss the application of results from nonlinear control theory for the analysis of the phenomenon of synchronization in chaotic systems. Two systems are said to synchronize when they evolve along identical trajectories in phase space.

Chaotic systems exhibit a sensitive dependence to initial conditions, i.e., two identical chaotic systems starting from nearby initial conditions, evolve along exponentially diverging trajectories. This sensitive dependence on initial conditions associated with chaotic evolution means that two identical chaotic systems are not expected to synchronize with each other. However, it has been recently shown that it is possible to achieve synchronization in chaotic systems also. Several different techniques have been proposed for this purpose.

In chapter 4 we present a unified framework for the analysis of the different techniques for synchronizing chaotic systems. We employ recent results from differential-geometry based nonlinear control theory for this purpose. It is shown that the different synchronization techniques are a different interpretation of **perfect control** of a system along a desired chaotic trajectory. By perfect control, we mean that the system (plant) output tracks its desired trajectory exactly for all $t \geq 0$. We illustrate the connection between synchronization and perfect control on the Rossler system.

It is not possible to synchronize several systems using many of the techniques currently available. The Rossler system is an example of such a system. These systems are classified as non-minimum phase systems in the control literature. These are the systems having zeros in the right-half plane. In the first part of the fifth chapter we employ a control scheme based on bifurcation theory for achieving chaotic synchronization in the Rossler system.

The synchronization problem is formulated as a problem of regulating the output

of a system using state feedback. The reference output tracking signal is generated by a nonlinear external system. This external system is selected such that the composite system consisting of the plant and the external system, has at least one zero on the imaginary axis. This permits application of the center manifold theorem for the derivation of the control law for regulating the output of the composite system.

Input multiplicity is a situation where different inputs can give the same output. A result of this is that the controlled system states cannot be stabilized at their desired steady-state. Systems exhibiting input multiplicity appear frequently in chemical engineering. A major limitation of many of the control techniques based on differential-geometry is their limited use for the control of systems exhibiting input multiplicity. In the second part of the fifth chapter we use the output regulation technique mentioned above to control an isothermal CSTR system, sustaining an autocatalytic reaction and exhibiting input multiplicity, around its steady-state.

Dedicated to
AP
and my family

Acknowledgements

Thanks are due to the Department of Chemical Engineering and my parents for providing the financial support during my stay here. Of the many facilities provided by the Institute, the Computer Centre was by far the best and unlimited use of the facilities are gratefully acknowledged.

Several people within and outside the department have lent a helping hand at various stages during the past seven and half years. Having Dr. Pushpavanam as my adviser benefited me immensely. As it eventually turned out, I could not have completed parts of this thesis without his encouragement.

Surely, I could have avoided stretching his patience to its very limits on numerous occasions. He, despite all this and more, allowed me to have a great degree of freedom. I thank him for this, for never refusing his time and for rarely losing his patience with me. I also thank Prof. J. P. Gupta for his advise and timely help without which it would have been difficult to wind up the thesis so quickly.

It only remains for me to thank all my friends for tolerating me inspite of the associated health hazards. Thanks are due to Alok, Appaji, Ashim, Behera, Bhadri, Bhaskar, Khulbe, Masterji, Murthy, Niranjana, Rajan, Ravindra, Shamsi and Sridhar. Working in the company of several sets of my lab-mates - especially the cheerful and enthusiastic Ravi, Venu, Joydeb, and above all Pandeyji - was a pleasure. Memories of the company provided by all the regular participants in the frequent *trips* will always remain with me. These would not have been so memorable were it not for the efforts of Abir, GK, Sankar, Swapna, Tapo and many others, not forgetting the different species of *scapegoats*.

The *online* help provided by Sairam from time to time is greatly appreciated. And finally, a word of thanks to Alok and Ramana for their friendship and support.

Contents

List of Figures	xi
List of Tables	xvii
1 Introduction	1
2 Nonlinear Dynamics of a Fed-Batch Reactor (FBR)	9
2.1 Introduction	10
2.2 Description of the Model	11
2.3 Method of Solution	13
2.3.1 Shooting Method	14
2.3.2 Arc-length Continuation Method	16
2.3.3 Stability	18
2.3.4 Simulations	19
2.3.5 Stroboscopic Map	19
2.4 Results and Discussion	19
2.5 Conclusions	39
3 Steady-state Behavior of a Reactor-Separator System	41
3.1 Introduction	42
3.2 Description of the Model	44
3.3 Steady-State Analysis	47
3.3.1 Isothermal and Isobaric Separation with (M_R, F_0) Fixed	48
3.3.2 Isothermal and Isobaric Separation with (M_R, F) Fixed	62
3.3.3 Isothermal and Isobaric Separation with (M_R, L) Fixed	66

3.3.4	Isothermal and Isobaric Separation with (F_0, F) Fixed	69
3.3.5	(T_F, L) Separation with (M_R, F_0) Fixed	73
3.4	Conclusions	77
4	A Unified Framework for the Analysis of Synchronization of Chaotic Systems	79
4.1	Introduction	79
4.2	Theoretical Analysis	83
4.3	Results and Discussion	88
4.4	Conclusions	95
5	Synchronization and Control of Non-Minimum Phase Systems	97
5.1	Introduction	97
5.2	Description of the Method	100
5.3	Results and Discussion	102
5.4	An Autocatalytic Reaction in a CSTR	107
5.5	Conclusions	122
	Bibliography	122
	Appendix	128
A	Singularity Theory	129

List of Figures

2.1	Bifurcation diagram for the CSTR for parameter sets 1 and 2 of Table 2.1, (—): stable steady-state; (···): unstable steady-state; (×): Hopf bifurcation point.	20
2.2	Bifurcation diagram of the 1P state for the FBR, parameter set 1, $R = 0.573875$, (—): stable 1P state; (···): unstable 1P state; (×): Period doubling bifurcation; (•): Torus bifurcation point.	21
2.3	Stroboscopic maps of the chaotic attractor showing the growth and collision of the chaotic attractor with the unstable fixed point (×), parameter set 1, $R = 0.573875$, (a) $P = 0.33515$; (b) $P = 0.342$ and (c) $P = 0.349$	24
2.4	Variation of the temperature T with dimensionless time ((a) and (b)) and the stroboscopic map ((c) and (d)) near the ignition point showing intermittency behaviour, parameter set 1, $R = 0.573875$, (a), (c): $P = 0.4105$; (b), (d): $P = 0.411$	27
2.5	Dependence of the largest Lyapunov exponent λ on P for the FBR, set 1, $R = 0.573875$	29
2.6	Stroboscopic map of the chaotic attractor, parameter set 1, $P = 0.635$, $R = 0.573875$	31
2.7	Bifurcation diagram of the 1P state for the FBR, parameter set 1, $R = 0.20$ and $R = 0.30$, (—): stable 1P state; (···): unstable 1P state; (•): Torus bifurcation point.	32
2.8	Dynamic behaviour for $R = 0.20$, parameter set 1, Stroboscopic maps for (a) $P = 0.13385$; (b) $P = 0.1385$; (c) $P = 0.20$	33

2.9	Bifurcation diagram of the 1P state for the FBR, parameter set 1, $R = 0.750$, (—): stable 1P state; (\cdots): unstable 1P state; (\times): Period doubling bifurcation; (\bullet): Torus bifurcation point.	34
2.10	Bifurcation diagram of the FBR for parameter set 2, (—): stable 1P state; (\cdots): unstable 1P state; (\bullet): Torus bifurcation point.	36
2.11	Stroboscopic map for the FBR showing quasi-periodic behavior, parameter set 2, $P = 0.28$, $R = 0.25$	37
2.12	Bifurcation diagram of the CSTR for parameter set 3, (—): stable steady-state; (\cdots): unstable steady-state; (\times): Hopf bifurcation point.	38
2.13	Bifurcation diagram of the FBR for parameter set 3. (—): stable 1P state; (\cdots): unstable 1P state.	38
3.1	Schematic diagram of the reactor-separator system with recycle.	45
3.2	Global classification of the steady-state bifurcation diagrams for (T_F, P) and (M_R, F_0) flash (Equation (3.14)) in the $x_e - y_e$ plane for $B = 15$, $\beta_0 = 4.0$, $Da_0 = 0.20$. BLS: Boundary limit set; BTS: Boundary tangent set; DCS: Double cross set; IV: Isola variety.	54
3.3	Global classification of the steady-state bifurcation diagrams for (T_F, P) and (M_R, F_0) (Equation (3.14)) in the $x_e - y_e$ plane for $B = 5$, $\beta_0 = 1.0$, $Da_0 = 0.20$. BLS: Boundary limit set; DCS: Double cross set; IV: Isola variety.	55
3.4	Schematic bifurcation diagrams of the steady-state for (T_F, P) and (M_R, F_0) flash (Equation (3.14)) describing the dependence of composition in the reactor on τ . Letters indicate regions in Fig. 3.2. The horizontal lines represent the feasibility boundaries $z = x_e$ and $z = y_e$ respectively ($x_e > y_e$).	58
3.5	Schematic bifurcation diagrams of the steady-state for (T_F, P) and (M_R, F_0) flash (Equation (3.14)) describing the dependence of composition in the reactor on τ . Letters indicate regions in Fig. 3.3. The horizontal lines represent the feasibility boundaries $z = x_e$ and $z = y_e$ respectively ($x_e > y_e$).	60

3.6	Global classification of the steady-state bifurcation diagrams for (T_F, P) and (M_R, F) flash (Equation (3.29)) in the $B - \beta_0$ plane for $x_e = 0.95$, $y_e = 0.1$, $Da_0 = 0.10$. BLS: Boundary limit set; BTS: Boundary tangent set; HV: Hysteresis variety; IV: Isola variety; LCS: Limit and cross set.	63
3.7	Schematic bifurcation diagrams of the steady-state (T_F, P) and (M_R, F) flash (Equation (3.29)) describing the dependence of composition in the reactor on τ_f . Letters indicate regions in Fig. 3.6. The horizontal lines represent the feasibility boundaries $z = x_e$ and $z = y_e$ respectively ($x_e > y_e$).	65
3.8	Global classification of the steady-state bifurcation diagrams for (T_F, P) and (M_R, L) flash (Equation (3.32)) in the $B - \beta_0$ plane for $x_e = 0.95$, $y_e = 0.1$, $Da_0 = 0.10$. HV: Hysteresis variety; IV: Isola variety.	68
3.9	Schematic bifurcation diagrams of the steady-state (T_F, P) and (M_R, L) flash (Equation (3.32)) describing the dependence of composition in the reactor on τ_l . Letters indicate regions in Fig. 3.8.	68
3.10	Global classification of the steady-state bifurcation diagrams for (T_F, P) and (F_0, F) flash (Equation (3.35)) in the $B - \beta_0$ plane for $x_e = 0.95$, $y_e = 0.1$, $Da_0 = 0.10$. BLS: Boundary limit set; HV: Hysteresis variety; IV: Isola variety.	71
3.11	Schematic bifurcation diagrams of the steady-state for (T_F, P) and (F_0, F) flash (Equation (3.35)) describing the dependence of temperature in the reactor on z . Letters indicate regions in Fig. 3.10. The vertical lines represent the feasibility boundaries $z = x_e$ and $z = y_e$ respectively ($x_e > y_e$).	72
3.12	Global classification of the steady-state bifurcation diagrams for (T_F, L) flash (Equation (3.38)) in the (α, β_0) plane.	74
3.13	Schematic bifurcation diagrams of the steady-state for (T_F, L) flash (Equation (3.38)) describing the dependence of temperature in the reactor on τ_f . Letters indicate regions in Fig. 3.12.	75
4.1	Schematic diagram of Pecora-Carroll synchronization.	80
4.2	Schematic diagram for detecting the occurrence of generalized synchronization in a given system.	81

4.3	Schematic diagram of the feedback control strategy.	82
4.4	Evolution of the state error $e_2 = Y_1 - Y_2$ with time for the case of $y = X_2$, $y_d = X_1$ and $u = p_1$	90
4.5	Evolution of the state errors $e_1 = (X_1 - X_2)$ and $e_3 = (Z_1 - Z_2)$ with time for the case of $y = Y_2$, $y_d = Y_1$ and $u = p_2$	91
4.6	Evolution of the error $e_1 = (X_1 - X_2)$ and $e_3 = (Z_1 - Z_2)$ with time for the case of $y = Y_2$, $y_d = Y_1$ and $u = p_2$. Parameter mis-match of $\pm 2\%$ between the model and the process was assumed.	91
4.7	Evolution of the state errors $e_1 = (X_1 - X_2)$, $e_2 = (Y_1 - Y_2)$ and $e_3 = (Z_1 - Z_2)$ with time for the case of $y = s_2$, $y_d = s_1$ and $u = u_{new}$. (a) No parameter mis-match; (b) mis-match of $+2\%$ and (c) mis-match of -2% between the model and the process parameters was assumed.	93
5.1	Schematic bifurcation diagrams for system showing input multiplicity.	98
5.2	Schematic diagram of the feedback control strategy for regulating the output of a nonlinear system.	99
5.3	Evolution of the errors and the manipulated variable with time. (a): $e_1 = (X_1 - X_2)$ and $e_2 = (Y_1 - Y_2)$; (b): $e_3 = (Z_1 - Z_2)$; (c): $e_{cm1} = (e_1 - \pi_1(w))$ and $e_{cm2} = (e_2 - \pi_2(w))$; (d): $e_{cm3} = (e_3 - \pi_3(w))$; (e) u . $\bar{a} = -1$, $k_1 = 12$, $k_2 = 4$ and $k_3 = -1$ in (5.24).	106
5.4	Steady-state bifurcation diagram depicting the dependence of the steady-states of (a) Y_1 and (b) Y_2 on τ	107
5.5	Response of the system states X and Y to a (a) $+10\%$ change and (b) -10% change in the input τ	109
5.6	Response of the system states ((a), (c)) and the input ((b), (d)) to a $+20\%$ change ((a), (b)) and -20% change ((c), (d)) in the set-point using the input-output linearization technique.	113
5.7	Response of the system states ((a), (c)) and the input ((b), (d)) to a $+20\%$ change ((a), (b)) and -20% change ((c), (d)) in the set-point using the output regulation technique. $\bar{w} = w^2$	114

5.8	Response of the system states ((a), (c)) and the input ((b), (d)) to unmeasured disturbances of +15% ((a), (b)) and -5% ((c), (d)) in β . $\bar{w} = w^2$	115
5.9	Response of the system states ((a), (c)) and the input ((b), (d)) to measured disturbances of +15% ((a), (b)) and -5% ((c), (d)) in β . $\bar{w} = w^2$	116
5.10	Response of the system states ((a), (c)) and the input ((b), (d)) to a +20% change ((a), (b)) and -20% change ((c), (d)) in the set-point using the input-output linearization technique.	118
5.11	Response of the system states ((a), (c)) and the input ((b), (d)) to a +20% change ((a), (b)) and -20% change ((c), (d)) in the set-point using the output regulation technique. $\bar{w} = w^2$	119
5.12	Response of the system states ((a), (c)) and the input ((b), (d)) to unmeasured disturbances of +15% ((a), (b)) and -5% ((c), (d)) in β . $\bar{w} = w^2$	120
5.13	Response of the system states ((a), (c)) and the input ((b), (d)) to measured disturbances of +15% ((a), (b)) and -5% ((c), (d)) in β . $\bar{w} = w^2$	121
A.1	Bifurcation diagrams showing the change in the multiplicity features (a) before crossing the hysteresis variety; (b) on the hysteresis variety and (c) after crossing the hysteresis variety.	132
A.2	Bifurcation diagrams showing the change in the multiplicity features (a) before crossing the isola variety; (b) on the isola variety and (c) after crossing the isola variety. Figures in the first and second rows are for the isola bifurcation and the simple bifurcation respectively.	133
A.3	Bifurcation diagrams showing the change in the multiplicity features in the presence of feasibility boundaries. (a) before crossing the boundary sets; (b) on the boundary sets and (c) after crossing the boundary sets. Figures in the first, second and third rows are for the BLS, the BTS and the DCS respectively.	135

A.4	Bifurcation diagrams showing the change in the multiplicity features for the case of (T_F, P) and (F, F_0) flash. (a) before crossing the BLS; (b) on the BLS and (c) after crossing the BLS.	135
A.5	Bifurcation diagrams showing the change in the multiplicity features for the case of (T_F, P) and (M_R, F) flash. (a) before crossing the LCS; (b) on the LCS and (c) after crossing the LCS.	136

List of Tables

2.1	Parameter values.	20
2.2	Bifurcation points of the FBR and summary of the dynamic behavior for parameter set 1 of Table 2.1, $R = 0.573875$	23
2.3	Period-adding and alternating periodic-chaotic regions, set 1, $R = 0.573875$	28
2.4	FBR bifurcation behavior.	36
4.1	Lyapunov exponents of the zero dynamics for the process system for different control configurations of the Rossler system.	95
5.1	Parameter values. $\beta_1 = 1$, for all cases.	111
5.2	Parameter values used in the output regulation technique. SP: Change in set-point; UMD: Unmeasured disturbance; MD: Measured disturbance.	112

Chapter 1

Introduction

In this dissertation we focus our attention on the behavior of nonlinear systems. We have chosen different model systems for our investigations and studied their open-loop and closed-loop characteristics. In chapter 2 we discuss the dynamic behavior exhibited by a discretely forced batch reactor. Chapter 3 is concerned with the analysis of the steady-state characteristics of a coupled reactor-separator network. We discuss the effect of different design specifications on the behavior of the system. In these two chapters we concern ourselves with the open-loop response of the respective systems.

In the fourth and fifth chapters we discuss the closed-loop performance of chaotic systems. In the fourth chapter we revisit the problem of designing a feedback controller with the objective of tracking a reference chaotic trajectory. We show that the study of this nonlinear control problem helps us to develop a unified framework for the analysis of the phenomenon of synchronization of chaotic systems. This technique is suitable only for a certain class of systems. In the fifth chapter we develop and apply a more general nonlinear control technique based on bifurcation theory for controlling a chaotic system. This technique is also employed for the control of a reactor system exhibiting input multiplicity.

In the remainder of this chapter we discuss the literature related to each of the above problems mentioned above. We also provide the motivation for the investigations undertaken in each of the following chapters.

The steady-state and dynamic behavior of the continuous stirred tank reactor (CSTR) has been the focus of several investigations over the last four decades. Even before the fifties, it was known that a few reaction systems could exhibit multiple

steady-states. Such behavior was first reported by Liljenroth in 1918[1]. Later Van Heerden[2] showed for the first time that the CSTR could exhibit similar phenomena. He determined the conditions for the existence of multiple steady-states in the reactor by considering the dependence of the rates of heat generation and heat removal on the reactor temperature. The subsequent interval has seen atleast four bursts of activity aimed at understanding the behavior of this system.

In the first phase, the emphasis was on developing a mathematical framework for understanding the uniqueness and multiplicity features of the CSTR. Most investigations considered the exothermic, irreversible reaction scheme $A \rightarrow B$ in a non-adiabatic CSTR. Bilous and Amundson[3] applied Lyapunov theory to carry out a linear stability analysis for this system. Their investigations revealed the existence of different types of steady-states for this system. They applied the concept of phase plane diagrams for explaining the nature of approach to the steady-state.

In the mid-seventies, the pioneering work of Poore and co-workers[4-6] resulted in a second burst of activity in investigations into the multiplicity features of the CSTR. This effort was mainly directed towards systematically characterizing the different possible types of steady-state multiplicity and dynamic features of this system. Bifurcation theory was used for this purpose. They introduced the bifurcation diagram for graphically representing the dependence of a state variable on a independent control parameter.

Multiplicity features in the context of non-isothermal reactions arise due to the presence of thermal feedback. This idea goes back to the work of Van Heerden[2]. Another class of reactions which have been widely investigated are the autocatalytic reactions. Here the multiplicity features arise because of feedback due to autocatalysis. Such autocatalytic mechanisms are of importance in catalytic and biochemical reaction systems. Gray and Scott[7, 8] have thoroughly investigated the multiplicity features of different types of autocatalytic reaction schemes in the CSTR. They showed that the autocatalytic mechanism by itself is sufficient for a system to exhibit a variety of multiple steady-state and dynamic behavior.

In the early eighties, the focus of the investigations shifted towards understanding the dynamic behavior of the CSTR. This was an outcome of the discovery that several simple nonlinear systems could exhibit complex dynamic behavior. Jorgensen and

Aris[9] demonstrated the richness of the dynamic behavior of the reaction $A \rightarrow B \rightarrow C$ in a CSTR. Such complex dynamic behavior has also been observed in non-isothermal autocatalytic reactions in a CSTR[10].

Some studies on the complex dynamics in CSTR's have considered the reaction $A \rightarrow B$ in a periodically forced system. It has been shown that periodic variation of the coolant temperature or the reactant flow rate can cause the system to exhibit complex dynamic behavior. Sincic and Bailey[11] have studied the dynamics of the first order, exothermic reaction in a periodically forced reactor. They investigated the dynamics under very fast forcing, very slow forcing and at intermediate values of the forcing frequency. They showed that it was possible for the system to exhibit sub-harmonic and quasi-periodic oscillations at intermediate ranges of the forcing frequency.

Several studies have been carried out to explain the mechanism through which such complex behavior can arise in the context of the CSTR. Aris and coworkers[12–15] have investigated the bifurcation features of different reaction schemes. Their objective was to study the effect of the bifurcation and multiplicity features of the unforced system on the system with forcing. They suggested mechanisms for explaining the occurrence of complex dynamic behavior in the periodically forced CSTR. Studies on verifying the universal features of such complex dynamics have also been reported in the literature. For example, Mankin and Hudson[16] have demonstrated the existence of a period doubling route to chaos and bistability for this system.

Other than its importance from the point of view of nonlinear dynamics, periodic operation of chemical reactors has been widely studied in the literature. In some cases, it may be advantageous to operate the reactor in a periodic manner. For example, under certain conditions of operation, the reactor may have multiple steady-states. Some of these states may possess undesirable features. For instance, a steady state could have a low conversion, and another could be at a very high temperature, for which a reactor may not be designed. Alternatively, a steady-state could be unstable. In such cases, periodic operation of the system can allow one to overcome many of the drawbacks associated with the presence of multiple steady-states while combining their advantages. It has been reported that use of periodically forced reactors can result in higher reaction rates, improved selectivity and better controllability characteristics[17]. The parameters which can be varied periodically include the feed flow

rate, feed concentration and the coolant temperature.

The above studies are based on the continuous forcing of a system. Another mode of a periodically forced operation of a reactor is discrete forcing, i.e., forcing at discrete times. Codell and Engel[18] were the first to investigate the performance of such a system. They considered the isothermal and adiabatic operations of a controlled cycled tank reactor (CCTR). The CCTR is a batch reactor in which a pre-determined fraction of the reactor contents are withdrawn and replaced with fresh feed after fixed intervals of time. They showed that for some reactions, the performance of the CCTR could be better than a CSTR and a plug flow reactor. Ausikaitis and Engel[19] experimentally studied the reaction between sodium thiosulphate and hydrogen peroxide in a CCTR. They showed that the CCTR offers better controllability characteristics in the case of exothermic reactions than a CSTR. Lin and Wu[20] have carried out a modelling and experimental study of the reaction between sodium thiosulphate and hydrogen peroxide in an adiabatic CCTR. They have considered a more general situation of the case considered by Ausikaitis and Engel[19], with the objective of predicting the approach to the steady periodic state. Another of their objectives was to compare the performance in the CCTR with that in the CSTR and the plug-flow reactor.

Kubickova *et al.*[21] have investigated the nonlinear dynamics of the first order, exothermic reaction in a non-adiabatic fed-batch reactor (FBR). This mode of operation of a reactor is an idealisation of the system considered by Codell and Engel[18], as they neglect the time of addition and withdrawal of fresh reactants and products respectively. They employed the arc-length continuation method to obtain the dependence of the periodic behavior of the system on the residence time in the reactor. They showed that the system could exhibit a variety of complex dynamic behavior.

In the next chapter, we investigate a more general model of the system considered by Kubickova *et al.*[21]. Operation of the FBR is considered to be to a mode between the batch and continuous modes of operation. The dynamics of the batch reactor are uninteresting as the reactor always proceeds towards a state of complete conversion, as we consider the reaction to be irreversible. The CSTR, on the contrary, can exhibit different types of steady-state and dynamic behaviour, i.e., hysteresis, isolas and limit cycles. For this reaction, the dynamics of the CSTR are well known. Our objective is to study the dynamics of the FBR, and, to compare it with that of a CSTR operating

under the same conditions. This would enable us to see how the dynamics of the FBR evolves from that of the CSTR. In particular, we study how the different bifurcations and multiplicity features of the CSTR manifest themselves in the FBR. With this in mind, we have used the arc-length continuation method to obtain the bifurcation diagrams of the FBR. The stability of the periodic solutions have been determined using Floquet theory. Extensive simulations have been carried out to corroborate the predictions of the stability theory.

The research on understanding the behavior of chemical reactors has been aided by the application of novel techniques from mathematics. The final burst of activity on investigations into the steady-state multiplicity features of chemical reactors followed the work of Balakotaiah and Luss[22–24]. In a series of papers, they demonstrated the application and usefulness of singularity theory in analysing the steady-state multiplicity features of several lumped parameter systems. Since then singularity theory has been shown to be a powerful tool specially for the steady-state analysis of systems containing a large number of parameters. Application of singularity theory has made it possible to obtain the steady-state multiplicity features of several single reactor systems with different types of nonlinearities.

Single units seldom occur in the process industries. It is typical to have several different types of units linked together by heat or mass exchange. Introduction of coupling through material and heat recycle in chemical processes alters the dynamics from that of single units. Therefore, even though the behavior of single units is well known, it is very difficult to predict the behavior of the coupled system. General features of the dynamic behavior of integrated plants have recently been reviewed by Morud and Skogestad[25, 26]. They have also ~~have~~ pointed out the need of obtaining some 'rules of thumb' which could be used as indicators for classifying different types of behavior of the coupled system.

Recent studies have analysed the steady-state and dynamic behavior of coupled reactor systems[10, 27]. These studies show that even when a model of the system is available, a comprehensive analysis of all the possible types of behavior of such systems is very difficult. In principle, currently available mathematical tools such as bifurcation theory and singularity theory, can be used to analyse a plant. However, these tools cannot be used to obtain a complete picture of the behavior of anything

but the simplest of such systems.

Luyben and co-workers[28–30] have studied the dynamics and control of binary and ternary recycle systems. They consider a process consisting of an isothermal CSTR coupled through recycle to a distillation column. The effect of operating the system under different design specifications on the steady-state economics and the controllability of the process were discussed. Starting with a given set of design parameters, their approach consists of developing a design procedure for the operation of the distillation column. The effect of changing the design parameters on the system variables was then studied. Based on their results, they have conjectured about the advantages of working with certain sets of design parameters. However, the complexity of the system in terms of the large number of variables, makes it impossible to obtain any firm results. In a later paper[31], Luyben analysed the effect of different control configurations on the snowball effect. The snowball effect is associated with a very large change in the recycle flow rate for a small change in the load variable. However, they did not provide any explanation for the origin of this phenomenon and ways for preventing its occurrence. In a later series of papers, they have extended their investigations to cover different cases of ternary systems[32–34]. In these studies, they consider several model reaction schemes, multiple separator units and multiple recycle streams.

In the third chapter of this dissertation, we study the steady-state behavior of a reactor-separator system with recycle. As mentioned earlier, the overall behavior of systems with material or heat recycle is very different from the behavior of the individual units. Further, it has been claimed that plant interconnections may introduce fundamental limitations in the performance of any control system[25, 26]. Knowledge of the performance of such plants is important for control design. Hence it is important to have a thorough knowledge of the steady-state and dynamic behavior of recycle systems. With this in mind, we have investigated the steady-state multiplicity features of a model reactor-separator system with recycle. The system selected is such that it permits the application of singularity theory[35]. Application of this technique enables us to obtain a comprehensive picture of the steady-state multiplicity features of this system. It is shown that this system exhibits some unusual features. For example, we find that the system cannot have any steady-states for some sets of the operating parameters. We provide a physical explanation for the origin of these unusual behav-

ior. The objective of this work is to obtain a qualitative picture about the types of steady-state behavior that can be expected for different sets of specifications of this system. For a plant with recycle streams, this study provides a starting point for a more detailed analysis and for understanding the different physical interactions.

Over the past decade, there have been major developments in the applications of nonlinear control schemes based on differential-geometry for the control of chemical engineering systems[36]. Extensive experimental and simulation studies on many systems, using several control techniques have been reported in the literature. In chapters 4 and 5 of this thesis, we show the applicability of results from nonlinear control theory to a problem which has been attracting widespread attention in the physics literature.

Since 1990, synchronization of chaos has been a topic of immense interest and puzzlement in the physics community. Two systems are said to synchronize if, after starting from different initial conditions, they evolve along the same trajectory in phase space. Synchronization between two identical chaotic systems has been considered to be an unlikely goal, because chaos is characterized by a sensitive dependence on initial conditions. However, Pecora and Carroll[37, 38] showed that two chaotic systems could be synchronized with each other. Within the last two years, two different types of synchronization have been reported in the literature. Rulkov *et al.*[39] and Kocarev and Parlitz[40] have studied the type of synchronization which they refer to as generalized synchronization. This type of synchronization is characterized by a nonlinear relationship between the drive and response system variables. Kocarev and Parlitz and their co-workers[41, 42] have reported a powerful new technique for achieving synchronization in chaotic systems. Their procedure, an active-passive decomposition (APD) technique involves creating a new system by defining a new variable as a function of the system variables and using this to drive the modified response system.

The importance of synchronization stems from several potential applications[40]. For example, it has been shown that synchronization can be used in secret communications and cryptography. Another potential application of synchronization is in the understanding of neural processes, where such a mechanism can be used to simulate neural behavior. There has also been much speculation in the literature about the role of synchronization governing the smooth functioning of the heart.

In the fourth chapter, we present an approach for the analysis of the different types

of chaotic synchronization in a unified framework. This approach results from the use of results from nonlinear control theory, which have been employed by chemical engineers in recent years.

Systems exhibiting input multiplicity are frequently encountered in chemical engineering. Input-multiplicity is a situation where different inputs can give the same output. Balakotaiah and Luss[45] have applied singularity theory to classify a parameter space into regions where it is possible to encounter input multiplicity. Koppel[43, 44] has carried out a detailed analysis of the effects of input multiplicity on different model control systems. However there has not been much progress in the development of control techniques for use on such systems. This is especially true for several of the methods based on differential-geometry. A limitation of many of these control techniques is that they can be used only for the control of minimum-phase systems. Hence they are of limited use for the control of systems exhibiting input multiplicity. A new technique for the output regulation of such systems has been recently proposed in the literature[46, 47].

In the fifth chapter, we apply the output regulation technique to achieve control and synchronization in two model systems. We consider the control of an autocatalytic reaction in an isothermal CSTR exhibiting input multiplicity. The technique is also applied to achieve synchronization in the Rossler system when the techniques discussed in chapter 4 fail.

Chapter 2

Nonlinear Dynamics of a Fed-Batch Reactor (FBR)

Nomenclature

B	Dimensionless heat of reaction.
C	Conversion.
k_0	Reaction rate constant.
P	Period of fed-batch operation.
R	Fraction of reaction volume withdrawn.
T	Dimensionless Temperature.
s	Arc-length in the continuation method.
t	Dimensionless Time.
t_c	Time of recharging.
t_d	Time of withdrawal.
β_0	Heat removal parameter.
β_1, β_2	Constants in Equation (2.9).
λ	Largest Lyapunov exponent.
τ	Residence time.

Subscripts

0	Initial state.
-, +	Before updating, after updating.

2.1 Introduction

In the previous chapter we reviewed the literature on the nonlinear dynamics of chemical reactors. Most of these studies have concentrated on investigating the dynamic behavior exhibited by the CSTR. The dynamics of several reaction schemes in (i) the autonomous CSTR and (ii) the periodically forced CSTR have been the subject of several detailed studies[10]. In comparison, the nonlinear dynamics of discretely forced systems have not been widely studied.

Discretely forced systems occur in a variety of contexts. In the area of medical sciences, periodic variation of drug concentration in the body is an example of such a system. Intake of the drug results in a sudden increase in its concentration in the body. Subsequently, ingestion of the drug results in a gradual decrease in its concentration. A similar situation also prevails in the periodic addition of fertilizers in farming. Discrete forcing is also widely used in the manufacture of various products involving biochemical reactions. Here, it is often desirable to add the substrate to a batch bio-reactor as the reaction proceeds. This addition is often done in discrete pulses, in order to optimize the reactor performance.

In this chapter we investigate the dynamic behavior of the first-order, irreversible and exothermic reaction in a non-adiabatic fed-batch reactor (FBR). The FBR is an example of a discretely forced batch system. The mode of operation of the FBR is in between the batch mode and the continuous mode. The dynamics of the batch reactor are uninteresting, as the reaction always proceeds in the direction of increasing conversion. The CSTR, on the other hand, exhibits a rich variety of dynamic behavior[6]. We wish to compare the dynamics of the FBR with that of a CSTR operating under the same conditions. In particular, we will be interested in investigating how the multiplicity, stability features and the nature of approach to the steady-state in the CSTR, influence the dynamics of the FBR. This would enable us to see how the dynamics of the FBR evolve from that of the corresponding CSTR. Therefore, our broad objective will be to investigate how the multiplicity features of the FBR depend on one of the system parameters. For this purpose, we have used an arc-length continuation method

to compute the bifurcation diagrams of the FBR. The shooting method has been used to compute the periodic solutions of the FBR model. The stability of the solutions have been determined using Floquet theory. Extensive simulations have been carried out to bring out the different types of complex dynamic behavior exhibited by the FBR.

We start by describing the FBR model. This is followed by a brief description of the method of solution. The results are presented in the third section and we conclude with a discussion of the results.

2.2 Description of the Model

The FBR discussed in this chapter is a periodically forced batch reactor. The operation consists of the following steps[21]:

1. The reactor is filled up to the desired volume with the reactants at the start of a operating cycle,
2. The reactor is well stirred and the reaction is carried out in the batch mode for time P (reaction step),
3. At the end of the reaction time, a fixed volume fraction R of the reactor volume is withdrawn over a time interval t_d (discharge step),
4. The reactor volume is made up to the final volume by the addition of fresh feed over a time t_c (recharge step),
5. The steps 2, 3 and 4 are repeated.

The FBR described above is different from that widely used for carrying out biochemical reactions. In the biochemical context, a FBR is a semi-batch reactor.

Throughout this study, we assume for simplicity that $t_c = t_d = 0$. This implies that steps 3 and 4 are instantaneous. The system we consider is the first order, exothermic, irreversible reaction $A \rightarrow B$ in a non-adiabatic FBR. Thus our model is the most general possible for this model reaction. The evolution of the concentration and the temperature in the reactor occurs during step 2. This evolution is modelled by the

following set of dimensionless equations, representing the material and energy balances respectively

$$\frac{dC}{dt} = k_0\tau(1 - C)e^T = f_1 \quad (2.1)$$

$$\frac{dT}{dt} = Bk_0\tau(1 - C)e^T - \beta_0\tau T = f_2$$

with the initial condition: $t = 0$: $C = 0$, $T = 0$.

Here we have assumed that the concentration and temperature characterising the initial state of the reactor (at the beginning of the reaction step of the first cycle) are equal to that of the fresh feed used for recharging the reactor. In the above equations, B , β_0 and k_0 represent the dimensionless heat of reaction, the heat removal parameter and the reaction rate constant respectively. The parameter $\tau (= P/R)$ is representative of the residence time in the reactor. We have used τ as the characteristic time scale to define the dimensionless time t . For simplicity, we have made the positive exponential approximation in the derivation of the above equations.

Equation (2.1) is valid only during the interval of batch operation. At the end of operation in the batch mode (of interval P actual time units), the discharge of products and the recharge of fresh feed updates the values of C and T in the reactor. In terms of the dimensionless time t , this is equivalent to updating after every integral multiple of R dimensionless time units. Therefore, at the end of each cycle of batch operation (of R dimensionless time units), the discharge of products and the recharge of fresh feed updates the values of C and T in the reactor according to

$$C_{t=R+} = (1 - R)C_{t=R-} \quad (2.2)$$

$$T_{t=R+} = (1 - R)T_{t=R-}$$

In the above equations, the subscripts $-$ and $+$ denote the values of the states before and after the updating respectively. Therefore, at the end of operation in the batch mode, there is a discontinuous variation of the conversion and temperature in the reactor governed by (2.2).

The model of the FBR appears to be an autonomous system as the independent variable t does not explicitly occur in the model. This system is a periodically forced system and is forced with a period P . The evolution of the system is therefore, determined not only by the current state of the system, but also by the time at which the

state is reached. Hence, if a state is reached at the end of the reaction step, it changes discontinuously according to (2.2), else its evolution is governed by (2.1). This is a characteristic of a non-autonomous system.

The FBR as described above, tends to a batch process in the limit of $R \rightarrow 0$. In this limit the reaction approaches a state of complete conversion with increasing time. This follows since the reaction is irreversible. For $R = 1$, we are at the limit of batch operation which is repeated every P time units. These two limits are uninteresting as far as the dynamic behavior of the reactor is concerned. However, for $0 < R < 1$, we have an open system which exchanges mass and heat with the environment periodically. We therefore, analyze the behavior of the system for $R \in (0, 1)$. For finite P and $R \in (0, 1)$, the mean residence time τ in the reactor can be defined as P/R . The dynamic characteristics of the FBR can hence be compared with that of a CSTR of the same residence time, for identical values of other system parameters. The true limit of the CSTR is reached in the limit $P \rightarrow 0$, $R \rightarrow 0$, such that

$$\lim_{R \rightarrow 0, P \rightarrow 0} \frac{P}{R} = \tau \text{ (finite)}$$

The CSTR of residence time τ_c , which is equivalent to the FBR described above can be represented by the following set of equations[6]

$$\frac{dC}{dt} = -C + k_0\tau_c(1 - C)e^T$$

$$\frac{dT}{dt} = -T + Bk_0\tau_c(1 - C)e^T - \beta_0\tau_cT$$

2.3 Method of Solution

The basic state of the CSTR is a steady-state. In the FBR, the equivalent state is a periodic state of the reactor which has a period P . Hence this is referred to as a 1P state. A state which is periodic and has a period mP with $m > 1$, is denoted as an mP state. This corresponds to sub-harmonic oscillations of the FBR. As mentioned earlier, the mP states ($m \geq 1$) are actually obtained as mR states, since we shall be using the dimensionless set of equations (2.1) and (2.2). However, we employ the mP notation to identify these periodic states of the FBR.

In the bifurcation study of a system, one investigates how a dependent variable varies with a control parameter. This is called the bifurcation parameter. For example, in the classical approach employed for understanding the bifurcation characteristics of the CSTR, one studies the dependence of the steady-state conversion or temperature on the bifurcation parameter (the residence time) in the reactor[6]. In this work we determine the multiplicity and stability features of the 1P state of the FBR. The parameter P is considered to be the bifurcation parameter. Changing P is equivalent to changing the residence time in the FBR.

We begin by describing the shooting method which has been used to generate the 1P solutions of (2.1) subject to (2.2). Later, we discuss the arc-length continuation method which has been used to generate the dependence of C and T on P . This is followed by a discussion on the determination of stability of the 1P solution. Details of all these techniques are available in[48].

2.3.1 Shooting Method

The 1P solution of (2.1) subject to (2.2) can be determined by integrating (2.1), once the initial conditions C_0 and T_0 of the periodic state have been determined. It is possible to determine these unknowns by formulating and solving a boundary-value problem using the shooting method. For a 1P solution, we require $C_{R+} = C_0$ and $T_{R+} = T_0$. This condition is represented as

$$\begin{aligned} G_1(C_0, C_{R+}, T_0) &= C_{R+} - C_0 = 0 \\ G_2(C_0, T_{R+}, T_0) &= T_{R+} - T_0 = 0 \end{aligned} \tag{2.3}$$

The equations (2.3) are a set of algebraic equations and these can be solved for the unknowns C_0 and T_0 using the Newton-Raphson method. The values of the variables before and after updating at $t = R$ (denoted by the subscripts $-$ and $+$ respectively) are dependent on the values at the beginning of the cycle (denoted by a subscript 0). These are determined by integrating (2.1) with the initial conditions (C_0, T_0) . This is followed by imposing the updating condition (2.2). The $(n + 1)^{th}$ iterate of the

unknowns is computed from the n^{th} iterate using

$$\begin{bmatrix} C_0 \\ T_0 \end{bmatrix}^{n+1} = \begin{bmatrix} C_0 \\ T_0 \end{bmatrix}^n - \begin{bmatrix} \frac{\partial C_{R+}}{\partial C_0} - 1 & \frac{\partial C_{R+}}{\partial T_0} \\ \frac{\partial T_{R+}}{\partial C_0} & \frac{\partial T_{R+}}{\partial T_0} - 1 \end{bmatrix}^{n-1} \begin{bmatrix} C_0 \\ T_0 \end{bmatrix}^n \quad (2.4)$$

The variations in C_{R+} , T_{R+} with C_0 and T_0 are obtained by solving the following set of four linear ordinary differential equations

$$\begin{aligned} \frac{d}{dt} \left(\frac{\partial C}{\partial C_0} \right) &= \left(\frac{\partial f_1}{\partial C} \right) \left(\frac{\partial C}{\partial C_0} \right) + \left(\frac{\partial f_1}{\partial T} \right) \left(\frac{\partial T}{\partial C_0} \right) \\ \frac{d}{dt} \left(\frac{\partial C}{\partial T_0} \right) &= \left(\frac{\partial f_1}{\partial C} \right) \left(\frac{\partial C}{\partial T_0} \right) + \left(\frac{\partial f_1}{\partial T} \right) \left(\frac{\partial T}{\partial T_0} \right) \\ \frac{d}{dt} \left(\frac{\partial T}{\partial C_0} \right) &= \left(\frac{\partial f_2}{\partial C} \right) \left(\frac{\partial C}{\partial C_0} \right) + \left(\frac{\partial f_2}{\partial T} \right) \left(\frac{\partial T}{\partial C_0} \right) \\ \frac{d}{dt} \left(\frac{\partial T}{\partial T_0} \right) &= \left(\frac{\partial f_2}{\partial C} \right) \left(\frac{\partial C}{\partial T_0} \right) + \left(\frac{\partial f_2}{\partial T} \right) \left(\frac{\partial T}{\partial T_0} \right) \end{aligned} \quad (2.5)$$

with the initial conditions

$$\text{At } t = 0, \quad \frac{\partial C}{\partial C_0} = 1, \quad \frac{\partial C}{\partial T_0} = 0, \quad \frac{\partial T}{\partial C_0} = 0, \quad \frac{\partial T}{\partial T_0} = 1.$$

and

$$\begin{bmatrix} \frac{\partial f_1}{\partial C} & \frac{\partial f_1}{\partial T} \\ \frac{\partial f_2}{\partial C} & \frac{\partial f_2}{\partial T} \end{bmatrix} = \begin{bmatrix} -k_0 \tau e^T & k_0 \tau (1 - C) e^T \\ -B k_0 \tau e^T & B k_0 \tau (1 - C) e^T - \beta_0 \tau \end{bmatrix}$$

The system of six equations (2.1) and (2.5) are integrated simultaneously. Dependence of these variables on the updating condition is accounted for, by imposing the updating condition on these variables. The values of the derivatives in the matrix of (2.4) are the values of the dependent variables in (2.5), at $t = R+$. We can thus obtain the solution C_0, T_0 using an iterative procedure (using (2.4)) for a fixed value of the system parameters B, k_0, P, R and β_0 . Once C_0, T_0 have been obtained, the 1P solution is obtained by integrating (2.1) using (2.2). Equation (2.3) is a periodic boundary condition. This ensures that the dependent variables C and T are periodic

with a period R . For the cases where multiple 1P solutions exist for (2.1), the solution to which we converge upon, depends on the initial guess of C_0 and T_0 .

Having determined the solution for a fixed set of parameters, we fix all the parameters except P . We study how the 1P solution changes as we vary P - the bifurcation parameter. The arc-length continuation method has been used to obtain the dependence of the 1P solutions of the system (2.1) on P . This method is described next.

2.3.2 Arc-length Continuation Method

It is well known that for the first order reaction, the bifurcation diagram of the CSTR can consist of different branches. Hence we may expect that for the FBR, the dependence of the 1P state on the bifurcation parameter P can consist of various branches. A technique which can be used to determine the dependence of the dependent variable on an independent variable is the arc-length continuation method[48]. We have employed this technique for generating the dependence of the 1P states of the FBR on P in a smooth manner. The method involves introducing a new parameter, the arc-length of the solution curve denoted by s , such that the system has a smooth set of solutions in (C, T, P) space. The method is based on starting with a solution for a given value of P , say P_0 . We use this solution as an initial guess to determine the solution at a new value $P + \delta P$ in the neighborhood of the initial point P_0 . We now describe the details of this technique.

Let s denote the arc-length along the solution curve. Having determined the 1P solution of (2.1) subject to (2.2) at an initial point P_0 , we denote that point by $s = 0$. Instead of studying the dependence of $C(t)$ and $T(t)$ on P , the problem is now transformed to that of studying the dependence of $C(t)$, $T(t)$ and P on the arc-length s , i.e., we are interested in determining the evolution of $C(t)$, $T(t)$ and P as s varies. The 1P solution of (2.1) subject to (2.2) is uniquely determined by its initial conditions C_0 and T_0 , for a given P . Therefore, the arc-length continuation procedure reduces to a problem of determining how C_0 , T_0 and P change, as we proceed along the arc-length

s. Differentiating (2.3) with respect to s , we have

$$\begin{aligned}\frac{dG_1}{ds} &= \left(\frac{\partial G_1}{\partial C_0}\right)\left(\frac{dC_0}{ds}\right) + \left(\frac{\partial G_1}{\partial T_0}\right)\left(\frac{dT_0}{ds}\right) + \left(\frac{\partial G_1}{\partial P}\right)\left(\frac{dP}{ds}\right) = 0 \\ \frac{dG_2}{ds} &= \left(\frac{\partial G_2}{\partial C_0}\right)\left(\frac{dC_0}{ds}\right) + \left(\frac{\partial G_2}{\partial T_0}\right)\left(\frac{dT_0}{ds}\right) + \left(\frac{\partial G_2}{\partial P}\right)\left(\frac{dP}{ds}\right) = 0\end{aligned}\quad (2.6)$$

The coefficients $\frac{\partial C_{R+}}{\partial P}$ and $\frac{\partial T_{R+}}{\partial P}$ occurring in the derivatives of G_1 and G_2 in (2.6) are obtained by integrating the following equations

$$\begin{aligned}\frac{d}{dt}\left(\frac{\partial C}{\partial P}\right) &= \left(\frac{\partial f_1}{\partial C}\right)\left(\frac{\partial C}{\partial P}\right) + \left(\frac{\partial f_1}{\partial T}\right)\left(\frac{\partial T}{\partial P}\right) + \left(\frac{\partial f_1}{\partial P}\right) \\ \frac{d}{dt}\left(\frac{\partial T}{\partial P}\right) &= \left(\frac{\partial f_2}{\partial C}\right)\left(\frac{\partial C}{\partial P}\right) + \left(\frac{\partial f_2}{\partial T}\right)\left(\frac{\partial T}{\partial P}\right) + \left(\frac{\partial f_2}{\partial P}\right)\end{aligned}\quad (2.7)$$

with the initial conditions: at $t = 0$: $\frac{\partial C}{\partial P} = 0$ and $\frac{\partial T}{\partial P} = 0$, followed by imposing the updating condition.

Equation (2.6) is a system of two linear homogenous equations in the three unknowns $\frac{dC_0}{ds}$, $\frac{dT_0}{ds}$ and $\frac{dP}{ds}$. A third equation is obtained using the normalisation condition from calculus

$$\left(\frac{dC_0}{ds}\right)^2 + \left(\frac{dT_0}{ds}\right)^2 + \left(\frac{dP}{ds}\right)^2 = 1 \quad (2.8)$$

From (2.6), we seek a solution of the form

$$\frac{dx_i}{ds} = \beta_i \frac{dx_k}{ds}, \quad i = 1, 2, k-1, k+1, \dots, n+1 \quad (2.9)$$

In the above equation, $x_1 = C_0$, $x_2 = T_0$, $x_3 = P$ and $n = 2$. We can thus determine β_1 and β_2 from (2.6) and solve (2.8) for $\frac{dx_k}{ds}$ to evaluate

$$\frac{dx_k}{ds} = \frac{1}{\pm \sqrt{1 + \beta_1^2 + \beta_2^2}} \quad (2.10)$$

The sign of the derivative $\frac{dx_k}{ds}$ is given by the orientation of s along the solution branch. Choosing the variable x_k and the sign of the solution to the above equation appropriately, enables us to traverse through the bifurcation points in a smooth manner.

We integrate (2.1), (2.5) and (2.7) simultaneously, with the updating conditions (2.2). Equation (2.9) is then solved for β_1 and β_2 using Gaussian elimination. We then obtain estimates of $\frac{dP}{ds}$, $\frac{dC_0}{ds}$ and $\frac{dT_0}{ds}$ from (2.9) and (2.10). This system of equations with the initial condition

At $s = 0$: $P = P_0$, $C = C_0$ and $T = T_0$

is integrated using the Euler method. This is the predictor step which yields new approximate values of P , C_0 , T_0 . These values of C_0 and T_0 are then used as initial guesses to solve (2.1) and (2.3) with the new value of P , using the shooting method described earlier. This shooting method step is the corrector step, used to obtain the accurate 1P solution with the new value of P . The Gaussian elimination, Euler integration and the shooting method are repeated with the new value of P computed above. This procedure eventually enables us to determine the dependence of the 1P solution on P in a continuous manner.

2.3.3 Stability

1P solutions of (2.1) subject to (2.2) computed using the shooting method can be stable or unstable. The solution on which we converge is solely determined by the initial guesses of C_0 and T_0 used in the scheme. Floquet theory[48] is used to determine the stability of the 1P solution. After a 1P solution is determined, its stability is determined by calculating the magnitudes of the eigenvalues of the variational matrix

$$\begin{bmatrix} \frac{\partial C_{R+}}{\partial C_0} & \frac{\partial C_{R+}}{\partial T_0} \\ \frac{\partial T_{R+}}{\partial C_0} & \frac{\partial T_{R+}}{\partial T_0} \end{bmatrix} \quad (2.11)$$

The solution is stable if both the eigenvalues of the above matrix lie inside the unit circle in the complex plane. As the bifurcation parameter P is varied, the eigenvalues can cross the unit circle in three ways. Therefore, there are three possible ways in which the 1P state can be de-stabilized. These are

1. One of the eigenvalues leaves the unit circle through -1 . This corresponds to a period doubling bifurcation. The 1P state of the FBR becomes unstable and another state with twice the original period branches off at this point.
2. An eigenvalue leaves the unit circle through $+1$. In the case of the FBR, this instability corresponds to the saddle-node bifurcation. At this bifurcation point, a 1P state changes its stability and another 1P state emanates from this point.

3. A complex-conjugate pair of eigenvalues leaves the unit circle. This corresponds to a torus bifurcation. Following this bifurcation, there is a change in the dimension of the attractor. We can now visualise the system as evolving on the surface of a torus.

2.3.4 Simulations

Extensive simulations were carried out to obtain a complete picture of the dynamic behaviour of the fed-batch reactor. Gear's method (Routine D02EBF of NAG library) was used for integrating (2.1). Integration was usually carried out till 5000 cycles of operation of the fed-batch reactor.

2.3.5 Stroboscopic Map

In general it is very difficult to identify the nature of the dynamics using time series data obtained from the simulations. In such cases, the stroboscopic map is useful for identifying the nature of evolution of the system. This is a standard technique used in the analysis of forced systems. This technique involves measuring one of the system states after definite intervals of time. The strobing is generally done at a frequency equal to the forcing frequency. Construction of the stroboscopic map therefore, involves plotting the value of a state variable $X(t)$ (either C or T) versus $X(t+R)$. In this work we have used the value of T at the end of reaction step, to generate the stroboscopic maps. The stroboscopic map for the FBR showing mP dynamics consists of m points. For a system undergoing quasi-periodic dynamics, the stroboscopic map yields a closed curve, indicating that the system evolves on the surface of a torus. A stroboscopic map in which the points are scattered is representative of chaotic dynamics. These points usually lie on dense segments, which is typical of deterministic chaos.

2.4 Results and Discussion

The dynamics of our model reaction in the CSTR has been thoroughly investigated by Uppal *et al.*[6]. They catalogued the different steady-state multiplicity features and the qualitative aspects of the dynamic behavior of the CSTR by classifying the parameter

Set	B	k_0	β_0
1	14.0	0.162	3.0
2	8.0	0.136	1.0
3	6.88	0.136	0.72

Table 2.1: Parameter values.

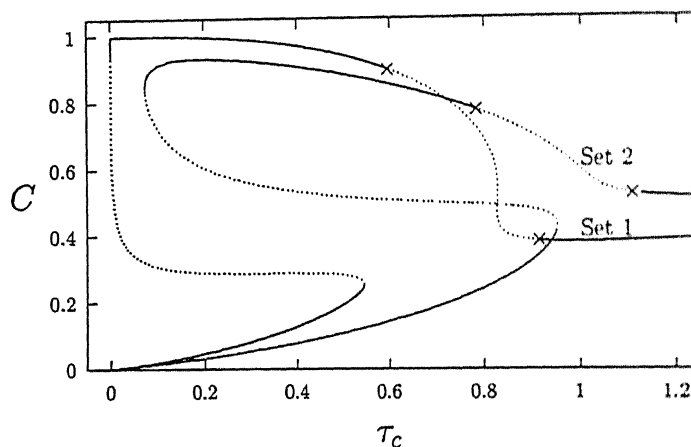


Figure 2.1: Bifurcation diagram for the CSTR for parameter sets 1 and 2 of Table 2.1, (—): stable steady-state; (\cdots): unstable steady-state; (\times): Hopf bifurcation point.

space into different regions. For the purpose of comparing the dynamic characteristics of the FBR with the CSTR, we have chosen three sets of parameter values for our investigation. These are listed in Table 2.1.

The parameter values in set 1 are identical to those chosen by Kubickova *et al.*[21]. For this set, the CSTR has multiple steady-states for $0.00183 < \tau_c < 0.5458$. The upper steady-state branch is unstable in the region $0.5963 < \tau_c < 0.9163$. This instability arises because of a Hopf bifurcation and the system exhibits oscillatory behavior in this region. The dependence of the steady-state conversion of the CSTR on τ_c is shown in Fig. 2.1. Kubickova *et al.*[21] have shown that the FBR exhibits periodic oscillations of different periods for parameter values of this set under the restriction $P = R$. In the present study, we generate the bifurcation diagram of the 1P state of the FBR

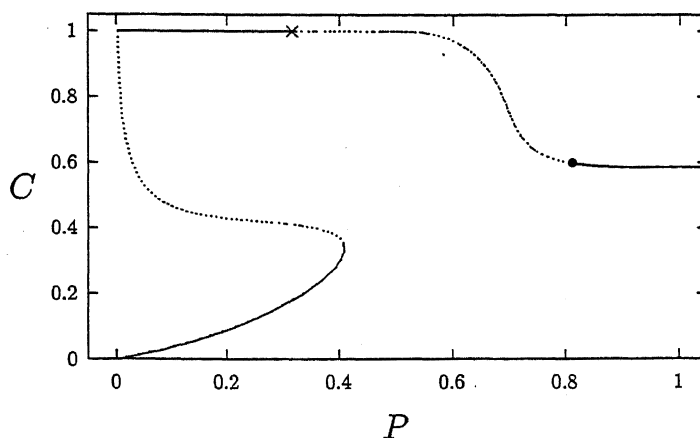


Figure 2.2: Bifurcation diagram of the 1P state for the FBR, parameter set 1, $R = 0.573875$, (—): stable 1P state; (···): unstable 1P state; (×): Period doubling bifurcation; (•): Torus bifurcation point.

by varying P , for a fixed value of R and the other parameters. This is equivalent to determining the effect of residence time on the 1P state of the FBR.

We concentrate only on the basic periodic behavior of the FBR. This is the periodic behavior with a period equal to the forcing period P . As mentioned earlier, we refer to this as a 1P state. This 1P state is analogous to the steady-state of the CSTR. We have shown the dependence of the 1P state on P for $R = 0.5738750$ in Fig. 2.2. The ordinate in the figure is the conversion at the end of a batch cycle before the updating. This corresponds to the composition of the product withdrawn from the reactor. The figure is qualitatively similar to the bifurcation diagram of the CSTR (Fig. 2.1). There is a region of τ where multiple 1P states exist and a region where the upper 1P state branch is unstable. The different features of Fig. 2.2 are discussed next in detail.

For $R = 0.573875$, as we increase P from zero, the conversion increases till $P = 0.410027$. At this point an eigenvalue of the variational matrix (2.11) moves out of the unit circle through $+1$ and the 1P state loses its stability via a saddle-node bifurcation. This corresponds to the ignition point of the system. The 1P state emerging as a result of this bifurcation is a saddle, as one eigenvalue of (2.11) lies inside the unit circle and the other is outside the unit circle in the complex plane. This unstable state exists

for $P < 0.410027$. This 1P state exists till $P = 0.00251$, where another saddle-node bifurcation occurs. Here an eigenvalue of (2.11) re-enters the unit circle through $+1$. The 1P state now regains its stability and it turns around. This point corresponds to the extinction point. The stable branch exists for $P > 0.00251$. As we continue along P on the top branch, an eigenvalue of (2.11) goes out of the unit circle through -1 at $P = 0.3186$. At this value of P , the 1P state loses its stability in a period doubling bifurcation. As P is increased past this value, the stable state of the FBR is a periodic state with a period of twice the forcing period. We now continue along this stable 2P state and study successive bifurcations. As we increase P , we encounter a sequence of period doubling bifurcations. The first five period-doubling bifurcation points are given by the first five values of P in Table 2.2. At each of these values of P , an eigenvalue of the stable $2^m P$ state ($m = 1$ to $m = 5$), existing to the left of the bifurcation point, moves out of the unit circle through -1 . The distance between successive values of P at which period doubling bifurcations occur decreases very rapidly. This is consistent with the classical period doubling route to chaos[49]. This cascade of period doubling bifurcations continue till the bifurcation points accumulate at a value of P close to 0.33513. We were unable to continue beyond the 32P state. This is because the bifurcations occur very rapidly.

As we vary the parameter P from 0.33515 to 0.351, i.e., just beyond the regions of period doubling bifurcations, the FBR exhibits interesting dynamic behavior. The stroboscopic map for $P = 0.33515$ is shown in Fig. 2.3(a). The last 2000 points out of 5000 cycles of the simulation were used to generate the map. This stroboscopic portrait can be described as two small islets facing each other. Further, the strobed points oscillate in the neighbourhood of $T = 4.5$ and $T = 6.6$. This dynamic behavior is typical of the emergence of chaotic behavior from the classical period doubling route to chaos. The stroboscopic maps for $P = 0.342$ and $P = 0.349$ are shown in Figs. 2.3(b) and 2.3(c). This type of the stroboscopic portrait is typical of a system exhibiting chaotic dynamics. The growth and the subsequent merging of the islets as we increase P is clear from Figs. 2.3(a)-2.3(c). The three cases considered above show that the system exhibits chaotic behavior, for values of P just beyond the accumulation point of the period doubling cascade. This behavior ends suddenly for values of P just beyond 0.351. For $0.351 < P < 0.410027$, i.e., till the ignition point, the only stable state of

Nature of FBR dynamics	P
1P-2P	0.3186
2P-4P	0.332955
4P-8P	0.334596
8P-16P	0.3350285
16P-32P	0.3351235
Chaos	0.33513-0.351
Crisis (lower 1P)	0.351-0.410027
Intermittency	0.410027-0.411
Mixed-mode oscillations (Table 2.3)	0.415-0.70
Torus bifurcation	0.8214

Table 2.2: Bifurcation points of the FBR and summary of the dynamic behavior for parameter set 1 of Table 2.1, $R = 0.573875$.

the FBR is the 1P state corresponding to the lower stable 1P branch in Fig. 2.2.

In this region the chaotic attractor loses its basin of attraction, i.e., points in phase space are no longer attracted to it. This is induced by the collision of the chaotic attractor with the upper unstable 1P state. This phenomenon is termed as a boundary crisis[50, 51]. This can be seen from the stroboscopic map for $P = 0.349$ shown in Fig. 2.3(c), which shows the chaotic attractor about to collide with the fixed point. Destruction of the chaotic attractor results from its collision with the upper unstable 1P state near $P = 0.351$. For values of $P > 0.351$, the system exhibits transient chaos, i.e., the trajectory stays in the vicinity of the chaotic attractor (which has disappeared now) for some time before being attracted to the lower 1P state. The crisis point is a bifurcation point as beyond this point the chaotic attractor disappears. This bifurcation involves two non-local attractors and hence is an example of a global bifurcation.

There is another sudden change in the dynamic behavior as we cross the value of P at the ignition point ($P = 0.410027$). For values of $P > 0.410027$, the lower 1P state does not exist, and the upper 1P state is unstable. The steady behavior of the system is such that it consists of a large number of small amplitude amplitude

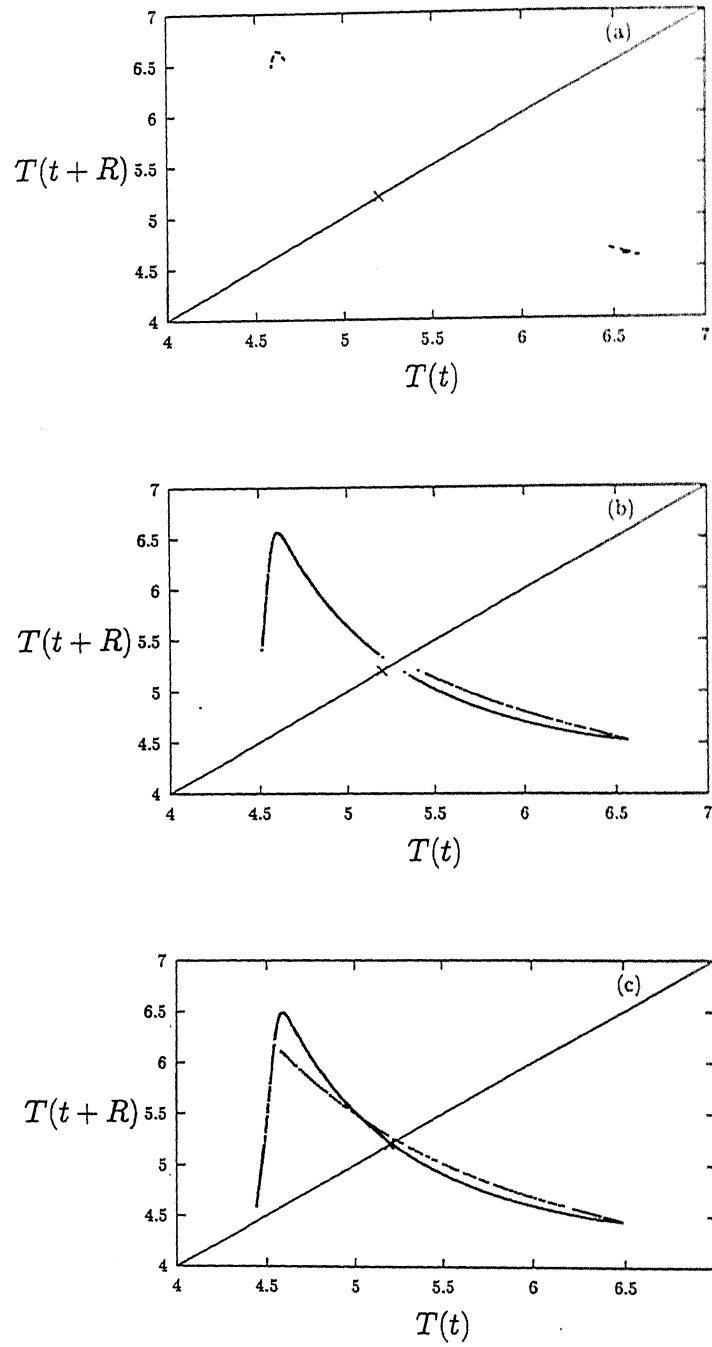
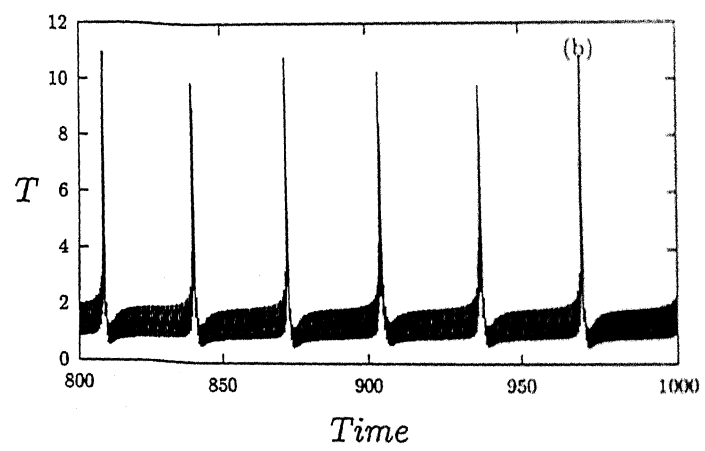
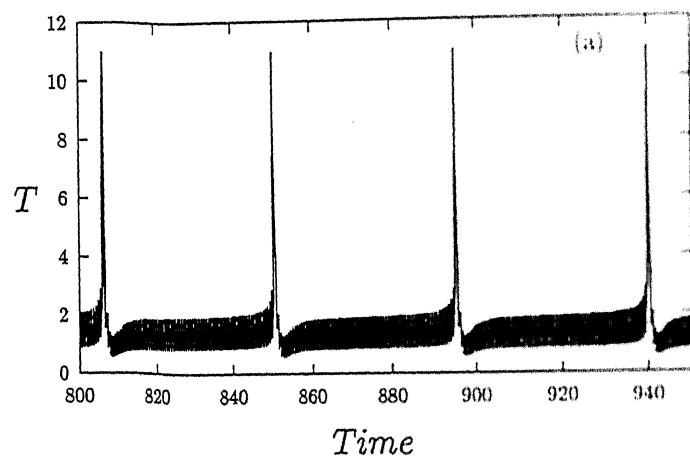


Figure 2.3: Stroboscopic maps of the chaotic attractor showing the growth and collision of the chaotic attractor with the unstable fixed point (\times), parameter set 1, $R = 0.573875$, (a) $P = 0.33515$; (b) $P = 0.342$ and (c) $P = 0.349$.

oscillations which are occasionally interrupted by a few large amplitude oscillations. This behavior is characteristic of a system exhibiting Type I intermittency[52, 53], where we have bursts of noisy behavior interrupting an otherwise quiescent evolution of the system. Figure 2.4(a) shows the variation of T with dimensionless time for $P = 0.4105$. This is actually a 78P state characterized by a large number of small amplitudes peaks and a few big amplitude peaks. Figure 2.4(b) shows the variation of T with time for $P = 0.4110$. The stroboscopic maps of the attractors for these two values of P are shown in Figs. 2.4(c) and 2.4(d). It is seen that the behavior of the system in the former (latter) case is periodic (chaotic). Closer to the ignition point, the system spends longer time near the lower state and the large amplitude oscillatory bursts become less frequent. This and the increase in the size of the attractor across the ignition point (occurrence of the large amplitude peaks) can be explained by invoking the reinjection property for one-dimensional maps[52, 53]. Here a trajectory leaving the vicinity of the lower 1P state, like it does when it exhibits a large amplitude oscillation, gets reinjected back close to the lower 1P state soon thereafter. This principle has been discussed in the context of homoclinic tangency and homoclinic orbits by Gaspard and Wang[54]. They show how such a behavior can explain the occurrence of mixed-mode oscillations.

The intermittency appears to be the fore-runner of a sequence of more complex dynamic behavior which we see in the region $0.415 < P < 0.70$. In this region the dynamic behavior alternates regularly between periodic and chaotic as the parameter P is varied. The periodic states are typical of mixed-mode oscillations consisting of a mixture of large amplitude and small amplitude oscillations. In this region we have observed a period adding sequence, different period doubling cascades as well as saddle-node bifurcations. A review detailing these characteristics can be found in Swinney[49].

The characteristics of the stable state of the system in the region $0.415 < P < 0.70$ are summarized in Table 2.3. Each chaotic state is represented by the letter C. Similarly, each periodic state is represented by the letter P. Each sub-harmonic oscillation having a period m times the forcing period is represented with the number m preceding the letter P. Each P is followed by one or more subscripts and superscripts. The subscript (superscript) denotes the number of consecutive small (large) amplitude peaks in the periodic state. Thus a $11P_9^2$ periodic state is characterized by two consecutive



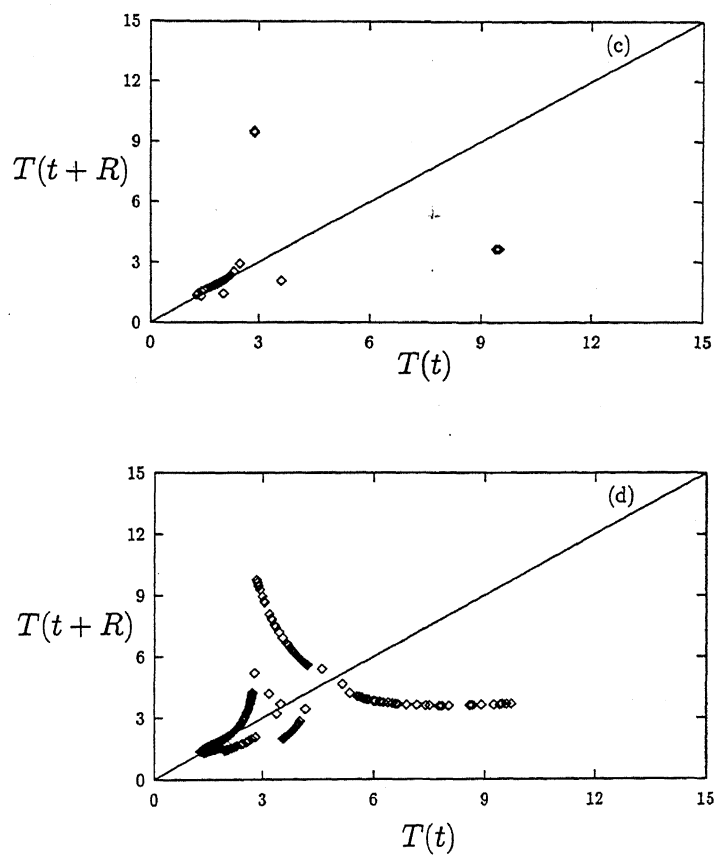


Figure 2.4: Variation of the temperature T with dimensionless time ((a) and (b)) and the stroboscopic map ((c) and (d)) near the ignition point showing intermittency behaviour, parameter set 1, $R = 0.573875$, (a), (c): $P = 0.4105$; (b), (d): $P = 0.411$.

mP	$27P_{25}^2$	$22P_{20}^2$	$21P_{19}^2$	$20P_{18}^2$	C	$19P_{17}^2$	$18P_{16}^2$	$17P_{15}^2$
P	0.417	0.418	0.4190	0.420	0.421	0.422	0.424	0.426
mP	$16P_{14}^2$	C	$15P_{13}^2$	$14P_{12}^2$	$29P_{12,12}^{2,3}$	$13P_{11}^2$	$25P_{11,11}^{2,1}$	$12P_{10}^2$
P	0.428	0.43	0.4320	0.434	0.439	0.440	0.446	0.448
mP	$12P_{10}^2$	C	$11P_9^2$	C	$10P_8^2$	$20P_{8,8}^{2,2}$	$9P_7^2$	$18P_{7,7}^{2,2}$
P	0.452	0.456	0.460	0.468	0.470	0.484	0.490	0.510
mP	C	$17P_{7,7}^{2,1}$	C	$8P_6^2$	$16P_{6,6}^{2,2}$	C	$15P_{6,6}^{2,1}$	$22P_{6,6,6}^{1,2,1}$
P	0.512	0.513	0.515	0.520	0.552	0.555	0.560	0.565
mP	$7P_5^2$	$14P_{5,5}^{2,2}$	$28P_{5,5,5,5}^{2,2,2,2}$	C	$13P_{5,5}^{2,1}$	$19P_{5,5,5}^{2,1,1}$	C	$6P_4^2$
P	0.58	0.628	0.630	0.635	0.640	0.660	0.670	0.700

Table 2.3: Period-adding and alternating periodic-chaotic regions, set 1, $R = 0.573875$.

large amplitude peaks and nine consecutive small amplitude peaks. Fig. 2.5 shows the dependence of the largest Lyapunov exponent λ on P . Chaotic dynamics are characterized by a sensitive dependence on initial conditions. This implies that one of the Lyapunov exponents is greater than zero. Since the system is dissipative, the other Lyapunov exponent is negative. The Lyapunov exponents were calculated using the method of Wolf *et al.*[56].

The main characteristic of Table 2.3 is the occurrence of chaotic behavior in between regions where the behavior is periodic. This occurrence of alternating periodic-chaotic behavior has been observed in several other systems[9, 57–59]. We have observed that the chaotic behavior in this region is generated through the period-doubling route.

The system exhibits a sequence of mP oscillations for successive integer values of m (22 to 6 are shown in Table 2.3). The periods of two successive states belonging to this basic sequence differ by 1P. Each periodic state exhibits 2 large amplitude peaks. Transition from one periodic state to another is initiated through a series of period

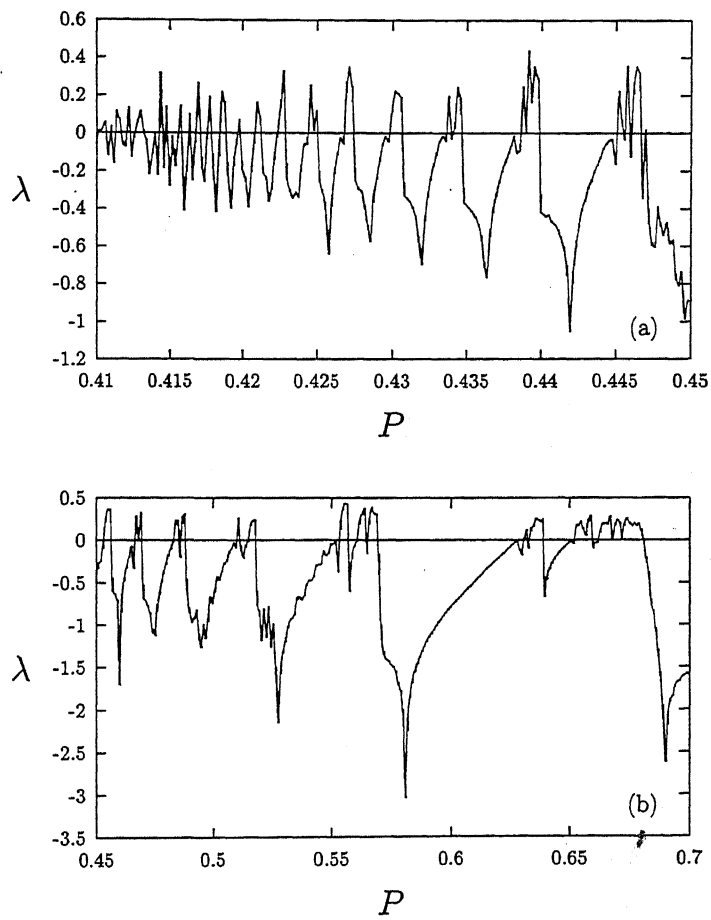


Figure 2.5: Dependence of the largest Lyapunov exponent λ on P for the FBR, set 1, $R = 0.573875$.

doubling bifurcations to chaos, followed by a recovery to the next periodic state in the period-adding sequence[58, 60]. Frequency locking type interaction of two neighbouring periodic states yields a new periodic state not belonging to this period-adding sequence. Here, between an nP and an $(n-1)P$ state, there is a $(2n-1)P$ state. The $(n-1)P$ and $(2n-1)P$ states again interact to give a $(3n-2)P$ state. Repetitive interactions of this nature give rise to stable periodic states of different periods. The region of stability of these periodic states with large periods is very small[9, 58]. We explain this next in the context of Table 2.3.

For $P = 0.56$, we see a $15P_{6,6}^{2,1}$ state. This is a 15P state with 6 small amplitude peaks, followed by 2 large amplitude peaks. This is followed by another sequence of 6 small amplitude peaks and a large amplitude peak. This particular state arises in the region between the $7P_5^2$ and $8P_6^2$ states which occur on either side of this value of P . We have observed that this 7P state becomes unstable through a limit point bifurcation. This unstable 7P state is of the form $7P_6^1$. The stable 8P state is of the form $8P_6^2$. It appears that the unstable 7P state interacts with the stable 8P state and yields the stable 15P state. Similarly, we observed the existence of a 22P state between the 15P and the 7P states. This corresponds to a $(3n-2)$ periodic state (discussed in the preceding paragraph) with $n = 8$. Similarly, 13P and 19P states exist between the 7P and the 6P states. We have also found a 25P state between the 13P and the 12P states of the period-adding sequence.

The existence of these periodic states can be explained with the help of the frequency locking type of interaction discussed earlier. It appears that for this interaction to occur, one of the members of the period-adding sequence must undergo a saddle-node bifurcation. We have confirmed this for the 7P state near $P = 0.56$, in the vicinity of which a stable 15P state exists. Similarly, it appears that the 6P and the 12P states undergo a saddle-node bifurcation to give stable 13P and 25P states respectively. This appears to be consistent with the total number of large and small amplitude peaks occurring in the 12P, 13P, 25P and the 6P, 7P, 13P states respectively in Table 2.3.

Kubickova *et al.*[21] have obtained bifurcation diagrams for a number of mP states as a function of $P = R$. They have observed saddle-node bifurcations for these periodic states. This provides further evidence that such bifurcations can occur for the different periodic states in the period-adding sequence, thereby causing an interaction between

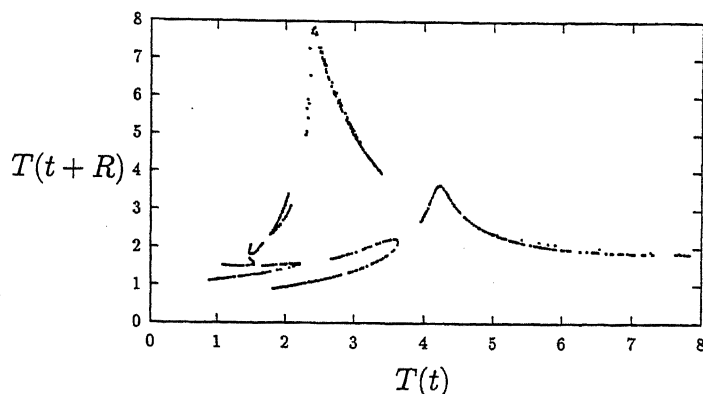


Figure 2.6: Stroboscopic map of the chaotic attractor, parameter set 1, $P = 0.635$, $R = 0.573875$.

two neighbouring periodic states.

Near $P = 0.628$, the 7P state undergoes a period doubling bifurcation. This gives rise to a stable 14P state. As P is increased, this 14P state again undergoes a period doubling bifurcation giving a stable 28P state. The period doubling of different mP states of periods $m = 8, 9$ and 10 have also been observed. It is very likely that there are other cascades of period doubling bifurcations of each of the members of the period adding sequence. This is another mechanism to generate the chaotic behavior (see Table 2.3). The stroboscopic map of a chaotic attractor for $P = 0.635$ is shown in Fig. 2.6. This arises from the period doubling of the sub-harmonic 7P state. This figure can be viewed as being composed of 7 islets.

With a view to determining the effect of the parameter R on the dynamic behavior of the FBR, we carried out extensive simulations for set 1 for $R = 0.2, 0.3$ and 0.75 . The bifurcation diagram depicting the dependence of the 1P state for $R = 0.20$ is also S-shaped (Fig. 2.7). The lower branch of the 1P state has an ignition point at $P = 0.12051$. On the upper branch, the 1P state is unstable between $0.1337 < P < 0.20475$. To the left of this interval, a complex-conjugate pair of eigenvalues leaves the unit circle. At the right end point of this interval, a complex-conjugate pair of eigenvalues re-enters the unit circle. These points correspond to torus bifurcation points. In this region we have observed the existence of quasi-periodic oscillations for $0.1337 < P < 0.1365$.

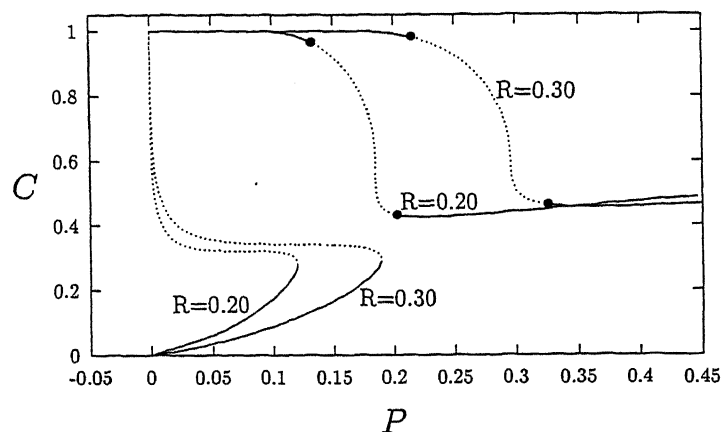


Figure 2.7: Bifurcation diagram of the 1P state for the FBR, parameter set 1, $R = 0.20$ and $R = 0.30$, (—): stable 1P state; (···): unstable 1P state; (•): Torus bifurcation point.

The FBR exhibits periodic, quasi-periodic and chaotic dynamic behavior in the region $0.1385 < P < 0.20475$. Chaotic behavior in this region appears to arise from a periodic - quasi-periodic - chaotic transition[49]. Figure 2.8(a) shows the stroboscopic map for the quasi-periodic behavior of the FBR with $P = 0.13385$. As expected, the map yields a closed curve. In Figs. 2.8(b) and 2.8(c), we show the stroboscopic maps of the dynamics for $P = 0.13850$ and 0.20 respectively. For $P = 0.13850$, we see that the closed curve has undergone ‘folding’. This is a typical feature of the stroboscopic maps in the region $0.1365 < P < 0.1385$. As P is increased past this value, the closed curve breaks up indicating a transition to chaotic behavior. The mapped points now lie on segments of disjoint curves. The onset of chaos is thus signalled by the folding and subsequent breaking up of the closed curve. Figure 2.8(c) is representative of the typical nature of the stroboscopic map of the behavior obtained for values of P in the region $0.1386 < P < 0.20475$. Further simulations indicate that the stroboscopic map remains similar to Fig. 2.8(c) till the second bifurcation point at $P = 0.20475$, where the 1P state regains its stability.

The bifurcation diagram of the 1P state of the FBR for $R = 0.75$ is shown in Fig. 2.9. The qualitative nature of the bifurcation diagram is very similar to that for

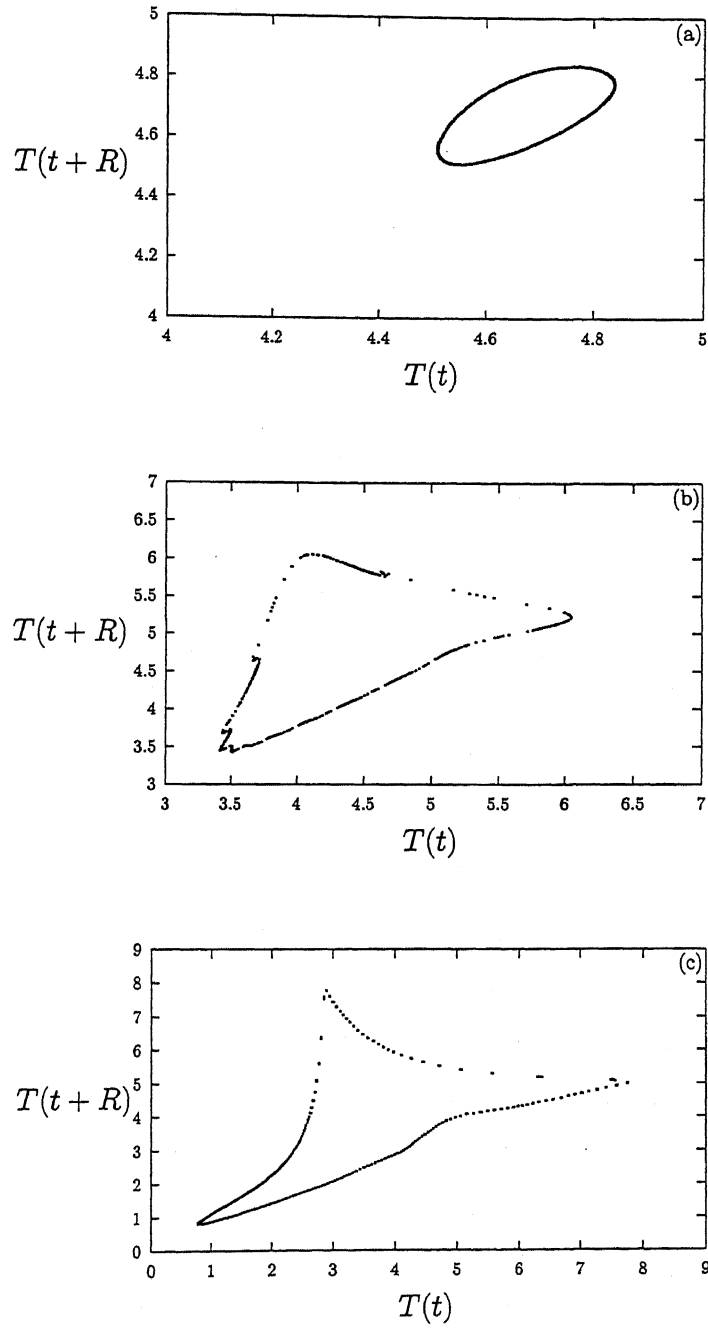


Figure 2.8: Dynamic behaviour for $R = 0.20$, parameter set 1, Stroboscopic maps for (a) $P = 0.13385$; (b) $P = 0.1385$; (c) $P = 0.20$.

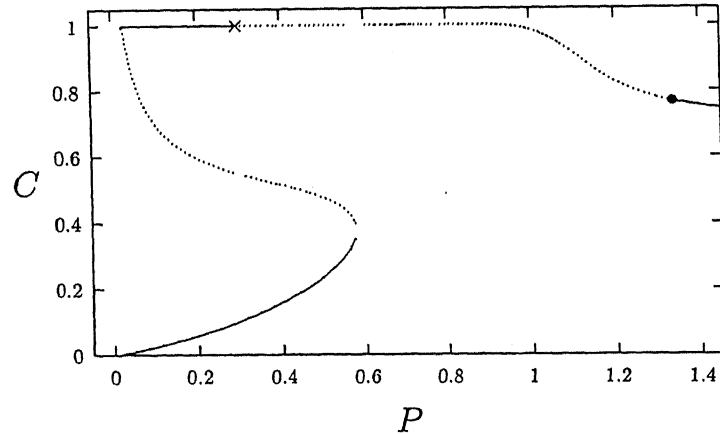


Figure 2.9: Bifurcation diagram of the 1P state for the FBR, parameter set 1, $R = 0.750$, (—): stable 1P state; (\cdots): unstable 1P state; (\times): Period doubling bifurcation; (\bullet): Torus bifurcation point.

$R = 0.573875$. We have a region of multiple 1P periodic states for $0.026 < P < 0.5776$. On the upper branch of the 1P state a period doubling cascade begins at $P = 0.299$. This proceeds according to the Feigenbaum scenario. Beyond the accumulation point of this cascade, the dynamics are chaotic and the stroboscopic maps are again 'islet' shaped. These islets grow in size and finally merge as P is increased, in much the same way as we saw for $R = 0.573875$ (Fig. 2.3(a)-2.3(c)). Simulations with P beyond 0.330 always end up on the lower stable 1P state. This was tested for a wide variety of initial conditions. It appears that the chaotic attractor has disappeared as a result of a boundary crisis. As in the case of $R = 0.573875$, this is due to the occurrence of a crisis. This persists till we cross the ignition point ($P = 0.5776$). Just beyond the ignition point, the behavior appears to be typical of intermittency, i.e., mainly small amplitude periodic behavior is interrupted by bursts of large amplitude oscillations. It appears that the dynamics of the FBR are essentially periodic in this region. This dynamic behavior consists of very large period oscillations. For example, simulations have revealed that at $P = 0.5777$, a 160P state exists. In the region $0.5777 < P < 1.340$, we have observed a period-adding sequence and regions of alternating periodic-chaotic behavior. The dynamic behavior is similar to that with $R = 0.573875$. A

complex-conjugate pair of eigenvalues re-enters the unit circle at $P = 1.34$ and the 1P state regains its stability.

The bifurcation diagram of the 1P state of the FBR for $R = 0.30$ is shown in Fig. 2.7. For this value of R , the dynamic behavior of the FBR in the region on the upper branch where the 1P state is unstable ($0.2164 < P < 0.3295$) is similar to that for $R = 0.20$ and $R = 0.573875$. As P is increased beyond 0.2164, a complex conjugate pair of eigenvalues leaves the unit circle. The dynamics of the FBR are quasi-periodic for this value of P . With further increase in P , the quasi-periodic dynamics disappear and the FBR exhibits chaotic dynamics. With further increase in P beyond 0.220, we see a period-adding sequence and regions of alternating periodic-chaotic behavior. Cascades of period doubling bifurcations also occur in the period-adding sequence.

For $R = 0.2$ and 0.30 , the region where the upper 1P state branch is unstable occurs to the right of the ignition point. Hence in these cases, we do not expect nor observe any crisis (Table 2.4).

Simulations for values of R beyond 0.90 have shown a decrease in the region where multiple 1P states exist. There is also a decrease in the size of the region on the upper branch where the 1P state is unstable. This conforms to the fact that the dynamics of the FBR approach that of the batch reactor for high R . For set 1, the high value of B perhaps necessitates going to such high values of R , in order for the transition to the batch reactor to be realized.

For the parameters in set 2 of Table 2.1, the CSTR has a region of multiple steady-states and a region where the upper steady-state branch is unstable and has limit cycles[6]. The bifurcation diagram for this set of parameters is shown in Fig. 2.1. The dependence of the 1P states of the FBR on P has been obtained for three values of R , viz., 0.25, 0.50, 0.75. This is shown in Fig. 2.10.

For $R = 0.250$, we have a region of multiple 1P behavior in the interval $0.0249 < P < 0.2715$. In the upper branch the stable 1P behavior becomes unstable via a torus bifurcation at $P = 0.227$. At $P = 0.3103$, a complex conjugate pair of eigenvalues re-enters the unit circle and the 1P state becomes stable again beyond this value of P . In the region $0.2715 < P < 0.3103$, immediately to the right of the ignition point, simulations reveal the existence of quasi-periodic behavior for several values of P . A typical stroboscopic map of such behavior for $P = 0.28$ is shown in Fig. 2.11. The

Set	R	Behavior observed
1	0.20	Multiplicity, periodic, quasi-periodic and chaotic behavior
	0.30	Multiplicity, quasi-periodic, chaotic behavior, period-adding giving rise to alternating periodic-chaotic behavior
	0.573875	Multiplicity, period doubling cascade to chaos, crisis, intermittency, mixed-mode oscillations, period-adding giving rise to alternating periodic-chaotic behavior
	0.75	Multiplicity, period doubling cascade to chaos, crisis, intermittency, mixed-mode oscillations, period-adding giving rise to alternating periodic-chaotic behavior,
2	0.25	Multiplicity and quasi-periodic behavior
	0.50	Multiplicity and quasi-periodic behavior
	0.75	Unique stable 1P state
3	0.25	Multiplicity and isola
	0.50	Multiplicity and isola
	0.75	Unique stable 1P state

Table 2.4: FBR bifurcation behavior.

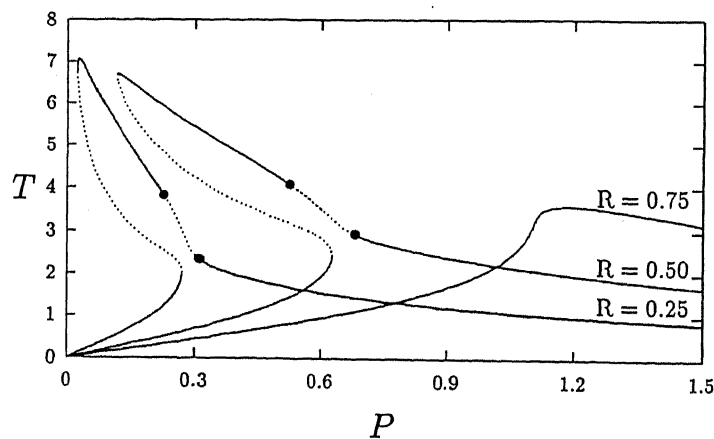


Figure 2.10: Bifurcation diagram of the FBR for parameter set 2, (—): stable 1P state; (---): unstable 1P state; (•): Torus bifurcation point.

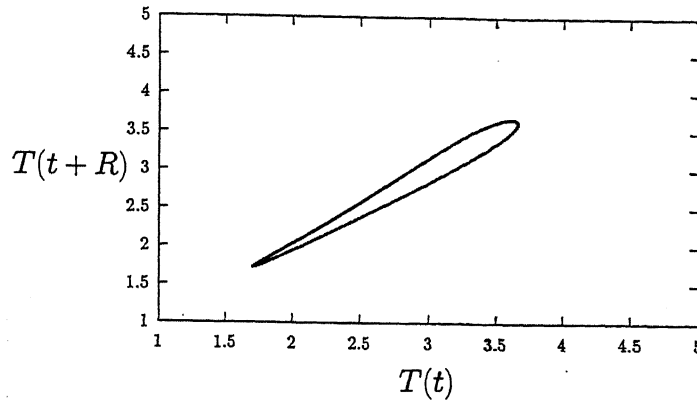


Figure 2.11: Stroboscopic map for the FBR showing quasi-periodic behavior, parameter set 2, $P = 0.28$, $R = 0.25$.

points trace out a continuous closed curve. In the region $0.227 < P < 0.2715$, immediately after the 1P state becomes unstable on the upper branch, simulations with different initial conditions always end up on the lower stable 1P state. This may be because the quasi-periodic attractor has been destroyed in a collision with the 1P periodic state at the saddle-node bifurcation point.

We notice a similar qualitative behavior for $R = 0.50$. For $R = 0.750$, the region of multiple 1P states and the region where the 1P state is unstable disappears (Fig. 2.10). The dynamics of the FBR, therefore approach the dynamics of the batch reactor for this and higher values of R . Unlike in set 1, we have not observed any period doubling bifurcations on the upper 1P state branch of the bifurcation diagram for all the values of R studied.

For the parameter values in set 3 of Table 2.1, the CSTR bifurcation diagram shows a region of multiple steady-states and an isola[6]. The bifurcation diagram for this set of parameters is shown in Fig. 2.12. For the FBR, we get a similar dependence of the basic 1P state on P for $R = 0.10$ and 0.20 . The dependence of the 1P behavior of the FBR for $R = 0.1$, $R = 0.20$ and $R = 0.50$ is shown in Fig. 2.13. For the first two values of R , we see a region of multiple 1P states and an isola. As we increase R from 0.10 to 0.20, the regions of existence of multiple 1P states and of the isola decreases. When R is increased further to 0.50, the isola and the multiple 1P states

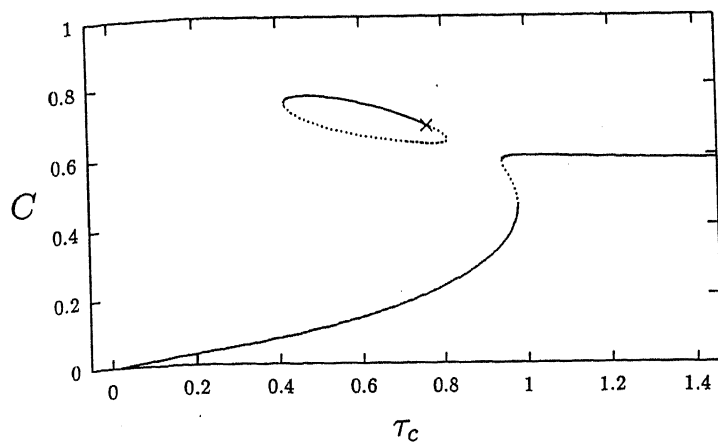


Figure 2.12: Bifurcation diagram of the CSTR for parameter set 3, (—): stable steady-state; (···): unstable steady-state; (×): Hopf bifurcation point.

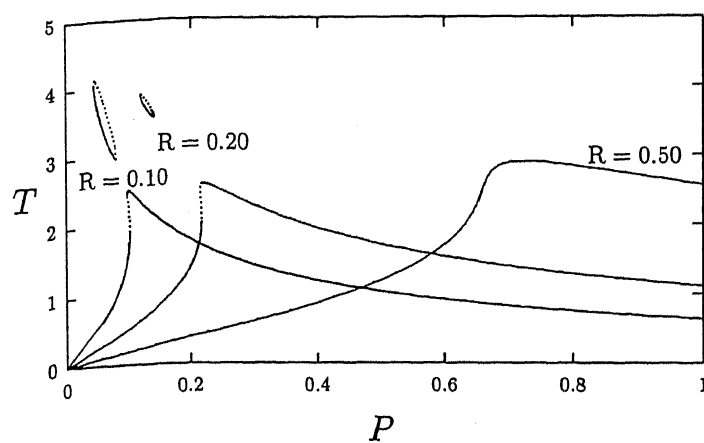


Figure 2.13: Bifurcation diagram of the FBR for parameter set 3. (—): stable 1P state; (···): unstable 1P state.

disappear. A unique stable 1P state exists for all values of P . Thus, again we approach the dynamics of the batch reactor at high values of R . Table 2.4 contains a summary of the bifurcation features we have observed for the FBR.

2.5 Conclusions

In this work we have presented bifurcation features of the FBR for selected values of the parameters B , β_0 and k_0 . Our objective was to study how the local bifurcations in the CSTR manifest themselves in the FBR. From the numerical evidence presented in the previous section, we may conclude that the steady-state bifurcation (saddle-node bifurcation) in the CSTR manifests itself as a saddle-node bifurcation in the FBR. The Hopf bifurcation in the CSTR can manifest itself as either a period doubling bifurcation or a torus bifurcation. It appears that complex, i.e., sub-harmonic, quasi-periodic and chaotic, oscillations occur in the FBR only in cases where the equivalent CSTR has a Hopf bifurcation. It also appears that the nature of the steady-states of the CSTR also influences the dynamics of the FBR. The node and saddle type steady-states manifest themselves in a similar way in the FBR. However the complex dynamics of the FBR appear to arise only when the equivalent CSTR has a focus type of steady-state.

A positive feature of this system is that it exhibits complex dynamic behavior over a sufficiently wide range of parameter values. In contrast, Jorgensen and Aris[9] report complex bifurcation sequences occurring over very narrow ranges of the bifurcation parameter.

The quasi-periodic, chaotic dynamics and regions of period-adding sequence reported above were obtained by simulating with a wide variety of initial conditions. However, the existence of other attractors in these regions cannot be ruled out[21]. The basin of attraction of these other attractors may be very small. A thorough investigation of the effect of initial conditions will be necessary to verify the existence of other attractors.

For this reactor system, we have shown the existence of a wide spectrum of complex dynamic behavior, i.e., the period doubling route to chaos, period-adding sequences resulting in alternating periodic-chaotic behavior and period doubling bifurcations of various members of the period-adding sequence, quasi-periodic oscillations, crisis and

intermittency behavior (Table 2.4). Such dynamic behavior is a universal characteristic of nonlinear systems of varying degrees of complexity, from the one-dimensional logistic map to systems of coupled ordinary differential equations. Nonlinear electrical circuits and chemical reactions have been known to exhibit some of these features. This behavior has been analysed in the literature, mainly in the context of discrete dynamical systems. The understanding of these features in the context of continuous time systems remains incomplete.

We have compared a CSTR operating at a particular residence time τ with the FBR with the same ratio of P/R . There is an infinity of P and R values of the FBR which yield a given τ . Hence the operation of a CSTR can be compared with an infinity of FBR's. As explained earlier, the FBR approaches the CSTR in the limit $P \rightarrow 0$, $R \rightarrow 0$ and for finite τ .

The periodically forced CSTR has been studied extensively in the literature. The unforced CSTR itself may have limit cycles and the interaction of the natural and forcing frequencies gives rise to complex dynamics. We have studied the forced operation of a batch reactor. The type of forcing used in the present study is discrete. This causes a discontinuous variation in the concentration and temperature. We have observed that, even though there is a basic difference in the way the system is being forced, the dynamic behavior is equally rich. It must be noted that that the system we are forcing, the batch reactor does not show any oscillations, whereas the CSTR our system tends to, can exhibit autonomous limit cycles.

We can also consider the FBR to be the most general form of the well-stirred reactor model. This is because both the batch reactor and the CSTR are the two limiting cases of FBR operation. From this point of view, it is perhaps natural that the FBR shows such complex behavior.

Chapter 3

Steady-state Behavior of a Reactor-Separator System

Nomenclature

B	Dimensionless heat of reaction.
Da_0	Damkohler number, reaction rate constant.
F_0	Molar flow rate of fresh feed to reactor.
F	Molar flow rate of feed to flash unit.
k	Equilibrium constant.
L	Molar flow rate of the liquid stream from flash unit.
M_R	Molar holdup of the reactor.
P	Pressure in the separator.
P^{sat}	Saturated vapor pressure.
R	Molar flow rate of the recycle stream.
T	Dimensionless temperature.
T_F	Dimensionless temperature of the separator.
V	Molar flow rate of the vapor stream from the separator.
x_e	Composition of the liquid (recycle) stream, mole fraction.
x_R	Composition of the material in the mixer, mole fraction.
y_e	Composition of the vapor (product) stream, mole fraction.
z	Composition of the material in the reactor, mole fraction.

Greek letters

α	Recycle rate per unit molar flow rate of fresh feed.
β_0	Heat removal parameter.
δx_e	Constant in section 3.3.
ρ	Molar density of mixture.
τ	M_R/F_0 .
τ_f	M_R/F .
τ_l	M_R/L .

Subscripts

i	Component i .
0	Conditions at reactor inlet.
1	Reactant.
2	Product.

3.1 Introduction

In the previous chapter we investigated the dynamic behavior of a discretely forced reactor system. Another class of systems which have only attracted attention in recent years are the reactor-separator systems coupled by recycle. In a continuing series of papers, Luyben and co-workers have investigated the steady-state features of several simple reactor-separator systems. However, as we pointed out in the first chapter, they have not made any attempts to carry out a systematic study and generalize the qualitative features of such systems. Recently Morud and Skogestad[25, 26] have presented reviews of the effect of recycle on the dynamics and control of plants. With the help of several examples, they catalog the different features of linear recycle systems. They also highlight the need for a systematic classification and analysis of effects which may introduce complex behavior in a plant. This is essential in order to enhance our understanding of the different phenomena and also to provide some indicators of when the phenomena occur.

In a series of papers, Luyben and co-workers[28–30] have studied the dynamics and control of binary and ternary recycle systems. They consider a process consisting

of an isothermal CSTR coupled through recycle to a distillation column. The effect of design on the steady-state economics and the controllability of the process were discussed. Starting with a given set of design parameters, their approach consists of developing a design procedure for the operation of the distillation column. The effect of changing the design parameters on the system variables was then studied. Based on their results, they have conjectured about the advantages of working with certain sets of design parameters. However, the complexity of the system in terms of the large number of variables, makes it impossible to obtain a generalization of their results. In a later paper[31], they analysed the effect of different control configurations on the snowball effect. The snowball effect manifests itself as a very large change in the recycle flow rate for a small change in the independent variable. However, they did not provide any explanation about the origin of this phenomenon and ways for preventing its occurrence. Recently, they have extended their investigations to cover different cases of ternary systems[32–34]. In these studies they consider several model reaction schemes, multiple separator units and multiple recycle streams.

In this chapter we study the steady-state characteristics of a coupled reactor-separator system. The reactor is assumed to be a non-adiabatic CSTR. It sustains the exothermic, irreversible first order reaction $A \rightarrow B$. The mixture leaving the reactor is sent to a separator which is modelled as a single stage flash unit. The reactor effluent stream is separated into a reactant rich liquid fraction and a product rich vapor fraction. The coupling between the two units is achieved through the recycle of the reactant rich liquid stream from the separator to the reactor (Fig. 3.1).

We study the behavior of this model nonlinear reactor-separator system. We determine the qualitative features of the steady-state behavior of the system for different possible combinations of the specified variables. This enables us to identify different combinations of the specified control variables which permit operation of the coupled system with separation, at a steady-state. A comprehensive analysis is carried out for the following sets of operation of the separator

1. Constant temperature and pressure, (T_F, P) flash,
2. Constant temperature and constant liquid recycle rate, (T_F, L) flash.

In the first case, operation of the flash is isothermal and isobaric. The vapor-liquid

equilibrium (VLE) considerations for the binary system then uniquely determine the compositions of the liquid and vapor streams. For this choice of the specified variables, separation into a product rich vapor fraction and a reactant rich liquid fraction, is possible only when the reactor effluent composition lies in between the equilibrium compositions of the liquid and vapor streams. As we shall show later, there exist choices of the specified variables for which this constraint is not satisfied. This results in the existence of regions in parameter space for which steady-state operation with separation is not possible.

In the second case, the flow rate of the liquid stream from the flash is fixed. Here, the pressure in the separator is not externally imposed. Consequently, the compositions of the overhead and bottom streams leaving the flash are not fixed. Since the recycle stream flow rate L is fixed, the system is forced to regulate itself such that the recycle rate is always at its specified value. This ensures that steady-state operation with separation is possible for all parameter values.

For each of the above cases, we study the different possible steady-state multiplicity behavior of the coupled system using singularity theory. Application of singularity theory enables us to classify a suitable parameter space into regions having different multiplicity features. The results are presented in the form of bifurcation diagrams. We also make a qualitative analysis of the dynamic behavior which can be expected once a choice of the set of variables to be specified has been made.

The model is described in the next section. In section 3.3 we study the steady-state multiplicity behavior for different sets of specifications of this coupled system, as a single control parameter is varied.

3.2 Description of the Model

The system under consideration is shown in Fig. 3.1. Fresh feed containing pure A is fed at a rate F_0 to the reactor. The effluent stream from the reactor passes through a heat exchanger which changes the temperature of that stream to the specified flash temperature T_F . This stream is then flashed into two fractions. The liquid stream is rich in the reactant, while the vapor stream is rich in the product. The vapor stream is drawn off and the liquid stream is recycled to the reactor through a mixer

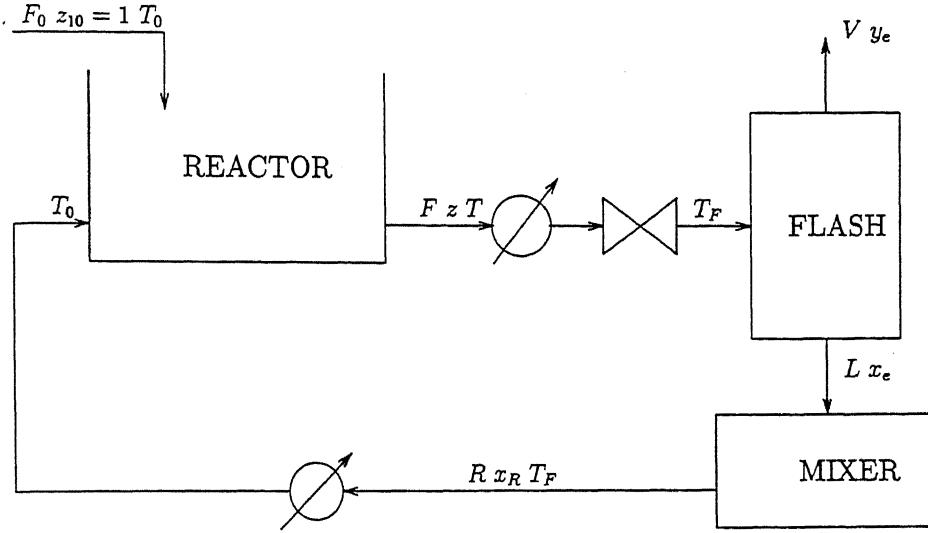


Figure 3.1: Schematic diagram of the reactor-separator system with recycle.

(where it mixes with the liquid already present) and a heat exchanger, which brings the temperature of the recycle stream to that of the fresh feed. The presence of the heat exchangers ensures that there is no thermal coupling between the two units. For simplicity, we neglect the dynamics of the heat exchangers. The coupling between the two units is therefore, only through the composition and the flow rate of the recycle stream.

Throughout this study, we assume the molar holdups of the reactor and the mixer to be constant. The material balance and the equilibrium relations modelling the separator usually involve the species composition expressed in terms of mole fractions z_i . The mass balance in the reactor is normally expressed in terms of the concentration of the different species c_i . To represent both the units on a common basis, we use mole fractions to model the system. This exploits the relationship

$$c_i = \rho z_i \quad (3.1)$$

We assume that the molar density in the liquid phase ρ is constant (i.e., independent of composition). The overall material balance and the dimensionless material (mole) and energy balance equations governing the evolution of the composition of the reactant z_1 and dimensionless temperature T in the reactor are given by the following equations

respectively

$$F = F_0 + R \quad (3.2)$$

$$\frac{dz_1}{dt} = 1 - z_1 - \frac{R}{F_0}(z_1 - x_R) - Da_0\tau e^T z_1 \quad (3.3)$$

$$\frac{dT}{dt} = -T\left(1 + \frac{R}{F_0} + \beta_0\tau\right) + BDa_0\tau e^T z_1 \quad (3.4)$$

Here B , β_0 and Da_0 represent the dimensionless heat of reaction, the dimensionless heat transfer coefficient and the Damkohler number (representing the reaction rate constant) respectively. We have used $\tau = M_R/F_0$ as the characteristic time to define the dimensionless time. We have made the exponential approximation in the derivation of the above equations. The overall and reactant mole balances for the equilibrium separation process are given by

$$F = V + L \quad (3.5)$$

$$Fz_1 = Vy_{e1} + Lx_{e1} \quad (3.6)$$

Subscript 1 (2) refers to the reactant (product). F , V and L represent molar flow rates of feed, vapor and liquid streams to and from the flash. The reactant rich liquid stream passes through a constant holdup mixer before being recycled to the reactor. Therefore, the recycle rate to the reactor is equal to the rate of the liquid stream entering the mixer (i.e., $R = L$). However, this rate is not constant but depends on x_{e1} , y_{e1} and z_1 . The evolution of the reactant composition in the mixer is governed by the following dimensionless equation

$$\frac{dx_{R1}}{dt} = \frac{R}{F_0}(x_{e1} - x_{R1}) \quad (3.7)$$

The separation process is governed by the vapor-liquid equilibrium relations relating the compositions (x_{ei} , y_{ei} , $i = 1, 2$) in both the phases. We assume the vapor and liquid phases to be ideal, so that Raoult's law is valid. The sum of the mole fractions in the liquid and the vapor phase must equal unity. Therefore, we have the following additional sets of equations

$$y_{e1} = k_1 x_{e1} \quad (3.8)$$

$$y_{e2} = k_2 x_{e2} \quad (3.9)$$

$$y_{e1} + y_{e2} = 1 \quad (3.10)$$

$$x_{e1} + x_{e2} = 1 \quad (3.11)$$

k_1 and k_2 are the equilibrium constants defined as $k_i = P_i^{sat}/P$, where P_i^{sat} is the saturation vapor pressure of component i . The saturation vapor pressures are assumed to be given by the Antoine relations. Then using (3.2), (3.5) and (3.6), the recycle rate per unit fresh feed entering the reactor, α , can be defined as

$$\alpha = \frac{L}{F_0} = \frac{R}{F_0} = \frac{y_{e1} - z_1}{z_1 - x_{e1}} \quad (3.12)$$

The set of equations (3.2)-(3.11) are a set of 10 equations in the 14 unknowns: $F_0, F, L, P, T, T_F, V, M_R, x_{e1}, x_{e2}, x_R, y_{e1}, y_{e2}$ and z_1 . Hence four additional variables need to be specified so that the above equations can be solved for the remaining variables.

In the following analysis, all the compositions are expressed as mole fraction of the reactant A , and hence the subscript 1 is suppressed.

3.3 Steady-State Analysis

In the first part of this section we consider the isothermal and isobaric (T_F, P) operation of the separator. This choice fixes two variables. We consider the following sets of specifications for specifying the remaining two variables.

1. (M_R, F_0) fixed: The reactor holdup M_R and the fresh feed flow rate F_0 are specified,
2. (M_R, F) fixed: The reactor holdup M_R and the reactor effluent stream flow rate F are specified,
3. (M_R, L) fixed: The reactor holdup M_R and the recycle stream flow rate L are specified.
4. (F_0, F) fixed: The fresh feed flow rate F_0 and the reactor effluent stream flow rate F are specified.

The overhead (vapor) and bottom (liquid) stream compositions for the case of isothermal and isobaric separation can be determined using (3.8)-(3.11). The model equations

(3.2)-(3.11) can then be reduced to a system of three coupled ordinary differential equations in z , T and x_R . The resulting model is solved for the steady state by setting the time derivatives to zero.

In subsection 3.3.5 we consider the flash temperature T_F and the liquid stream flow rate from the separator L to be fixed. We also consider the molar holdup of the reactor M_R and the fresh feed flow rate F_0 to the reactor to be fixed. With this set of specifications, the pressure of the separator remains an unknown quantity. The equilibrium constants k_1 and k_2 are not known and the equilibrium compositions x_{ei} and y_{ei} have to be calculated by solving the set of equations (3.2)-(3.11) simultaneously.

3.3.1 Isothermal and Isobaric Separation with (M_R, F_0) Fixed

We begin by considering the case when the holdup in the reactor M_R and the fresh feed flow rate F_0 are the specified variables. The recycle stream flow rate and the reactor effluent stream flow rates are now unknown and are dependent on the composition in the reactor. At steady-state, the resulting system of coupled nonlinear algebraic equations (3.2)-(3.11) can be reduced to the following single equation in the unknown T

$$\begin{aligned} H(T, p, \tau) = & Da_0\tau(x_e - y_e)Te^T + x_eDa_0\tau\beta_0\tau Te^T - x_eBDa_0\tau(1 - y_e)e^T \\ & - \beta_0\tau(1 - y_e)T + B(1 - y_e)^2 = 0 \end{aligned} \quad (3.13)$$

In the unknown z , the corresponding equation is

$$G(z, p, \tau) = \ln \left[\frac{1 - y_e}{Da_0\tau z} \right] [x_e - y_e + \beta_0\tau(x_e - z)] - B(1 - y_e)(x_e - z) = 0 \quad (3.14)$$

Here p represents the parameter set $(B, \beta_0, Da_0, x_e, y_e)$. The parameter τ is defined as the ratio of the molar holdup in the reactor M_R and the molar flow rate of fresh feed F_0 to the reactor. τ is considered to be the bifurcation parameter and is hence given a special identity in (3.13) and (3.14). The residence time in the reactor is dependent on F_0 and the recycle rate R , which in turn is dependent on the reactor effluent stream composition. It must be emphasised that τ does not represent the residence time in the reactor, since it depends only on F_0 and not on the reactor effluent stream flow rate.

The nonlinear equations (3.13) and (3.14) in the unknowns T and z respectively can have multiple solutions for a fixed set of parameters. We investigate the multiplicity features of (3.13) and (3.14) using singularity theory[35]. Singularity theory enables us to obtain a complete picture of the different possible steady-state multiplicity features of a system. A brief summary of singularity theory is presented in the appendix. We now present the singularity theory analysis of (3.13) and (3.14) in detail.

The set of equations (the subscripts T , z and τ indicate differentiation w.r.t. the respective variables)

$$H = H_T = H_{TT} = 0 \quad (3.15)$$

has the solution

$$T = \sqrt{4 - \frac{4x_e B(1 - y_e)}{(x_e - y_e)}}, \quad \tau = \frac{B(1 - y_e)}{\beta_0(T - 2)} \quad (3.16)$$

This solution is infeasible, since $T < 2$ and hence $\tau < 0$. The corresponding solution for z satisfying the set of equations

$$G = G_z = G_{zz} = 0 \quad (3.17)$$

is given by: $z = (1 - y_e)/Da_0\tau e^T$, with T and τ given by (3.16). This implies that (3.13) or (3.14) can only have a maximum of two solutions for any given set of the operating parameters. Equations (3.13) and (3.14) *behave* like quadratic equations, and therefore, there exists the possibility that for certain operating conditions, the system will not have any steady states. This is discussed in detail later. Such behavior is in contrast to the CSTR where we can have a maximum of three solutions for any given set of parameters[6, 23].

Further, the set of equations

$$G = G_z = G_\tau = \det[d^2G] = 0 \quad (3.18)$$

where $\det[d^2G]$ is the determinant of the matrix $\begin{bmatrix} G_{zz} & G_{z\tau} \\ G_{\tau z} & G_{\tau\tau} \end{bmatrix}$

has the solution given by

$$x_e = y_e = z = \frac{\beta_0}{BDa_0 e^1}, \quad T = 1, \quad \tau = \frac{B(1 - y_e)}{\beta_0} \quad (3.19)$$

After specifying B , β_0 and Da_0 , we solved (3.18) for the unknowns z , τ , x_e and y_e . The solution to (3.18) could not be obtained analytically. The numerically computed values of x_e and y_e satisfying this set of equations appeared to be equal to each other for several values of B , β_0 and Da_0 . It was possible to solve and obtain the singular point (3.19) after substituting $x_e = y_e$ in (3.18). This singular point is a point in parameter space p where the function (3.14) is degenerate, i.e., it satisfies the equality conditions (3.18). The system has a highest order singularity when x_e and y_e take the above values for fixed values of the parameters (B, β_0, Da_0) .

Irrespective of conditions in the reactor, the compositions of the vapor and liquid streams exiting the flash are fixed, since we have assumed isothermal and isobaric separation. A steady-state is defined to be feasible if it permits steady-state operation of the coupled system with separation. Hence a steady-state of the coupled system is feasible only if $y_e < z < x_e$. Therefore, the singular point (3.19) lies in the infeasible region of operation, i.e., it cannot be achieved in practice.

When $x_e = y_e = z$, the separator acts as a stream splitter. The solution of (3.14) given by (3.19) does not model the physical process under consideration (reaction and separation). Under these conditions, Equations (3.5), (3.6) and (3.8)-(3.11) are no longer valid, as no separation is effected. The reactor system can still be modelled using (3.3) and (3.4). However, we need to fix (arbitrarily) R/F_0 . The model equations (3.3) and (3.4) would now represent the dimensionless material and energy balance equations for the CSTR without recycle ($R/F_0 = 0$) and with recycle (for a positive non-zero R/F_0). The implications of the presence of infeasible regions on the steady-state behavior of the coupled system are discussed next.

As the steady-state value of z approaches y_e , more and more of the feed to the separator goes into the vapor phase and the recycle rate approaches zero. Consequently, in the limit of $z = y_e$, the coupled system reduces to a system connected in series. In this case, the flash unit does not affect the behavior of the CSTR. Further, as the steady-state value of z approaches x_e , i.e., for low conversions in the reactor, a larger proportion of the feed entering the flash goes into the liquid phase and the recycle rate (Equation (3.12)) tends to infinity. This results in a paradoxical situation in the limit of $z = x_e$, where we have total recycle of the reactor effluent stream. This contradicts the assumption of steady-state operation under constant molar holdup of the reactor

and the mixer, with fresh feed also entering the reactor at a constant rate. To overcome this situation, we impose the following bounds on the conversion in the reactor, for a feasible steady-state operation of the coupled system

$$y_e < z < x_e - \delta x_e$$

Here δx_e is a small positive constant incorporated to exclude the possibility of total recycle in the process and its governing system of equations. This bound is imposed on the conversion to enable a feasible steady-state operation of the coupled system. The inclusion of a non-zero δx_e is equivalent to specifying an upper bound on the recycle stream flow rate. An additional feature of singularity theory is that it can systematically account for the changes in the multiplicity features resulting from the presence of such feasibility boundaries on the state variables.

From (3.12), it can be seen that in the limit $z \rightarrow x_e$, a small change in the fresh feed stream flow rate is associated with a large change in the recycle stream flow rate. This is the snowball effect observed by Luyben[30]. In general, the snowballing increases in magnitude only when perturbations acting on the system cause z to approach x_e .

To determine the normal form of the singularity, we evaluate the eigenvector v corresponding to the zero eigenvalue of the Hessian matrix $[d^2G]$. The only non-zero element of the Hessian matrix $[d^2G]$ is $G_{zz} = 2\beta_0\tau/z$. The eigenvector v is therefore, determined to be $[0 \ 1]^T$. It is also necessary to determine the directional derivatives of G along v [35]. The directional derivative G_v is defined as

$$G_v = G_{v1} = [G_z \ G_\tau] [0 \ 1]^T \quad (3.20)$$

At the singular point, $G_v = 0$. Similarly, G_{vv} , G_{vvv} , G_{vvvv} and G_{vvz} are given by

$$G_{vv} = G_{v2} = [G_{v1z} \ G_{v1\tau}] [0 \ 1]^T \quad (3.21)$$

$$G_{vvv} = G_{v3} = [G_{v2z} \ G_{v2\tau}] [0 \ 1]^T \quad (3.22)$$

$$G_{vvvv} = G_{v4} = [G_{v3z} \ G_{v3\tau}] [0 \ 1]^T \quad (3.23)$$

$$G_{vvz} = [G_{v2z} \ G_{v2z}] [0 \ 1]^T \quad (3.24)$$

In the above expressions, the subscripts z and τ indicate differentiation with respect to these variables. At the singular point given by (3.19)

$$G_{vv} = G_{vvv} = G_{vvvv} = 0, \ G_{vvz} = \beta_0/\tau \text{ and } (G_{vvvv}G_{zz}) - G_{vvz}^2 \neq 0 \quad (3.25)$$

The normal form of the singularity is $x^2 - \lambda^4 = 0$ [35], where λ is the bifurcation parameter. This singularity is of co-dimension three and its universal unfolding is given by

$$x^2 - \lambda^4 + \bar{\alpha} + \bar{\beta}\lambda + \bar{\gamma}\lambda^2 = 0 \quad (3.26)$$

where $\bar{\alpha}$, $\bar{\beta}$ and $\bar{\gamma}$ are auxiliary parameters. In a neighborhood of the singular point given by (3.19), the multiplicity features of the coupled system are similar to the multiplicity features of this polynomial equation near the origin in the $(\bar{\alpha}, \bar{\beta}, \bar{\gamma})$ parameter space. As mentioned earlier, the singular point (3.19) lies in the infeasible region of operation. However, we can still obtain the multiplicity features in a neighborhood of this singular point. As explained in the appendix, singularity theory enables us to identify and locate the critical surfaces in parameter space across which the multiplicity features change[23, 24]. For the set of the specified variables under consideration, the hysteresis variety does not exist in the feasible region of parameter space (since on this $\tau < 0$). Hence the multiplicity features can change only when the isola variety is crossed. The nature of the bifurcation across the isola variety is determined by the sign of the determinant of the Hessian matrix $[d^2G]$. For positive (negative) values of the determinant, we have a simple (isola) bifurcation. Computing the isola variety enables us to demarcate a suitable subset of the parameter space p into regions having different multiplicity features. As mentioned earlier, the singular point of the coupled system is of co-dimension three. For a singularity of co-dimension three, all the multiplicity features can only be obtained by representing the varieties in a three-dimensional parameter space. However, for ease of representation, the surfaces of the different boundaries are projected onto the $x_e - y_e$ plane. This is equivalent to representing the behavior in the (T_F, P) plane of flash operation.

As mentioned earlier, for an isothermal and isobaric flash, a steady-state of the coupled system given by (3.14) is feasible only when $y_e < z < x_e - \delta x_e$. For the sake of convenience, we take $\delta x_e = 0$. These constraints appear as feasibility boundaries in the bifurcation diagrams. The steady-states of the coupled system are not feasible when z lies outside the feasibility region. New types of multiplicity features arise depending on the manner in which the boundaries are crossed. Singularity theory can also be employed to account for these new kinds of multiplicity features in a systematic

way. Special parameter sets have been defined to account for the presence of the feasibility boundaries[24, 35]. These enable us to demarcate the locus of the feasibility boundaries in parameter space. These are summarized in the appendix. Next we study the existence of these sets for the system.

- **Boundary limit set (BLS):** The parameter set corresponding to which a turning point of the steady-state branch in the bifurcation diagram lies on the feasibility boundary forms the BLS.

For the turning point on the x_e boundary, the value of x_e is determined to be

$$x_e = y_e / (1 - B(1 - y_e)) \quad (3.27)$$

For all y_e in the feasible region $(0, 1)$, x_e predicted by (3.27) is always outside the feasible region. Consequently, the BLS exists only for $z = y_e$.

- **Boundary tangent set (BTS):** For parameter values belonging to this set, the steady-state branch in the bifurcation diagram is tangential to the feasibility boundary.

The BTS for $z = x_e$ corresponds to the diagonal $x_e = y_e$. This lies in the infeasible region in the parameter space. Whether or not the locus of the BTS corresponding to the crossing of the $z = y_e$ boundary exists, depends on the values of the parameters B , β_0 and Da_0 .

- **Double cross set (DCS):** This is given by the values of $x_e - y_e$ for which two branches of the bifurcation diagram cross the feasibility boundaries simultaneously.

The three boundary sets were computed numerically. The isola variety and these three boundary sets divide the $x_e - y_e$ plane into different regions. For the case of (M_R, F_0) fixed and isothermal and isobaric separation, these are the only surfaces in parameter space across which the multiplicity features change. These are depicted in Fig. 3.2 and 3.3 for two sets of the parameters B , β_0 and Da_0 . In Fig. 3.2 and 3.3, an isola bifurcation occurs along the curve AB, while a simple bifurcation occurs along

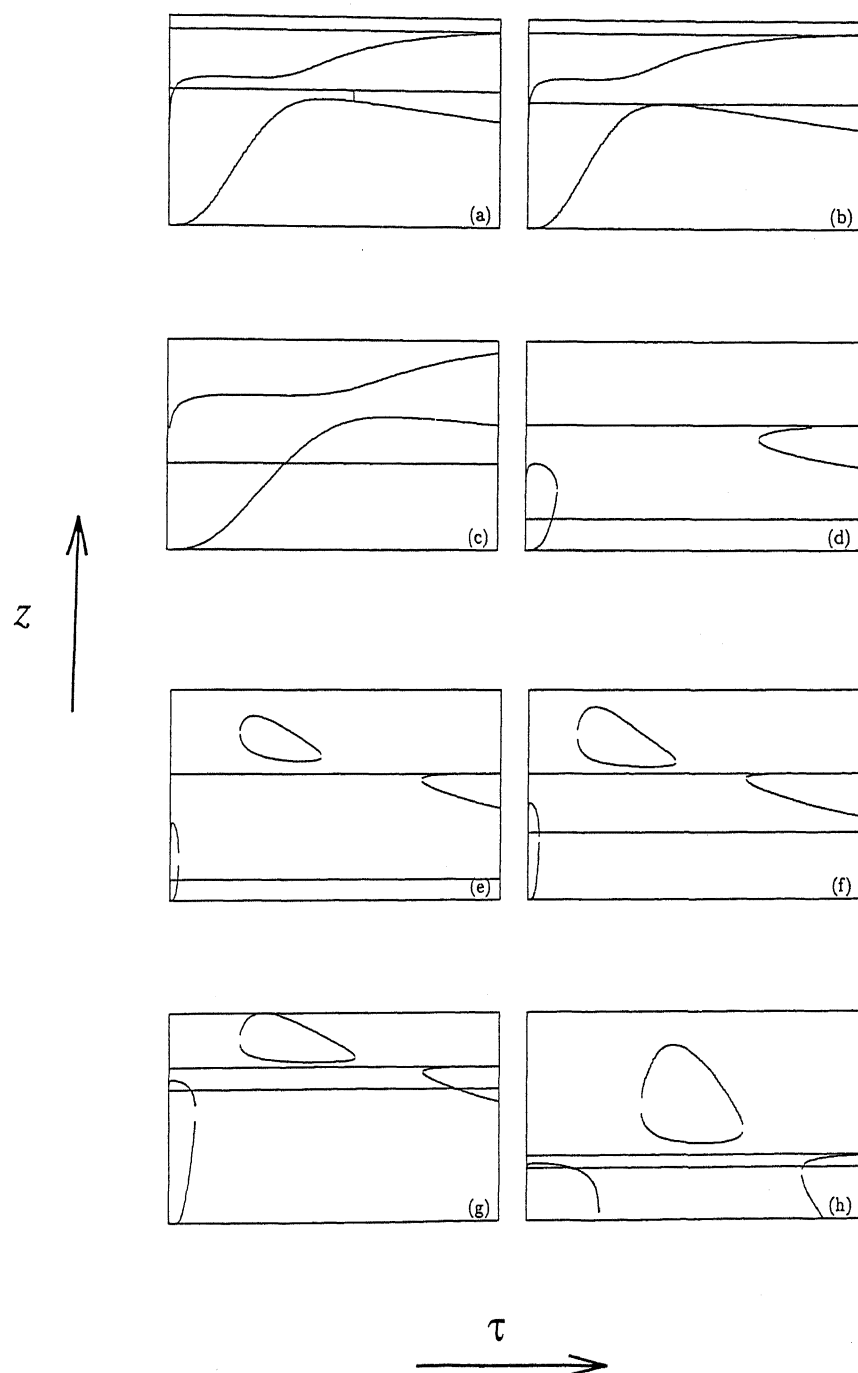
BC. The isola variety and the three boundary sets divide the $x_e - y_e$ plane of Fig. 3.2 [Fig. 3.3] into twelve (eleven) regions.

The bifurcation diagrams in the different regions of Figs. 3.2 and 3.3 are shown in Figs. 3.4 and 3.5. For a fixed set of the operating parameters, either zero or two solutions exist for a given value of τ in the bifurcation diagrams. However, the feasibility limits on z can give rise to regions where a unique feasible solution exists. The changes in the bifurcation diagrams due to crossing of the various boundaries in Fig. 3.2 is explained next for a few cases. As we move from region (e) to region (f), we cross the BLS ($z = y_e$). Thus, in the two bifurcation diagrams corresponding to these regions [Fig. 3.4(e) and 3.4(f)], the turning point lies above and below the feasibility boundary for $z = y_e$. Similarly, as we move from region (b) to region (c), we cross the DCS. In both regions, the bifurcation diagrams are such that the number of feasible solutions changes as $1 - 2 - 1$ as τ is varied [Fig. 3.4(b) and 3.4(c)]. The solution branch crosses the $z = y_e$ boundary first (at a lower value of τ) in region (b), while it crosses the $z = x_e$ boundary first in region (c).

The bifurcation diagrams on either side of the BTS of Fig. 3.2 are shown in Fig. 3.4(a) and 3.4(b). In Fig. 3.4(a) the lower steady-state branch lies in the infeasible region ($z < y_e$). A small part of the lower steady-state branch lies in the feasible region in Fig. 3.4(b). This is not clearly seen in the figure. When we cross curve AB of the isola variety in Fig. 3.2, an isola is born or disappears. This can be seen from the bifurcation diagrams in Fig. 3.4(d) and 3.4(e) respectively. In Fig. 3.4(e), there is an additional isolated branch in the bifurcation diagram. The curve BC of the isola variety represents the parameter set for which a simple bifurcation occurs at a certain value of τ . The bifurcation diagrams on either side of this curve are shown in Fig. 3.4(c) and 3.4(d).

The BLS and BTS corresponding to $z = x_e - \delta x_e$ depicted in Figs. 3.2 and 3.3 have been obtained by assuming $\delta x_e = 0$, i.e., for $z = x_e$. For small nonzero δx_e , these sets are shifted slightly from their present position (the diagonal $x = y$), thus, giving rise to new sets of multiplicity features. These new multiplicity features occur in very small regions in parameter space and hence are not considered in this study.

In the case of the CSTR, we are assured of the existence of at least one steady-state for all combinations of parameters. In complete contrast, it can be seen from the



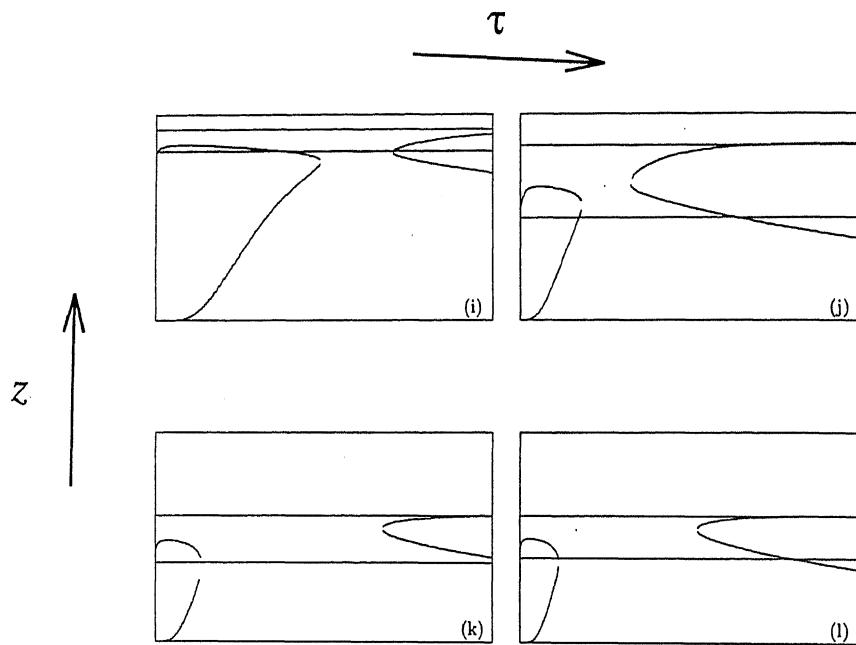
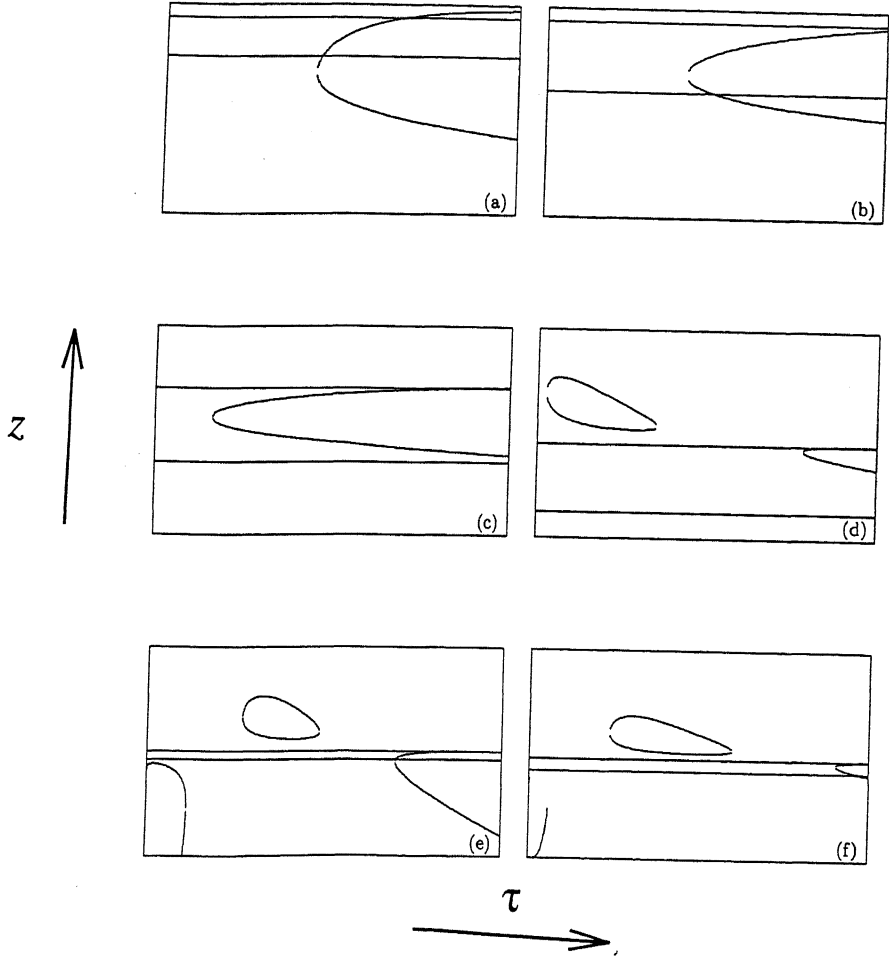


Figure 3.4: Schematic bifurcation diagrams of the steady-state for (T_F, P) and (M_R, F_0) flash (Equation (3.14)) describing the dependence of composition in the reactor on τ . Letters indicate regions in Fig. 3.2. The horizontal lines represent the feasibility boundaries $z = x_e$ and $z = y_e$ respectively ($x_e > y_e$).



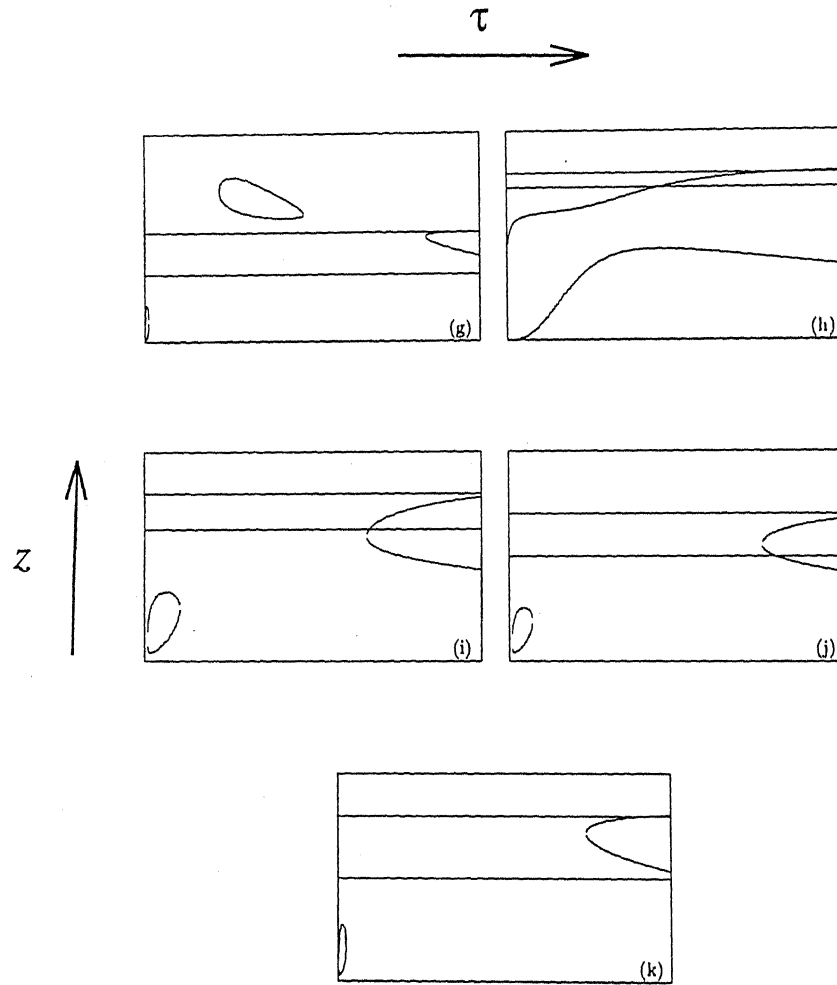


Figure 3.5: Schematic bifurcation diagrams of the steady-state for (T_F, P) and (M_R, F_0) flash (Equation (3.14)) describing the dependence of composition in the reactor on τ . Letters indicate regions in Fig. 3.3. The horizontal lines represent the feasibility boundaries $z = x_e$ and $z = y_e$ respectively ($x_e > y_e$).

bifurcation diagrams that there exist regions of τ where no solution exists. This is a result of the particular choice of the specified variables. Specifying M_R and F_0 and having an isothermal-isobaric flash operation constrains the performance of the coupled system. This is because the vapor flow rate and vapor composition are determined apriori irrespective of the residence time in the reactor. The overall mole balance determines V to be equal to F_0 . The VLE considerations determine y_e for the binary system. As a result, the performance of the coupled system is not allowed to be influenced by the interactions between the two individual units. The system behavior here is determined solely by the parameters (T_F, P) and (M_R, F_0) and not by the other conditions in the reactor. Our results indicate that under some operating conditions, such a constrained system may not have any steady-states.

Luyben[30] has studied the effect of different control structures on the steady-state characteristics of several recycle systems. They report the possibility of occurrence of the snowball effect with some control structures. The analysis presented earlier in this section, indicates that snowballing increases in magnitude as $z \rightarrow x_e$. This occurs only because x_e is fixed, since we assume an isothermal and isobaric flash operation. In addition, we have assumed a fresh feed stream entering the reactor at a constant rate.

The region in the (x_e, y_e) plane that is important in practical situations is the one corresponding to $x_e \rightarrow 1$ and $y_e \rightarrow 0$. This corresponds to operation in region (c) and (d) of Fig. 3.2 and region (c) of Fig. 3.3. The corresponding bifurcation diagrams are shown in Fig. 3.4 and Fig. 3.5 respectively. Operating the system around the lower steady-state branch of the bifurcation diagrams should make it possible to avoid the possibility of very large internal flow rates, associated with the presence of the snowball effect.

The steady-state equation for the temperature in the reactor (3.13) can be similarly analysed. It can be shown that the set of equations

$$H = H_T = H_\tau = \det[d^2H] = 0 \quad \text{and} \quad H_{vvv} \neq 0 \quad (3.28)$$

also has the solution given by (3.19). The equation (3.13) is contact equivalent to $x^2 - \lambda^3 = 0$ at the singular point. The differences in the normal forms for temperature and composition in reactor problems is well known[23]. We have however, not employed this equation to determine the multiplicity features as the feasibility constraints do not

affect this variable directly.

3.3.2 Isothermal and Isobaric Separation with (M_R, F) Fixed

We now consider the case when the reactor effluent flow rate F is the specified variable, in addition to the molar holdup in the reactor M_R . The fresh feed flow rate F_0 to the reactor is now an unknown quantity and must be computed from the model equations. Since the flash is isothermal and isobaric, the compositions of the streams leaving the flash are fixed. The reactor composition z and temperature T , the recycle stream flow rate R and the fresh feed flow rate F_0 all change such that the reactor effluent stream flow rate F is at its specified value. The dimensionless time in the model governing the dynamic behavior of the system (obtained from Equations (3.2)-(3.11)) is now defined with respect to the actual residence time in the reactor. At steady-state, these equations can be rearranged to yield the following single equation in z

$$G_1(z, p, \tau_f) = B(1 - y_e)(z - x_e) - (1 + \beta_0 \tau_f)(y_e - x_e) \left[\frac{(1 - y_e)(z - x_e)}{Da_0 \tau_f z (y_e - x_e)} \right] = 0 \quad (3.29)$$

τ_f in the above equation represents the actual residence time in the reactor. The parameter set p represents the parameters $(B, \beta_0, Da_0, x_e, y_e)$. The solution to the set of equations

$$G_1 = G_{1z} = G_{1zz} = G_{1\tau_f} = 0 \quad (3.30)$$

is given by

$$z = x_e/2, \quad \tau_f = \frac{1 - y_e}{Da_0(x_e - y_e)e^2}, \quad B = \frac{8(x_e - y_e)}{x_e(1 - y_e)}, \quad \beta_0 = \frac{Da_0(x_e - y_e)e^2}{1 - y_e}$$

It can be shown analytically that there is no solution to the winged cusp singularity, i.e., there is no solution satisfying the set of equations

$$G_1 = G_{1z} = G_{1zz} = G_{1\tau_f} = G_{1z\tau_f} = 0 \quad (3.31)$$

Therefore, for this set of specified variables, the system has a pitchfork singularity at its most singular point.

A typical projection of the numerically computed hysteresis and isola varieties and the boundary sets (BLS and BTS for $z = y_e$) in the (B, β_0) plane is shown in Fig. 3.6.

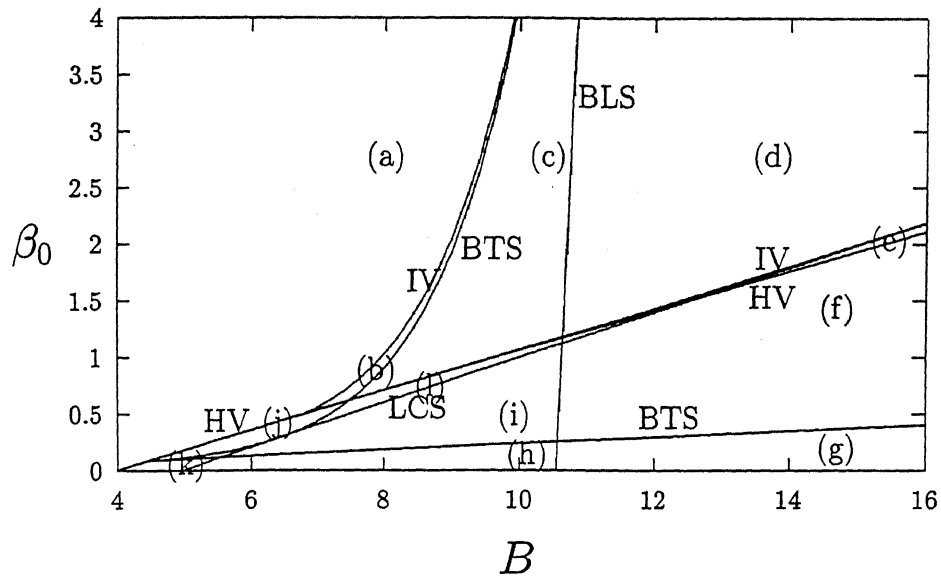
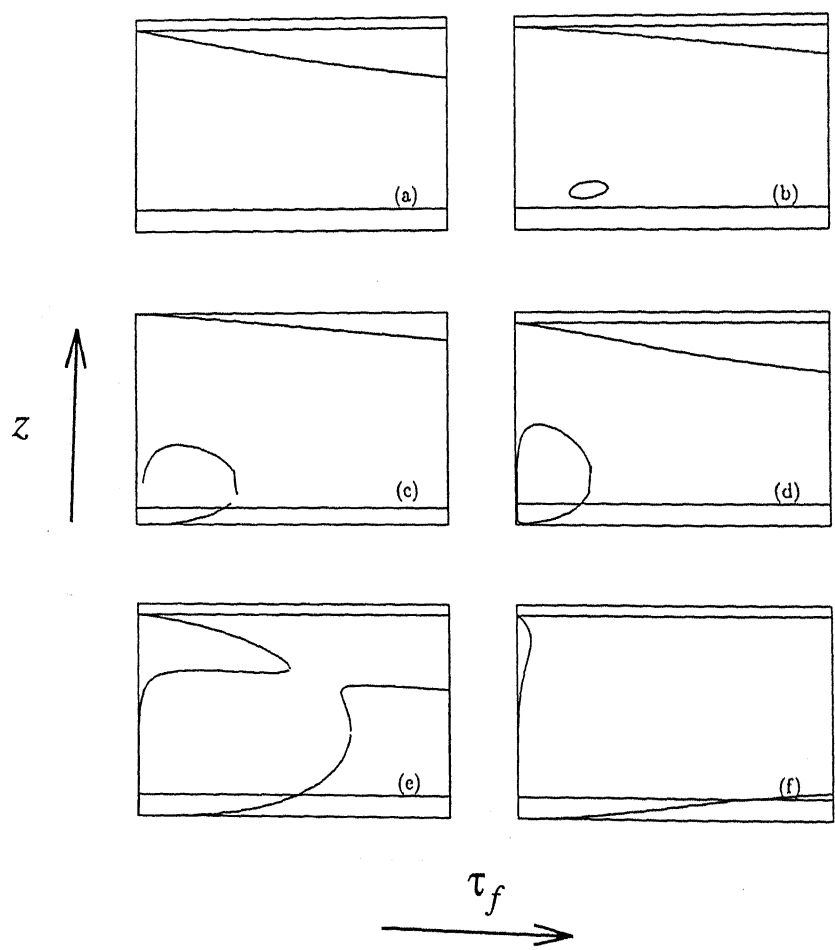


Figure 3.6: Global classification of the steady-state bifurcation diagrams for (T_F, P) and (M_R, F) flash (Equation (3.29)) in the $B - \beta_0$ plane for $x_e = 0.95$, $y_e = 0.1$, $Da_0 = 0.10$. BLS: Boundary limit set; BTS: Boundary tangent set; HV: Hysteresis variety; IV: Isola variety; LCS: Limit and cross set.



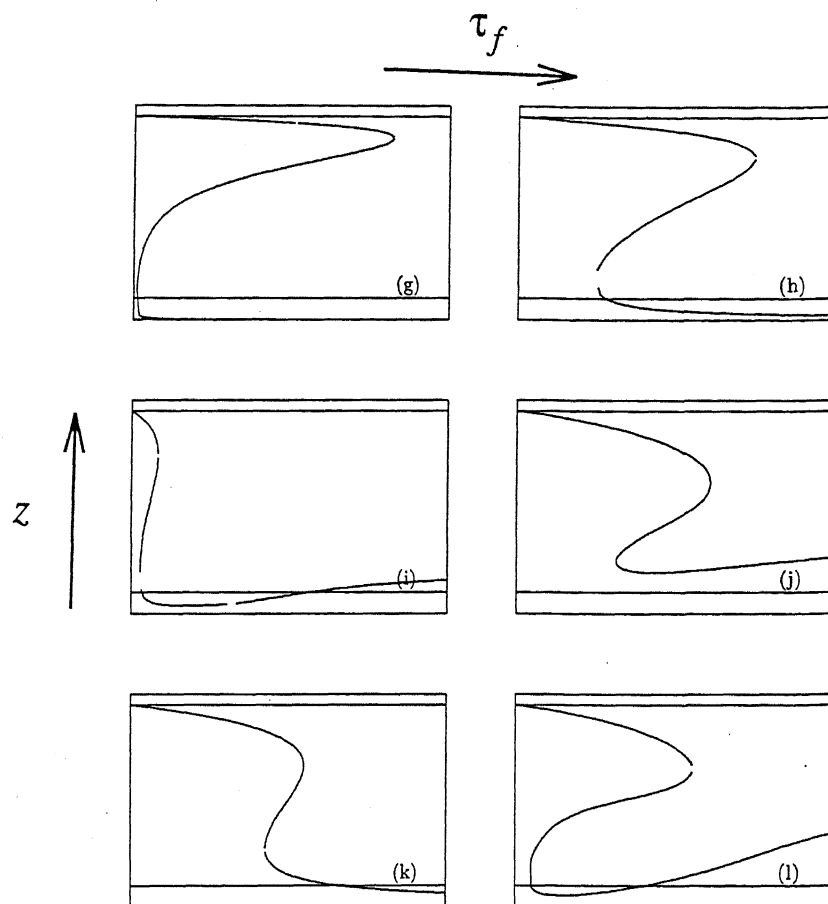


Figure 3.7: Schematic bifurcation diagrams of the steady-state (T_F, P) and (M_R, F) flash (Equation (3.29)) describing the dependence of composition in the reactor on τ_f . Letters indicate regions in Fig. 3.6. The horizontal lines represent the feasibility boundaries $z = x_e$ and $z = y_e$ respectively ($x_e > y_e$).

Equation (3.29) *behaves* as a cubic equation, and therefore we will have at least one steady-state for all values of the operating parameters, although this can be infeasible. For this set of the specified variables, the absence of feasible steady states is a consequence of the presence of the feasibility bounds on the conversion in the reactor.

The coupled system cannot have a feasibility boundary at $z = x_e$. This is because fixing the reactor effluent stream flow rate implies that the reactor composition z cannot equal x_e , since this implies complete recycle of the recycle effluent stream. Complete recycle of the product from the separator and the assumption of constant holdup in the reactor, force F_0 to be equal to zero. As a result the product stream flow rate also equals zero, resulting in the process operating in the batch mode. This in turn leads to an increase in the conversion, i.e., a decrease in z .

The coupled system can still behave as a system without recycle, even though the reactor effluent stream rate has been specified. This corresponds to the case where we have complete vaporisation of the feed to the separator. The reactor conversion z in this case would then be less than y_e . Therefore, in this case only the feasibility boundary corresponding to $z = y_e$, exists.

The bifurcation diagrams in the different regions are shown in Fig. 3.7. From Fig. 3.7 it can be seen that for some ranges of τ_f , there are no feasible steady states for the coupled system. The multiplicity features of the coupled system are essentially similar to that of a CSTR[23]. The isola and hysteresis varieties (Fig. 3.6) reduce to those of the CSTR in the limit of $x_e = 1$ and $y_e = 0$. The nature of the changes in the bifurcation diagrams when the boundary sets are crossed are explained in the appendix.

Practical considerations for an efficient operation of the coupled system require that the feasibility boundaries should be avoided. From Fig. 3.6 and the bifurcation diagrams shown in Fig. 3.7, it can be seen that this is possible provided we operate the system in regions (a), (b) and (j) of Fig. 3.6.

3.3.3 Isothermal and Isobaric Separation with (M_R, L) Fixed

We now consider operation of the coupled system when the liquid rate L leaving the flash is the specified variable, in addition to the molar holdup in the reactor M_R .

The fresh feed flow rate F_0 to the reactor and the reactor effluent flow rate F are now the unknown quantities, which must be computed from the model equations. The dimensionless time in the model governing the dynamic behavior of the system (obtained from Equations (3.2)-(3.11)) is now defined with respect to the recycle stream rate entering the reactor. At steady-state, these equations can be rearranged to yield the following single equation in z

$$G_2(z, p, \tau_l) = B(z - x_e)(1 - y_e) - [y_e - x_e + \beta_0 \tau_l (y_e - z)] \ln \left[\frac{(z - x_e)(1 - y_e)}{Da_0 \tau_l z (y_e - z)} \right] = 0 \quad (3.32)$$

τ_l in the above equation represents the quantity M_R/L . The parameter set p represents the parameters $(B, \beta_0, Da_0, x_e, y_e)$. The solution to the set of equations

$$G_2 = G_{2z} = G_{2zz} = G_{2\tau_l} = 0 \quad (3.33)$$

was computed numerically with z , τ_l , B and β_0 as the unknowns and with several sets of values for Da_0 , x_e and y_e . It was observed that the solution to the pitchfork singularity lies in the feasible region of the unknowns. From the computations, it appears that there is no solution to the winged cusp singularity, i.e., there is no solution to the set of equations

$$G_2 = G_{2z} = G_{2zz} = G_{2\tau_l} = G_{2z\tau_l} = 0 \quad (3.34)$$

Therefore, for this set of specified variables, it appears the system has a pitchfork singularity at its most singular point.

The hysteresis and isola varieties were computed numerically. A typical projection of the varieties in the (B, β_0) plane is shown in Fig. 3.8. The bifurcation diagrams in the different regions are shown in Fig. 3.9. At least one steady-state exists for all values of τ_l as is to be expected since now the normal form would be a cubic. The multiplicity features of the steady-states for this system are again similar to that of a CSTR[23].

The generic guideline proposed by Luyben to avoid the snowball effect[29], is that for isothermal recycle systems, the recycle rate should be a specified variable. We find that this need not be true in the case of non-isothermal recycle systems, though for this choice of the specified variables, feasibility boundaries do not influence the multiplicity features of the system. This is because fixing the recycle flow rate, constrains the conversion in the reactor to always lie within the bounds imposed by the vapor and

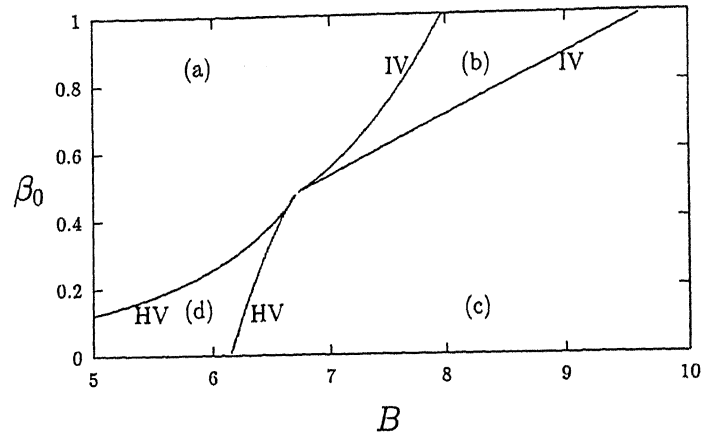


Figure 3.8: Global classification of the steady-state bifurcation diagrams for (T_F, P) and (M_R, L) flash (Equation (3.32)) in the $B - \beta_0$ plane for $x_e = 0.95$, $y_e = 0.1$, $Da_0 = 0.10$. HV: Hysteresis variety; IV: Isola variety.

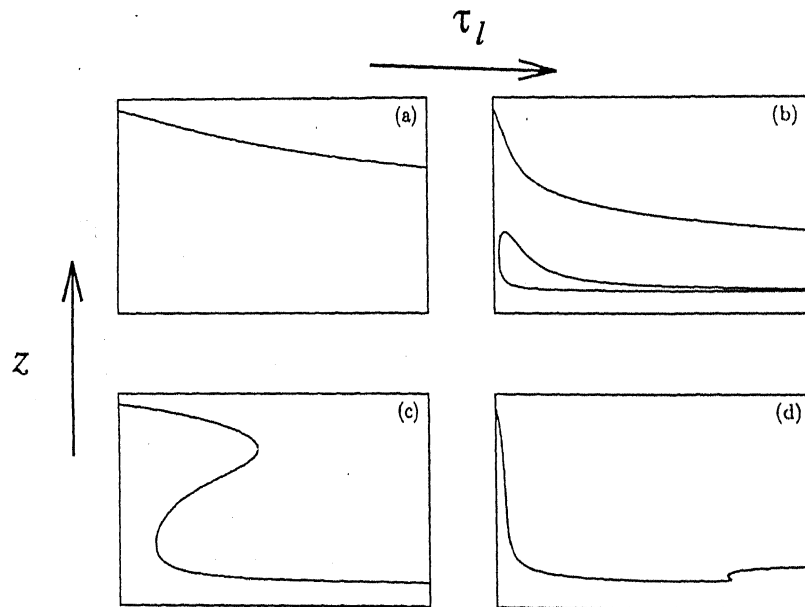


Figure 3.9: Schematic bifurcation diagrams of the steady-state (T_F, P) and (M_R, L) flash (Equation (3.32)) describing the dependence of composition in the reactor on τ_l . Letters indicate regions in Fig. 3.8.

liquid stream compositions exiting the separator. The reactor conversion z cannot equal y_e , since this would mean that the recycle rate goes to zero. Neither can the reactor conversion z equal x_e , since this would result in the fresh feed rate going to zero. As explained for the case $((M_R, F)$ separation), this results in a situation where we do not have any product stream exiting the system. As a result, we have the system operating in batch mode, leading to an increase in the conversion and hence a decrease in z . Such a situation again arises only because we have already fixed the operating conditions (T_F, P) in the separator.

However, in the case of $z \rightarrow y_e$, i.e., at high conversions, the amount of recycle going into the liquid fraction decreases. Hence for a small decrease in z , the amount of fresh feed added to maintain the recycle rate at its specified value, increases. This results in a decrease in the residence time in the reactor. In the case of non-isothermal reactions, this decrease in the residence time in the reactor can result in the appearance of run-away like conditions. Another effect of such an interaction is in the appearance of the snowball effect, since a small decrease in z results in a very large increase in the fresh feed flow rate to the reactor.

3.3.4 Isothermal and Isobaric Separation with (F_0, F) Fixed

We now consider the case when both the fresh feed flow rate F_0 and the reactor effluent flow rate are the specified variables. Since we assume isothermal and isobaric separation, the material balance and equilibrium equations governing the flash (Equations (3.5), (3.6) and (3.8)-(3.11)) determine the composition z of the reactor effluent stream. Hence this composition can be treated as a bifurcation parameter. The molar holdup M_R , the temperature T in the reactor, and the recycle flow rate L are now unknown. The dimensionless time in the model governing the dynamic behavior of the system (obtained from Equations (3.2)-(3.11)) is now defined with respect to the (unknown) actual residence time in the reactor. At steady-state, these equations can be rearranged to yield the following single equation in T

$$G_3(T, p, z) = B(1 - y_e)Da_0z(z - x_e) - T \left[Da_0z(y_e - x_e) + \beta_0(1 - y_e)(z - x_e)e^{-T} \right] = 0 \quad (3.35)$$

The reactor conversion z is now considered to be the bifurcation parameter. This

implies that we operate the reactor at a specified conversion. The parameter set p represents the parameters $(B, \beta_0, Da_0, x_e, y_e)$. The solution to the set of equations

$$G_3 = G_{3T} = G_{3TT} = G_{3z} = 0 \quad (3.36)$$

is given by

$$T = 2, \quad z = \frac{x_e(1 - y_e)}{1 - 2y_e}, \quad B = \frac{2(x_e - y_e)}{x(1 - y_e)}, \quad \beta_0 = \frac{Da_0(x_e - y_e)e^2}{1 - y}$$

This solution to the pitchfork singularity lies in the feasible region. Further, it can be shown that there is no solution to the winged cusp singularity, i.e., there is no solution to the set of equations

$$G_3 = G_{3T} = G_{3TT} = G_{3Tz} = G_{3Tz} = 0 \quad (3.37)$$

Therefore, for this set of specified variables, the system has a pitchfork singularity at its most singular point.

A typical projection of the hysteresis and isola varieties and the boundary sets in the (B, β_0) plane is shown in Fig. 3.10. The bifurcation diagrams in the different regions are shown in Fig. 3.11. It can be seen from the figure that atleast one steady-state exists for all feasible values of the bifurcation parameter z . The multiplicity features of the steady states for this system are essentially similar to that of a CSTR[23]. As mentioned earlier, for this set of the specified variables, the conversion z and all the flow rates to and from the reactor are determined by the material balance and equilibrium relations for the flash. Since we are considering isothermal and isobaric separation, the bounds on the conversion z still exist. Feasibility boundaries in this case arise due to the following bounds on the bifurcation parameter

$$y_e < z < x_e$$

The two vertical lines in the bifurcation diagrams in Fig. 3.11 represent the feasibility boundaries corresponding to y_e and x_e ($x_e > y_e$). Specifying the rates of the fresh feed stream to the reactor and the reactor effluent stream, implies that z cannot equal x_e . Therefore, only the feasibility boundary corresponding to $z = y_e$ exists for this case.

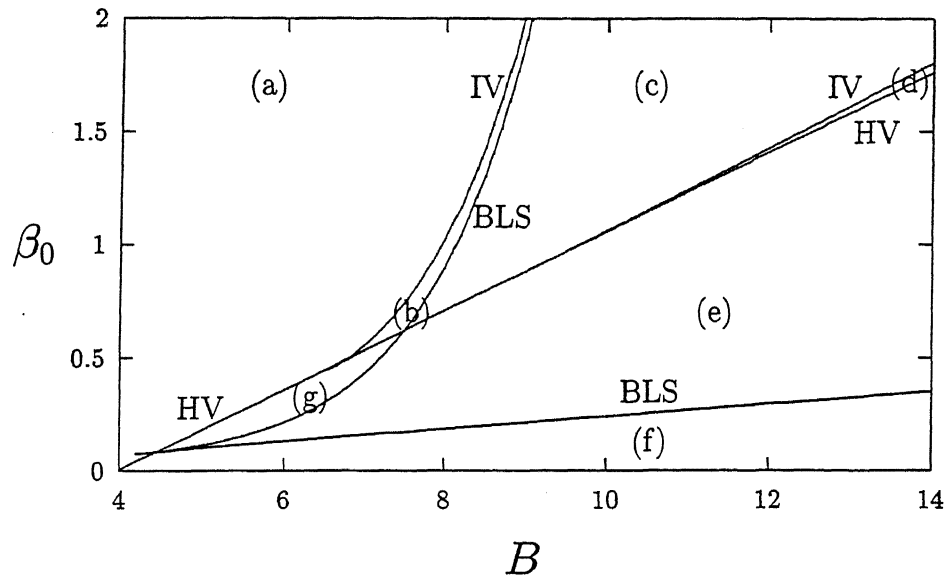


Figure 3.10: Global classification of the steady-state bifurcation diagrams for (T_F, P) and (F_0, F) flash (Equation (3.35)) in the $B - \beta_0$ plane for $x_e = 0.95$, $y_e = 0.1$, $Da_0 = 0.10$. BLS: Boundary limit set; HV: Hysteresis variety; IV: Isola variety.

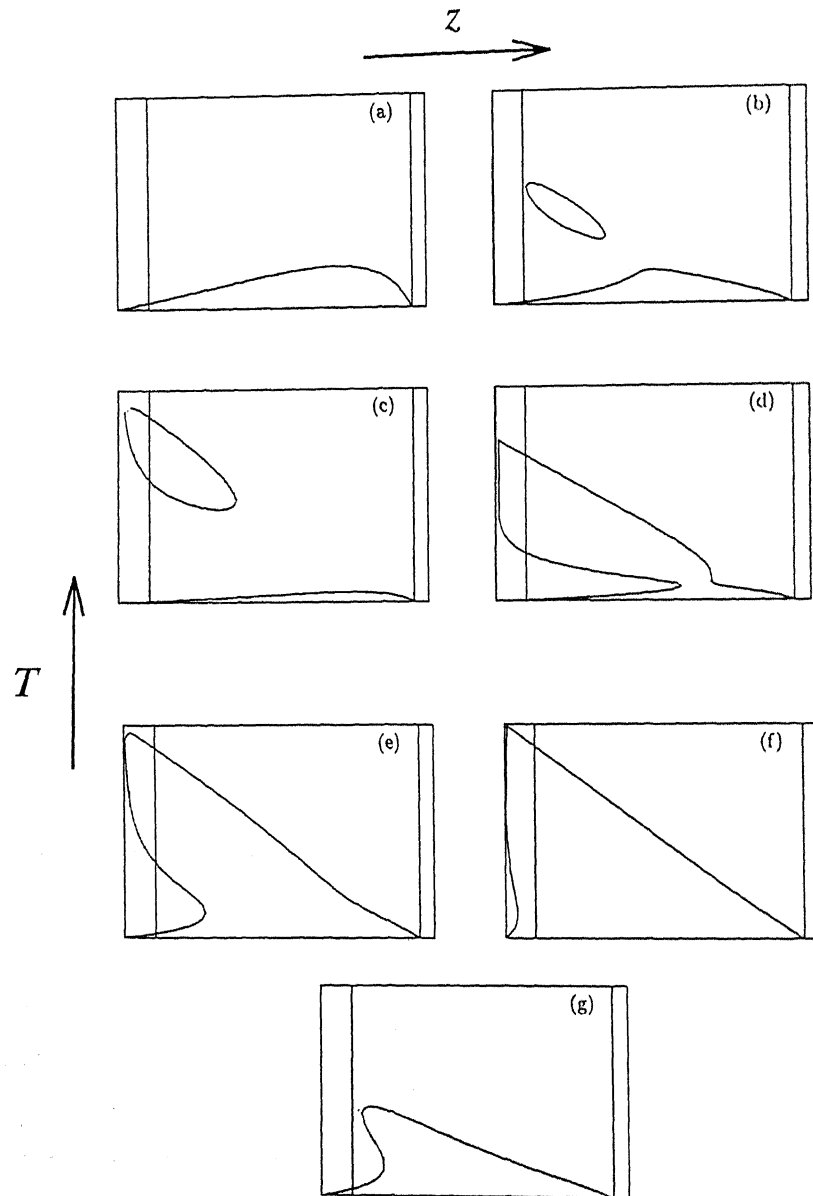


Figure 3.11: Schematic bifurcation diagrams of the steady-state for (T_F, P) and (F_0, F) flash (Equation (3.35)) describing the dependence of temperature in the reactor on z . Letters indicate regions in Fig. 3.10. The vertical lines represent the feasibility boundaries $z = x_e$ and $z = y_e$ respectively ($x_e > y_e$).

This situation corresponds to the coupled system behaving like a system in series, i.e., without recycle. The boundary limit set (BLS) for $z = y_e$ is shown in Fig. 3.10. The effect of this boundary on the multiplicity features of the coupled system is shown in Fig. 3.11. The part of the bifurcation diagram to the left of the $z = y_e$ line (the vertical line to the left) lies in the infeasible region and hence is of no physical significance. This corresponds to a negative value of one of the flow rates. At the limit of $z \rightarrow x_e$, the value of T approaches zero. This corresponds to a situation where we have very low residence times in the reactor and a very low amount of fresh feed entering the reactor.

Practical considerations for a smooth operation of the coupled system mean that the system has to be operated at low values of B and high values of β_0 . Selection of these parameters such that the bifurcation diagrams are of the type shown in Fig. 3.11(a), (b) or (g) ensures that the feasibility boundary does not influence operation of the system at the steady-state.

3.3.5 (T_F, L) Separation with (M_R, F_0) Fixed

We finally consider the case when the liquid rate L leaving the flash is the specified variable in addition to the fresh feed flow rate F_0 and the molar holdup in the reactor. The reactor and mixer holdups are assumed to be constant. Therefore, the reactor effluent stream rate is now a known quantity. This enables us to define the dimensionless time in the model governing the dynamic behavior of the system (obtained from Equations (3.2)-(3.11)) with respect to the actual residence time in the reactor. The pressure P in the separator is now an unknown quantity which must be computed by solving the set of model equations simultaneously. At steady-state, these equations can be rearranged to yield the following single equation in x_e

$$G_4(x_e, p, \tau_f) = B(1-x_e) - [1+x_e(\gamma-1)][1+\alpha+\beta_0\tau_f] \ln \left[\frac{(1-x_e)(\alpha+1)}{Da_0\tau_f[x_e(\alpha+1) + \alpha x_e^2(\gamma-1)]} \right] = 0 \quad (3.38)$$

In the above equation, γ is defined as P_1^{sat}/P_2^{sat} . τ_f represents the actual residence time in the reactor. The parameter set represents the parameters $(B, \beta_0, Da_0, \gamma, \alpha)$. The solution to the set of equations

$$G_4 = G_{4x_e} = G_{4x_e x_e} = G_{4\tau_f} = 0 \quad (3.39)$$

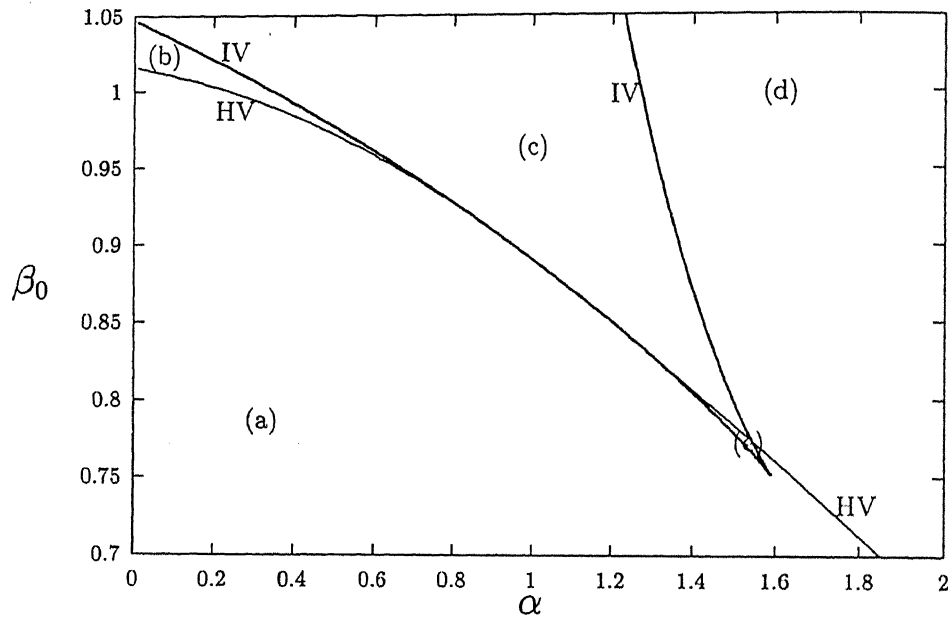


Figure 3.12: Global classification of the steady-state bifurcation diagrams for (T_F, L) flash (Equation (3.38)) in the (α, β_0) plane.

was computed numerically with x_e , τ_f , α and γ as the unknowns and with several sets of values for B , Da_0 , and β_0 . It was observed that the solution to the pitchfork singularity lies in the feasible region of the unknowns. It can be shown that there is no solution to the winged cusp singularity i.e., there is no solution to the set of equations

$$G_4 = G_{4x_e} = G_{4x_e x_e} = G_{4\tau_f} = G_{4x_e \tau_f} = 0 \quad (3.40)$$

From the computations, it appears that for this set of specified variables $((T_F, L)$ flash) the system has a pitchfork singularity at its most singular point.

The hysteresis and isola varieties were computed numerically. A typical projection of the varieties in the (α, β_0) plane is shown in Fig. 3.12. The bifurcation diagrams in the different regions are shown in Fig. 3.13. At least one steady-state exists for all values of τ_f . This is to be expected since now the normal form would be a cubic. The multiplicity features of the steady-states for this system are again similar to that of a CSTR[23].

In the present mode of operation, the choice of the specified variables is such that

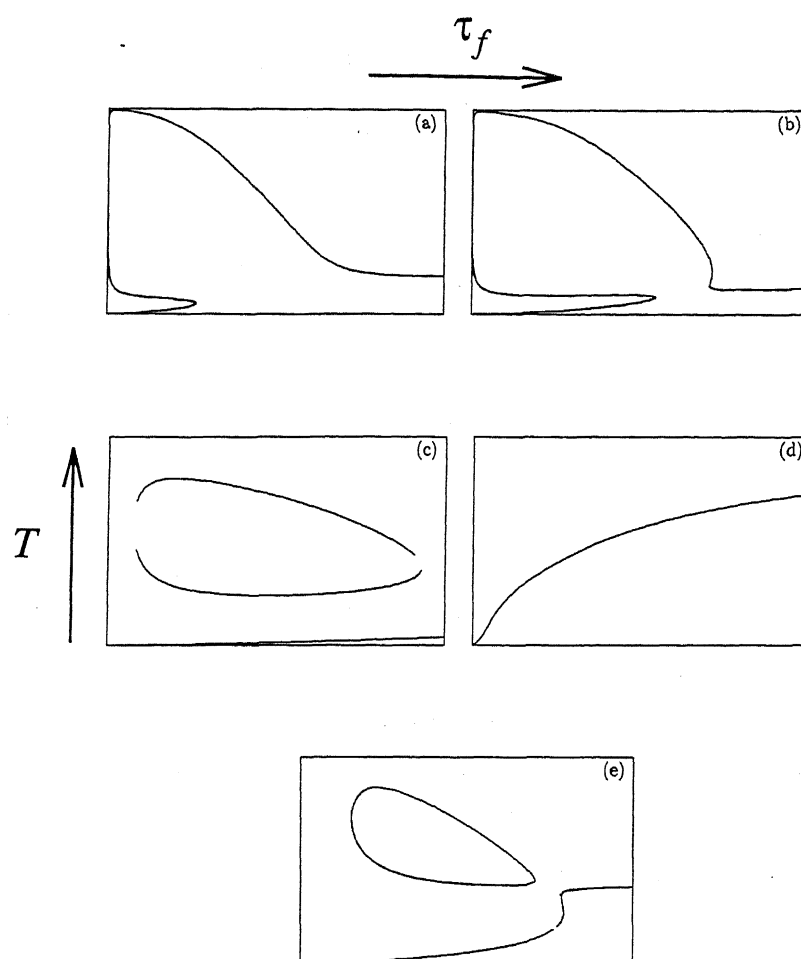


Figure 3.13: Schematic bifurcation diagrams of the steady-state for (T_F, L) flash (Equation (3.38)) describing the dependence of temperature in the reactor on τ_f . Letters indicate regions in Fig. 3.12.

there are no pre-determined composition constraints acting on the system, since the pressure in the separator is an unknown quantity. We can visualise the system as having to evolve to a state, which satisfies the constraint imposed by fixing the recycle flow rate to the reactor. For example, the problem can be considered to be one of determining the composition of the feed stream to the separator and the pressure in the separator, such that the flow rate of the liquid fraction exiting the flash equals its specified value. The absence of feasibility boundaries on the reactor conversion implies that the coupled system can regulate itself in this manner for all combinations of the operating parameters. For this reason we have depicted the dependence of the temperature in the reactor in the bifurcation diagrams.

Investigating the different modes of operation of the system enables us to explain the reason for the non-existence of steady states observed in the (T_F, P) and (M_R, F_0) flash operation. The fundamental difference between this and the other modes can be best understood by considering the overall system performance.

For the case of isothermal and isobaric separation when (M_R, F_0) are the specified variables, it was seen that the interactions between the two units (through recycle) is not allowed to affect the performance of the coupled system. This is because specifying the above four variables fixes the product rate and the product quality of the system. Therefore, this choice of combination of the specified variables constrains the performance of the coupled system. Non-existence of steady-states for certain values of parameters can be viewed as a failure of the coupled system to satisfy the constraints.

For all other combinations of the specified variables, either the product flow rate or its quality is constrained. Therefore, for all these combinations of the specified variables, the interactions between the two units (through recycle) can affect the performance of the coupled system, through the unconstrained variable. The system is thus free to evolve, and does evolve, to a state such that all the constraints are satisfied. Therefore, we do not have any regions in parameter space where both the feasible and infeasible steady-states of the single steady-state equation are non-existent. In these cases, the nature of the imposed constraints determines the presence or absence of the feasibility boundaries.

Interpretation of the results presented in this section can also be undertaken from the mathematical point of view. Absence of steady states for the case discussed in sub-

section 3.3.1 arises because the equation (3.14) is *contact equivalent* to a quadratic. All the other cases considered (sections 3.3.2-3.3.5) have a pitchfork singularity. Singularity theory predicts that the normal form for each of these cases is cubic in nature. This assures us of the presence of at least one steady-state for all operating conditions. However, the presence of bounds on the conversion in the reactor can result in the existence of regions in parameter space where we do not have any feasible steady states.

In Figs. 3.7 and 3.9, for the cases of (M_R, F) flash (subsection 3.3.2) and (M_R, L) flash (subsection 3.3.3), we see that for very low residence times in the reactor, the steady-state conversion z approaches x_e . Having $z \rightarrow x_e$ in these cases, corresponds to a situation where we have a very low amount of fresh feed entering the reactor.

The analysis carried out in this section shows that it is possible to cross the $z = y_e$ boundary for some sets of specifications. Operation near this boundary this can lead to unsafe conditions, since this boundary would typically correspond to a state of high conversion and high temperature in the reactor.

In the above discussion, we have concerned ourselves only with analysing the steady-state behavior of the system. The dynamic behavior has not been considered at all. The nature of the dependence of the steady-state composition and the temperature in the reactor (represented in the bifurcation diagrams) on an independent variable can be considered to be obtained by slowly varying the bifurcation parameter. Considering such a quasi-static variation of the control parameter together with the arguments presented earlier in this section enables us to obtain useful information about the dynamic behavior of the system.

During its approach to the steady-state, i.e., during the transient evolution, the system can evolve towards and cross the feasibility boundaries represented by x_e or y_e . As discussed earlier in this section, such an evolution of the system can result in the failure of operation of the coupled system, if appropriate corrective action is not taken.

3.4 Conclusions

In this work we have investigated the behavior of a coupled reactor-separator system. The steady-state multiplicity features were studied using singularity theory. It was shown that the choice of the specified variables drastically changes the multiplicity

features of the system. It was shown that for a particular choice of the specified variables ((M_R, F_0, T_F, P) operation), the maximum number of feasible steady-states of the system is two. For this choice of the specified variables, there exist ranges of parameter values for which a steady-state of the coupled system can be non-existent. In this case, the non-existence of the steady-states arises because the performance of the coupled system (in terms of production rate and product composition) is completely determined by the VLE considerations and the overall mole balance of the coupled system. The performance of the coupled system is not allowed to be influenced by the dynamics and interaction between the individual units. In contrast, the multiplicity features with the other sets of specifications, are essentially similar to that of the CSTR, which has a maximum of three steady-states. The only difference is in the presence of additional multiplicity features resulting from the presence of feasibility boundaries.

An important feature of this system is that the multiplicity features are influenced by feasibility constraints generated by the VLE considerations in the flash. This is true only for isothermal and isobaric separation. When either the temperature or the pressure in the flash are not specified, the VLE relations do not impose any constraints on the system. Therefore, in this case, even though some of the flow rates are constrained, the vapor composition can vary since the pressure in the flash is not fixed. In this case the system can regulate itself, such that the flow constraints are satisfied. As a result, we observe that the feasibility boundaries on the conversion do not exist.

It is a common practice in industry to operate a distillation column by maintaining the compositions of the top and bottom streams at constant values. Operating a reactor with constant fresh feed flow rate is also very common. This control configuration, however, may not be the best option for a recycle system. Our results indicate that for a simple recycle system consisting of a reactor and a separator, such an operation can lead to severe problems in the operation of the system.

Chapter 4

A Unified Framework for the Analysis of Synchronization of Chaotic Systems

Nomenclature

p_1, p_2, p_3	Inputs in the Rossler system.
r	Relative order of the system.
t	Time.
u	Manipulated input.
\mathbf{x}_m	States of the reference system.
\mathbf{x}_p	States of the process system.
y	Process output.
y_d	Desired or reference output.
\mathbf{z}	Co-ordinates in the transformed co-ordinate system.

4.1 Introduction

The temporal evolution of systems which exhibit chaotic behavior is characterized by a sensitive dependence on initial conditions. This implies that the trajectories along which two identical systems starting from nearby initial states evolve, diverge from each other. Mathematically, such an evolution is characterized by a positive value of

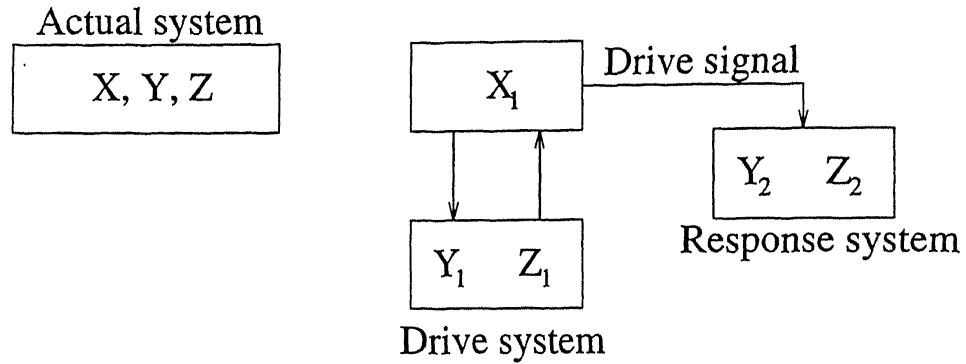


Figure 4.1: Schematic diagram of Pecora-Carroll synchronization.

one or more Lyapunov exponents. The Lyapunov exponents, which characterize the nature of a trajectory along which a system evolves, are analogous to eigenvalues which determine the stability of a steady-state of a system. Positive (negative) values of the Lyapunov exponents, are a measure of the rate at which two nearby states diverge from (approach) each other, as the system evolves.

Synchronization refers to the ability of all the states of two identical systems, starting from nearby initial states, to evolve identically with time. It would hence appear that two chaotic systems cannot be made to synchronize with each other. However, Pecora and Carroll[37, 38] showed that two chaotic systems could be synchronized with one another. They achieved synchronization between two chaotic systems by linking them with a common signal. A schematic representation of their technique is shown in Fig. 4.1. They considered a three-dimensional system represented by the state variables X, Y and Z . The state variables of the first and second systems are denoted by the subscripts 1 and 2 respectively. System 1, characterized by X_1, Y_1 and Z_1 is called the drive system. System 2, characterized by X_2, Y_2 and Z_2 is called the response system. Pecora and Carroll studied the evolution of the *response system*, represented by the states Y_2 and Z_2 , when X_2 was equal to X_1 , i.e., when the Y_2, Z_2 system was *driven* by the X_1 signal. Mathematically, this can be represented by the following system of

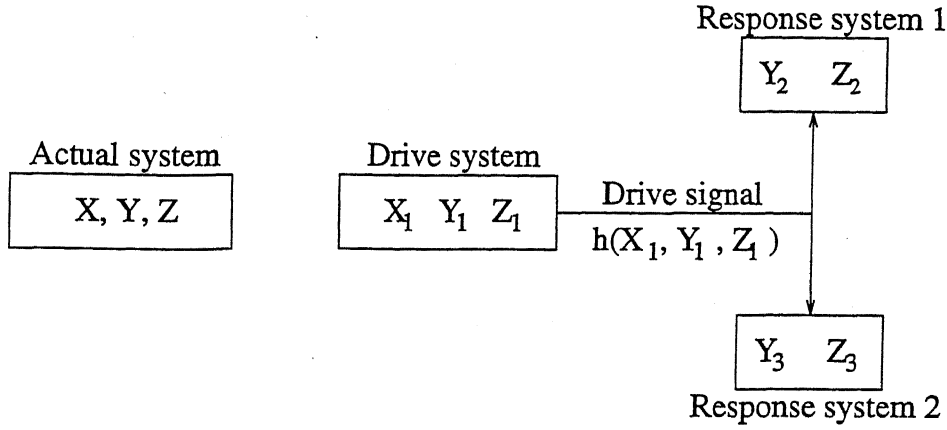


Figure 4.2: Schematic diagram for detecting the occurrence of generalized synchronization in a given system.

equations

$$\begin{aligned}\dot{X}_1 &= F_1(X_1, Y_1, Z_1) \\ \dot{Y}_1 &= F_2(X_1, Y_1, Z_1) & \dot{Y}_2 &= F_2(X_1, Y_2, Z_2) \\ \dot{Z}_1 &= F_3(X_1, Y_1, Z_1) & \dot{Z}_2 &= F_3(X_1, Y_2, Z_2)\end{aligned}$$

Since the driving signal X_1 is chaotic, the evolution of the response system is also chaotic. The drive and the response systems are said to have synchronized, if the difference between the corresponding states of the two systems, i.e., $(Y_1 - Y_2)$ and $(Z_1 - Z_2)$, goes to zero as $t \rightarrow \infty$. Pecora and Carroll showed that synchronization of the drive and response systems was possible, if the response system has only negative Lyapunov exponents. As mentioned in the first chapter, the importance of synchronization stems from its possible applications in several disciplines of science.

Recently, two different types of synchronization have been reported in the literature. Rulkov *et al.*[39] and Kocarev and Parlitz[40] have studied a type of synchronization, which they refer to as generalized synchronization (GS). The driving signal (Fig. 4.2) is now a function (possibly nonlinear) of the states of the drive system, i.e., it is achieved by substituting the driving variable (X_2) with the driving signal in the response system. Using such a driving signal generally results in a nonlinear relationship between the states of the driving system and the corresponding states of the response system. A

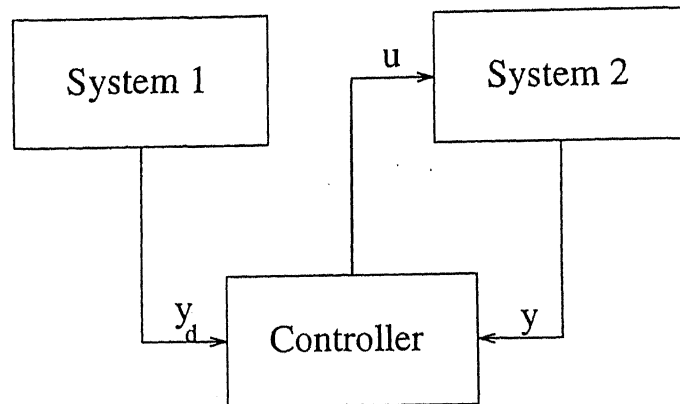


Figure 4.3: Schematic diagram of the feedback control strategy.

simple way of detecting whether or not synchronization is achieved involves constructing a replica of the response system (Fig. 4.2). The response system is said to have the ability to synchronize if the errors $(Y_2 - Y_3)$ and $(Z_2 - Z_3)$ go to zero as $t \rightarrow \infty$. Kocarev and Parlitz and their co-workers[41, 42] have reported a powerful new technique for achieving synchronization in chaotic systems. Their procedure, an active-passive decomposition (APD) technique, involves creating a new system by defining a new variable as a function of the drive system variables. The new variable is used as the driving signal to drive the modified response system. This is discussed in greater detail in the third section of this chapter.

In this chapter we present a general framework for the analysis of the above techniques for synchronizing chaotic systems. We show that the above techniques are a different interpretation of the use of feedback, to achieve **perfect control** of a process along a desired (chaotic) trajectory. By perfect control, we mean that the controlled output tracks the desired output exactly for all time $t \geq 0$. We show that the three types of synchronization mentioned above are different cases of perfect control of a single input-single output (SISO) system. The connection between synchronization and perfect control is illustrated on a modified form of the Rossler system.

4.2 Theoretical Analysis

Figure 4.3 shows a schematic diagram of the feedback control problem. System 1 represents a model whose output y_d generates the desired (reference) behavior of the process. System 2 represents the actual process with an output y . We assume that the model represents the process exactly. The difference between the evolution of the two systems arises due to the differences in the initial conditions of the state variables \mathbf{x}_m and \mathbf{x}_p . The process output y cannot track the desired output y_d in the absence of control, because of the chaotic behavior of the system. It is desired to match (synchronize) the process output y along a desired trajectory y_d for $t \geq 0$ using output feedback control. This objective is different from the conventional control goal, where it is desired that synchronization occurs as time $t \rightarrow \infty$.

Analysis and design of a controller for achieving perfect control in a nonlinear system requires the use of results from nonlinear systems and nonlinear control theories. These theories for nonlinear systems which are linear in the input or manipulated variable are well developed. They are an extension to nonlinear systems, of the Laplace transform method for linear systems. Recent developments in differential-geometry based nonlinear control theory[46, 62, 63], have made it possible to devise control schemes for the perfect control of nonlinear systems. We next present the formulation of the control problem and its solution. Complete details are available in[62, 63].

We consider the desired output and the process to be represented by the following n -dimensional single input-single output (SISO) models

$$\dot{\mathbf{x}}_m = \mathbf{f}(\mathbf{x}_m) + \mathbf{g}(\mathbf{x}_m)u_0 \quad (4.1)$$

$$y_d = h(\mathbf{x}_m) \quad (4.2)$$

$$\dot{\mathbf{x}}_p = \mathbf{f}(\mathbf{x}_p) + \mathbf{g}(\mathbf{x}_p)u \quad (4.3)$$

$$y = h(\mathbf{x}_p) \quad (4.4)$$

The overdot indicates differentiation with respect to time. $\mathbf{x}_m, \mathbf{x}_p \in \mathbb{R}^n$ are the reference and process states, u_0 and u are scalars representing the nominal and the manipulated inputs respectively. For the purpose of showing the equivalence between synchronization and perfect control, it is sufficient to assume that only one element in the vector $\mathbf{g}(\mathbf{x}_p)$ is non-zero. This implies that the input u , directly affects only one of

the states of the system. y is the scalar measured output, and y_d denotes the scalar desired output to be tracked. Our objective is to apply suitable parametric perturbations on u , such that the process output y tracks the desired output y_d exactly, i.e.,

$$y_d - y = 0 \quad \text{for } t \geq 0$$

Differentiating (4.4) repeatedly, the relationship between the output y and the state variable \mathbf{x}_p can be expressed as

$$\begin{aligned} y &= h(\mathbf{x}_p) \\ \frac{dy}{dt} &= L_f h(\mathbf{x}_p) \\ \vdots &\quad \quad \quad \vdots \\ \frac{d^{r-1}y}{dt^{r-1}} &= L_f^{r-1} h(\mathbf{x}_p) \\ \frac{d^r y}{dt^r} &= L_f^r h(\mathbf{x}_p) + L_g L_f^{r-1} h(\mathbf{x}_p) u \end{aligned} \tag{4.5}$$

The index r is a measure of how directly the input u affects the output y . It is called the **relative order** of the system and represents the number of differentiation operations which must be performed on the output, in order to obtain an explicit dependence of the output on the input u . The relative order is defined as the smallest integer r such that

$$L_g L_f^{r-1} h(\mathbf{x}_p) \neq 0$$

where $L_f h(\mathbf{x}_p)$ is the Lie derivative of a function $h(\mathbf{x}_p)$ with respect to $\mathbf{f}(\mathbf{x}_p)$ and is defined as

$$L_f h(\mathbf{x}_p) = \sum_{k=1}^n \mathbf{f}_k(\mathbf{x}_p) \frac{\partial h(\mathbf{x}_p)}{\partial x_k}$$

Higher order Lie derivatives with the same vector argument are defined recursively as

$$L_f^m = L_f L_f^{m-1}$$

The relationship between the manipulated input u and the process output y , can then be expressed as

$$u = \frac{y^r - L_f^r h(\mathbf{x}_p)}{L_g L_f^{r-1} h(\mathbf{x}_p)} \quad (4.6)$$

where y^r is the r^{th} order derivative of the process output. For the problem under consideration, the measured and the desired outputs are specified by the designer. In order to obtain the control law which achieves the objective of perfect control, we set the output tracking error $e = y - y_d$ equal to zero. On differentiating this r times, we obtain the following equation relating the input u to the output tracking error e .

$$e^r = y^r - y_d^r = 0$$

The control law which achieves the objective of perfect control is obtained by solving the above equation for u . Equivalently, this is given by replacing y^r in (4.6) by y_d^r . It follows that, by implementing the control law, the desired trajectory can be tracked perfectly, i.e., $y(t) = y_d(t)$ for all $t \geq 0$.

The tracking error equation above is of order r . In most cases $r \leq n$, and the tracking error equation accounts only for a part of the dynamics of the closed-loop system. The effect of this is to render part of the process dynamics unobservable from an input-output point of view. This part of the system dynamics is called the **internal dynamics** of the system, because the input-output relationship provides no information about the behavior of the states representing the internal dynamics of the system. The control is successful only if the internal dynamics are stable. Stability of the system representing the internal dynamics can be obtained by defining the **zero dynamics** of the system. The zero dynamics are an intrinsic feature of nonlinear systems and are defined as the internal dynamics, when the process output is kept at its desired value by the input.

Information about internal stability of the process (i.e., whether all the process states of that part of the system representing the internal dynamics, also approach their desired trajectories), can be obtained from a stability analysis of the zero dynamics of the process. Systems with asymptotically stable zero dynamics are said to be **minimum-phase systems**. Next we outline the method for obtaining the zero dynamics of a system.

Generalization of the analysis, for obtaining the zero dynamics is possible by working in transformed co-ordinates. Since $L_{\mathbf{f}}^k h(\mathbf{x}_{\mathbf{p}})$, $k = 0, \dots, r-1$ are linearly independent functions, we can choose these to be the first r elements in defining a transformed co-ordinate system \mathbf{z} , i.e.,

$$z_k = L_{\mathbf{f}}^{k-1} h(\mathbf{x}_{\mathbf{p}}) \quad k = 1, 2, \dots, r$$

It is also possible to define $(n-r)$ additional co-ordinates, $z_k = \phi_k(\mathbf{x}_{\mathbf{p}})$, $k = (r+1), \dots, n$, such that their time derivatives are independent of u [46, 64]. These additional co-ordinates can be obtained from the $(n-1)$ solutions $w(\mathbf{x})$ of the partial differential equation

$$g_1(\mathbf{x}_{\mathbf{p}}) \frac{\partial w}{\partial x_{p1}} + g_2(\mathbf{x}_{\mathbf{p}}) \frac{\partial w}{\partial x_{p2}} + \dots + g_n(\mathbf{x}_{\mathbf{p}}) \frac{\partial w}{\partial x_{pn}} = 0$$

The $(n-1)$ solutions to the above partial differential equation are obtained by defining

$$x_{p,i+1} = \psi_i(x_{p1}, \zeta_1, \dots, \zeta_{n-1}), \quad i = 1, \dots, n-1 \quad (4.7)$$

to be the solution of

$$\frac{dx_{pi}}{dx_{p1}} = \frac{g_i(\mathbf{x}_{\mathbf{p}})}{g_1(\mathbf{x}_{\mathbf{p}})}, \quad x_{pi}(0) = \zeta_i, \quad i = 2, \dots, n$$

Then the equations in (4.7) above, are solvable for $\zeta_1, \dots, \zeta_{n-1}$, i.e.,

$$\zeta_i = \phi_i(\mathbf{x}_{\mathbf{p}})$$

Further, the scalar fields $z_k = \phi_k(\mathbf{x}_{\mathbf{p}})$, $k = 1, 2, \dots, (n-r)$ thus obtained, are linearly independent and satisfy the above partial differential equation.

In the \mathbf{z} co-ordinates, the SISO nonlinear system can be represented in its **normal form**

$$\begin{aligned} \dot{z}_1 &= z_2 & \dot{z}_{r+1} &= q_{r+1}(\mathbf{z}) \\ \vdots & & \vdots & \\ \dot{z}_r &= \bar{b}(\mathbf{z}) + \bar{a}(\mathbf{z})u & \dot{z}_n &= q_n(\mathbf{z}) \\ y &= z_1 \end{aligned}$$

where

$$\begin{aligned} \bar{a}(\mathbf{z}) &= L_{\mathbf{g}} L_{\mathbf{f}}^{r-1} h[\phi^{-1}(\mathbf{z})], \quad \bar{b}(\mathbf{z}) = L_{\mathbf{f}}^r h[\phi^{-1}(\mathbf{z})] \quad \text{and} \\ q_k(\mathbf{z}) &= L_{\mathbf{f}} \phi_{k+r}[\phi^{-1}(\mathbf{z})] \quad k = 1, \dots, (n-r) \end{aligned}$$

A minimal-order realization of the inverse (MORI) of the system is obtained by replacing u in the normal form above by (4.6), after a suitable change of co-ordinates. The advantage of using the normal form representation of nonlinear SISO system is that its inverse is effectively of dimension $(n - r)$. The zero dynamics of a system are defined as the dynamics of a MORI. As mentioned earlier, they represent the internal system dynamics when the process output is constrained to be the desired output. The dynamical system representing the internal dynamics of the system is given by the last $(n - r)$ equations of the normal form.

Before showing the equivalence of synchronization and control with examples, we explain how the three types of synchronization, result from consideration of the control problem. Examples are presented in the next section to show that synchronization is another interpretation of perfect control when $r = 1$.

The synchronization technique proposed by Pecora and Carroll[37] results from the case when both the desired and measured outputs are states ($y_d = x_{mi}$ and $y = x_{pi}$, for an $i \in (1, n)$). GS[39, 40] results from considering the desired output as a function of states $y_d = h_1(\mathbf{x}_m)$ and $y = h_2(\mathbf{x}_p) = x_{pi}$, $1 \leq i \leq n$. For the case of synchronization using the APD technique, we rewrite one of the system variables (after neglecting the subscripts) as

$$\dot{x}_i = f_i(\mathbf{x}) + g_i(\mathbf{x})u + e(\mathbf{x}) - e(\mathbf{x})$$

where $e(\mathbf{x})$ is an arbitrary function of the states \mathbf{x} . We can define a new variable x_{n+1} , as the complete (or part of) function $f_i(\mathbf{x}) + g_i(\mathbf{x})u + e(\mathbf{x})$. Further, we can represent the evolution of this new variable by an arbitrary equation, containing a new input u_{new} . The model and process can now be represented by equations of the form

$$\begin{aligned}\dot{\mathbf{x}} &= \bar{\mathbf{f}}(\mathbf{x}) + \bar{\mathbf{g}}(\mathbf{x})x_{n+1} - \mathbf{e}(\mathbf{x}) \\ x_{n+1} &= f_i(\mathbf{x}) + g_i(\mathbf{x})u + e(\mathbf{x}) \\ \dot{x}_{n+1} &= d(\mathbf{x}) + u_{new}\end{aligned}$$

Now consider the case where the desired and process output are given by $y_d = x_{m,n+1}$ and $y = x_{p,n+1}$, and the manipulated input is u_{new} . Perfect control, for this case, is the control analog of synchronization using APD. From the point of view of synchronization, the exact functional form of $d(\mathbf{x})$ is not required since the desired trajectory

$y_d = x_{m,n+1}$, is directly obtained from a knowledge of the model states \mathbf{x}_m . Several examples of this case can be found in Table 1 of Parlitz *et al.*[42].

4.3 Results and Discussion

In this section we demonstrate the connection between perfect control and synchronization with the help of an example. The Rossler system is one of the extensively studied models in the nonlinear dynamics literature. Further, different aspects of chaotic synchronization of this system have been studied[37, 38, 42]. For these reasons, we have considered this system in this work. Our objective will be design the controller such that the process output tracks the the desired output exactly. This enables us to show the equivalence between the three different types of synchronization and perfect control of a process of relative order one. As mentioned in the previous section, we consider that the reference system models the process system exactly. We represent the reference system (system 1) and the process (system 2) as

$$\dot{X}_1 = -Y_1 - Z_1 \quad (4.8) \quad \dot{X}_2 = -Y_2 - Z_2 + p_1 \quad (4.11)$$

$$\dot{Y}_1 = X_1 + aY_1 \quad (4.9) \quad \dot{Y}_2 = X_2 + aY_2 + p_2 \quad (4.12)$$

$$\dot{Z}_1 = b + Z_1(X_1 - c) \quad (4.10) \quad \dot{Z}_2 = b + Z_2(X_2 - c) + p_3 \quad (4.13)$$

The system parameters a , b and c are taken to be the same for both the systems. We have chosen $a = b = 0.20$ and $c = 9$ for our studies. The system exhibits chaotic behavior for these values of the parameters. We have introduced p_1 , p_2 and p_3 as additively occurring auxiliary inputs in the process system. These are used as the manipulated inputs for achieving the control objective. We also assume that only one of the auxiliary inputs (p_1, p_2, p_3) is non-zero. This is the manipulated input.

Consider the case where $y = X_2$, $u = p_1$ (with $p_2 = p_3 = 0$) and $y_d = X_1$. The manipulated input p_1 occurs in the governing differential equation of the controlled output X_2 and hence $r = 1$. For perfect control, we require that $y = y_d$ for $t \geq 0$. This means that at $t = 0$, we require $X_2 = X_1$. The control law for tracking the desired trajectory y_d is

$$u = p_1 = \dot{y}_d - (-Y_2 - Z_2) \quad (4.14)$$

Substituting this back in the equations of the process (4.11)-(4.13), we get

$$\dot{X}_2 = \dot{y}_d \quad (4.15)$$

$$\dot{Y}_2 = y_d + aY_2 \quad (4.16)$$

$$\dot{Z}_2 = b + Z_2(y_d - c) \quad (4.17)$$

Applying the control action computed using the control law (4.14) ensures that the desired output can be tracked exactly, i.e., $y = y_d$ and $X_2 = X_1$, for $t \geq 0$. However, this provides no information about the behavior of the remaining system states, Y_2 and Z_2 . Information about the behavior of these states can be obtained by studying the stability of the internal dynamics of the process system. We now address the issue of internal stability of the process.

The system (4.11)-(4.13) is in its normal form. The co-ordinates z of the system in its normal form are the process system states. Hence the states Y_2 and Z_2 constitute the states of the internal dynamics of this system. The dynamical system representing the internal dynamics is given by (4.12) and (4.13). The zero dynamics are obtained by replacing $y = X_2$ in these equations by y_d (Equations (4.16) and (4.17)). The stability of the zero dynamics can be obtained by carrying out a stability analysis of the zero dynamics of the system. Since the desired trajectory is chaotic, the necessary condition for asymptotic stability of the zero dynamics (Equations (4.16) and (4.17)) is that its Lyapunov exponents must be negative[37]. These were calculated to be +0.20 and -8.87. This indicates that the zero dynamics is unstable (the system is non-minimum phase), and hence the process is not internally stable, i.e., the variables Y_2 and Z_2 do not approach their respective trajectories. This can also be seen by taking the error between the states Y_1 and Y_2 . Defining e_2 to be the error ($Y_1 - Y_2$), we have

$$\dot{e}_2 = a(Y_1 - Y_2) = ae_2$$

This *system*, representing a part of the internal dynamics of the process system, is unstable. The Lyapunov exponent of this part of the internal dynamics is a , i.e., 0.20. The growth of the error e_2 with time is shown in Fig. 4.4.

The set of equations (4.8)-(4.10), (4.16) and (4.17), is identical to the case of X drive in the approach of Pecora and Carroll. This is because the control parameter p_1

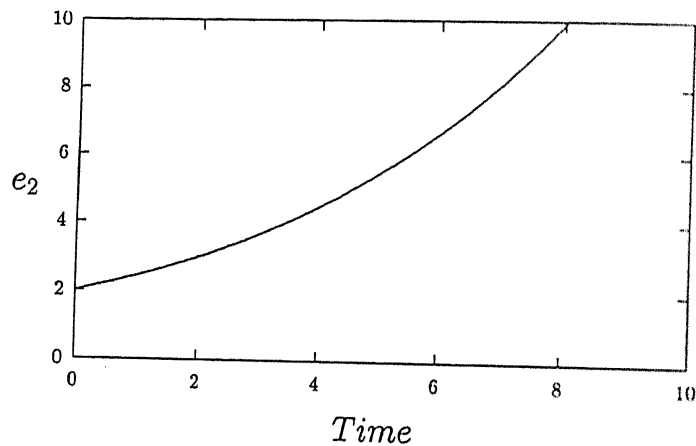


Figure 4.4: Evolution of the state error $e_2 = Y_1 - Y_2$ with time for the case of $y = X_2$, $y_d = X_1$ and $u = p_1$.

occurs only in the equation of the controlled output X_2 . Also the idea of a sub-system defined by them is identical to the notion of MORI (and the zero dynamics) in the control literature. Formulation and solution of the perfect control problem has allowed us to establish that the synchronization considered by Pecora and Carroll is a different interpretation of the perfect control problem.

Synchronization using Y drive and Z drive can be shown to be identical to requesting perfect control of Y_2 using p_2 as the manipulated input and perfect control of Z_2 using p_3 as the manipulated input, respectively. Fig. 4.5 shows the evolution of the errors $e_1 = (X_1 - X_2)$ and $e_3 = (Z_1 - Z_3)$ with time for the case when $y = Y_2$, $y_d = Y_1$ and $u = p_2$ (Y drive). Again, the system (4.11)-(4.13) is in its normal form. The coordinates of the system in its normal form are again the process system states. The states X_2 and Z_2 represent the states of the internal dynamics of the system. For this case, the Lyapunov exponents of the zero dynamics (Equations (4.11) and (4.13)) are negative (-0.024 and -8.8), indicating that the internal dynamics are asymptotically stable. As expected, the process synchronizes with the reference system.

In the above discussion, we have assumed that the model represents the process exactly. This cannot, however, be realised in practice. A mis-match between the systems can occur due to differences in the system parameters a , b and c . Hence it is

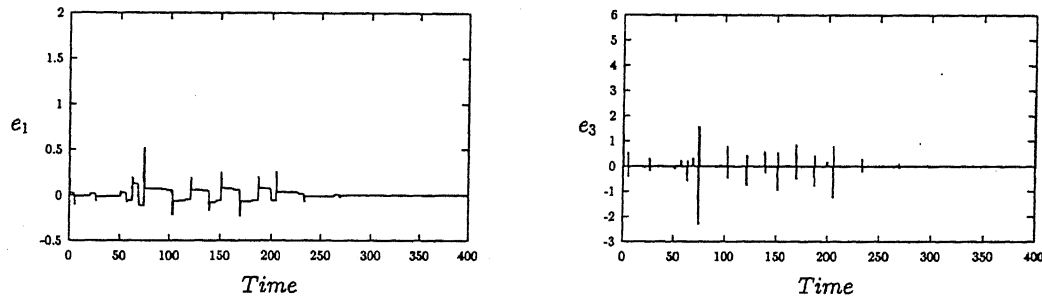


Figure 4.5: Evolution of the state errors $e_1 = (X_1 - X_2)$ and $e_3 = (Z_1 - Z_2)$ with time for the case of $y = Y_2$, $y_d = Y_1$ and $u = p_2$.

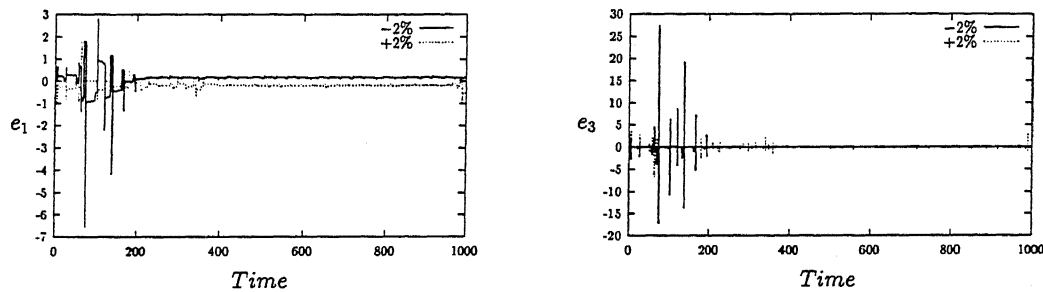


Figure 4.6: Evolution of the error $e_1 = (X_1 - X_2)$ and $e_3 = (Z_1 - Z_2)$ with time for the case of $y = Y_2$, $y_d = Y_1$ and $u = p_2$. Parameter mis-match of $\pm 2\%$ between the model and the process was assumed.

important to study the dynamics of the response system, by considering the effect of parameter mis-match. We illustrate the results for the case of $y = Y_2$, $y_d = Y_1$ and $u = p_2$ (Y drive). Figure 4.6 shows the evolution of the errors $e_1 = (X_1 - X_2)$ and $e_3 = (Z_1 - Z_2)$ when there is a $+2\%$ and -2% mis-match between all the parameters of the model and the process. The reduction in the quality of synchronization is clearly seen from the figure. Some amount of off-set appears to exist for the e_1 component of the error.

Next we show the equivalence between perfect control and GS[40]. We consider the

following control problem

$$y_d = X_1 + Y_1 + Z_1, \quad y = X_2 \quad \text{and} \quad u = p_1$$

This corresponds to synchronization with the driving variable being a function of the states of the drive system. For this case, $r = 1$ and the system (4.11)-(4.13) is in its normal form. As mentioned earlier (discussion following Fig. 4.4), control (synchronization) cannot be obtained with this choice of the output (drive), since the zero dynamics (Equations (4.16) and (4.17)) are unstable. For the Rossler system, it is possible to achieve GS using the same desired output but by considering $y = Y_2$ and $u = p_2$.

For an example of synchronization using the APD technique, we begin by defining a new variable $x_{n+1} = s = 1.2Y_1$. Using this, the Y component of the model (4.8)-(4.13) can be rewritten as

$$\dot{Y}_1 = X_1 - Y_1 + s_1 \quad \text{and} \quad \dot{Y}_2 = X_2 - Y_2 + s_2 \quad (4.18)$$

This new variable is selected such that the response system consisting of the states X_2 , Y_2 and Z_2 , is asymptotically stable. We now assume that the evolution of this new variable is given by an equation of the form

$$\dot{x}_{n+1} = \dot{s} = d(\mathbf{x}) + u_{new} \quad (4.19)$$

where $d(\mathbf{x})$ is an arbitrary function of the states \mathbf{x} . The dynamical system representing the reference and the process systems obtained by incorporating this new variable can then be obtained using the above equations for \dot{Y}_1 and \dot{Y}_2 . The perfect control objective $y = s_2$, $y_d = s_1 = 1.2Y_1$ with $u = p_2$ is the control analog of synchronization using the APD technique. The process system is in its normal form and the equations (4.11), (4.13) and the equation for the evolution of Y_2 given in (4.18), now constitute the dynamical system representing the internal dynamics of the modified system.

We integrate the resulting system of equations by assuming $s_2 = s_1$. This obviates the need to specify the function $d(\mathbf{x})$. Figure 4.7 shows the evolution of the state errors with time. When the model represents the process exactly, the tracking error goes to zero very rapidly. This is shown in Fig. 4.7(a). However the performance of the

designing a nonlinear controller for a system of relative order greater than one, i.e., we consider perfect control of the process when the manipulated input u , does not directly affect the controlled output y . We illustrate the method by considering X_2 to be the controlled output ($y = X_2$ and $y_d = X_1$) and p_2 to be the manipulated input ($u = p_2$). An explicit relationship between the input and the output can be obtained after performing two differentiation operations on the output. Hence we have $r = 2$ for this case. Proceeding as described in the previous section, the control law is obtained as

$$u = p_2 = -\ddot{y}_d - \dot{Z}_2 - y_d - aY_2 \quad (4.20)$$

Substituting the control law back into the equations describing the process (4.11)-(4.13), we get

$$\dot{X}_2 = \dot{y}_d = \dot{X}_1 \quad (4.21)$$

$$\dot{Y}_2 = -\ddot{y}_d - \dot{Z}_2 = \dot{Y}_1 + \dot{Z}_1 - \dot{Z}_2 \quad (4.22)$$

$$\dot{Z}_2 = b + Z_2(y_d - c) \quad (4.23)$$

Requiring perfect control on initiating the process setting $X_2 = X_1$ ($y = y_d$) at $t = 0$ requires that $\dot{X}_2 = \dot{X}_1$ for $t \geq 0$. On rearranging, this yields: $Y_2 = -\dot{y}_d - Z_2$. This implies that manipulating p_2 in order to make X_2 track X_1 , constrains Y_2 to evolve such that the above relation is satisfied. Hence it is only possible to achieve perfect control if at $t = 0$, $Y_2 = -\dot{y}_d - Z_2$. The co-ordinates z of the process system in its normal form are related to the actual co-ordinates by the relations

$$z_1 = X_2, \quad z_2 = -Y_2 - Z_2, \quad z_3 = Z_2$$

The normal form of the system is represented by the following system of equations

$$\dot{z}_1 = z_2, \quad \dot{z}_2 = \bar{b}(z) + \bar{a}(z)p_2 \quad \text{and} \quad \dot{z}_3 = q(z)$$

$$\text{where } \bar{a}(z) = 1, \quad \bar{b}(z) = z_1 + a(-z_2 - z_3), \quad \text{and} \quad q(z) = b + z_3(z_1 - c)$$

The internal stability of the process is now dependent on the asymptotic stability of the zero dynamics, given by (4.23). This system has a negative Lyapunov exponent equal to -8.87 , indicating that synchronization between the process and the reference system

	p_1	p_2	p_3
X_2	0.20 -8.87	-8.87	0.20
Y_2	-8.87	-0.024 -8.8	
Z_2	0.20		0.10 0.10

Table 4.1: Lyapunov exponents of the zero dynamics for the process system for different control configurations of the Rossler system.

can be obtained using feedback control. The evolution of the error $e_3 = (Z_1 - Z_2)$ with time is similar to that shown in Fig. 4.5.

Lyapunov exponents of the zero dynamics for each combination of the input-output (output=state) are given in Table 4.1(a). These are analogous to the conditional Lyapunov exponents of [37, 38]. The diagonal cases correspond to synchronization using X , Y and Z drives in the approach of Pecora and Carroll. Non-diagonal cases for which we have only one Lyapunov exponent can be considered to be similar to synchronization with a two variable drive in the approach of Pecora and Carroll [37, 38]. The absence of zero dynamics for the $Y_2 - p_3$ and $Z_2 - p_2$ configurations indicates that the Lyapunov exponents are equal to zero, for these cases [63]. The implication of this is that in order to achieve perfect control with these combinations of the input and the output, we need to fix all the initial states of the process.

4.4 Conclusions

In conclusion, we have presented a nonlinear control technique, to achieve perfect control of a system along a desired trajectory. An important result of this work is that it connects the idea of perfect control, with the synchronization phenomenon discussed in the physics literature. In this connection, we have presented results from the control literature, to show that chaotic synchronization can be analysed within the framework

of nonlinear control theory.

Several methods have been proposed in the literature for the control of chaotic systems[65]. Very little attention has been given to providing a theoretical basis for most of these techniques. Also very little attention has been given to applying the results from conventional control theory to the problem at hand. The need therefore, appears to point towards applying results from control theory, to provide the theoretical framework for several of the methods proposed in the physics literature. This can also result in a common theoretical framework of techniques for control of chaotic systems. An advantage of this could be that a technique suitable for the problem at hand, could then be selected from the different options available.

Chapter 5

Synchronization and Control of Non-Minimum Phase Systems

Nomenclature

\bar{a}	Constant in Equations (5.17) and (5.30).
k	Dimensionless reaction rate constant for the autocatalytic reaction.
t	Time.
u	Manipulated input.
w	State of the exo-system.
\mathbf{x}_m	States of the reference system.
\mathbf{x}_p	States of the process system.
y	Process output.
y_d	Desired or reference output.
β	Dimensionless feed concentration of B in the CSTR.
τ	Dimensionless characteristic time in the CSTR.

5.1 Introduction

In the previous chapter, we illustrated how results from nonlinear control theory can be employed to show the equivalence between synchronization of chaos and perfect control of a system along a desired trajectory. We also saw that not all systems can be

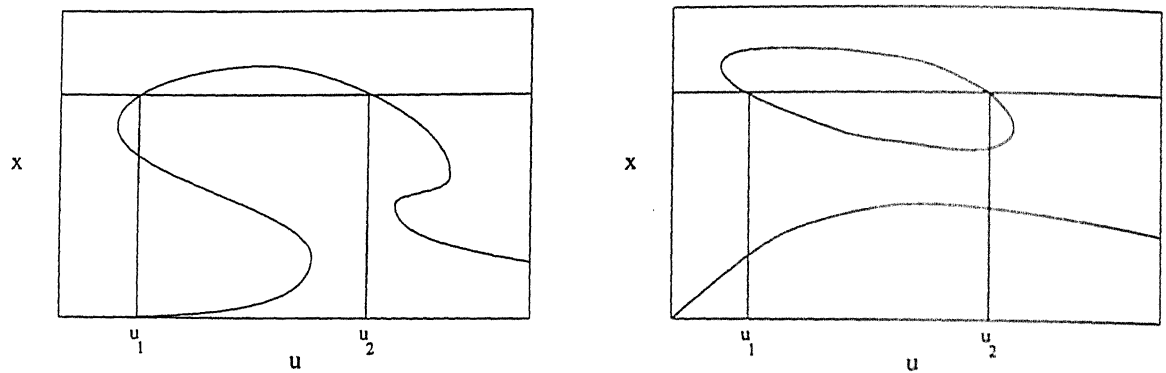


Figure 5.1: Schematic bifurcation diagrams for system showing input multiplicity.

synchronized using the approach of Pecora and Carroll. An example of such a situation is when we use the X drive of the Rossler system[37, 38]. As we saw in the previous chapter, it is not possible to achieve with this drive since the zero dynamics of the system for this choice of the output (X) and the input p_1 is unstable. Systems with unstable zero dynamics are classified as non-minimum phase systems in the control literature.

An important class of non-minimum phase systems of importance in chemical engineering are the systems exhibiting input multiplicity[43–45]. In these systems, it is possible to have more than one possible value of the control input, for a given value of the output. Figure 5.1 shows a schematic representation of two typical steady-state bifurcation diagrams for such systems. For the desired choice of the controlled output x (denoted by the horizontal line), we have two possible choices u_1 and u_2 of the manipulated input u . Unmeasured disturbances acting on the plant can destabilize the controlled system from its original set-point (at u_1) and cause the system to reach the other steady-state (at u_2). Though the controlled output has the same value for each of these inputs, the values of the process states, corresponding to the value of the input u_2 will be different from the desired values.

In recent years, there have been major developments in the application of nonlinear control techniques based on differential-geometry for the control of chemical engineering systems[36, 62, 63]. Experimental and computational studies have been carried out to

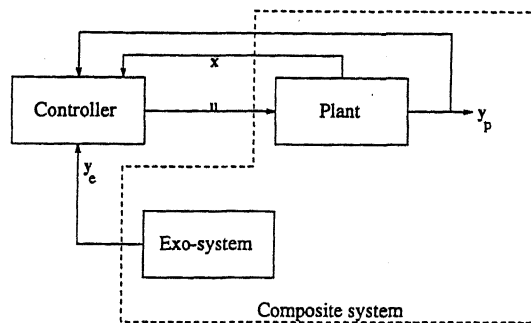


Figure 5.2: Schematic diagram of the feedback control strategy for regulating the output of a nonlinear system.

develop and test a variety of techniques. A limitation of most of these techniques is that they are valid only for systems with stable zero dynamics, i.e., for minimum-phase systems. Hence they are of limited use for the control of systems which can exhibit input multiplicity. Recently Isidori and Byrnes[47] have developed a technique for the regulating the output of nonlinear systems. Their method is based on bifurcation theory and is suitable for the control of non-minimum phase systems.

Their technique is aimed at controlling a nonlinear system (plant) in order to have its output track a reference signal generated by an external system (exo-system)[46, 47]. The technique involves considering a composite system consisting of the plant and the exo-system (Fig. 5.2). The exo-system is selected such that its linearization has all eigenvalues on the imaginary axis. This choice ensures that the composite system has at least one eigenvalue on the imaginary axis. Such a choice of the exo-system guarantees the existence of a center manifold for the composite system. Isidori and Byrnes show that the regulator problem can be solved by selecting the feedback control law, such that the center manifold is rendered invariant, i.e., the trajectories which begin on this manifold, remain on it for all time. Once the center manifold of the composite system has been computed, a choice of the feedback control law is made such that this center manifold is rendered invariant. Selecting such a control law causes the output of the composite system to be zero at each point on the center manifold, thereby ensuring that the plant output is regulated. The only necessary condition for the solution of the

regulator problem is that the plant be exponentially stabilizable by feedback.

In the first part of this chapter, we describe how this technique can be used to formulate and solve the control problem. In the second part of this chapter, we apply the technique to achieve synchronization of the Rossler system along a desired chaotic trajectory. We employ the technique to track a reference chaotic trajectory. Finally, we consider the cubic autocatalytic reaction in an isothermal CSTR[8]. We apply the method for the control of this reactor system which shows input multiplicity.

5.2 Description of the Method

We consider the SISO nonlinear process and the exo-system to be given by the following system of equations

$$\dot{\mathbf{x}} = \mathbf{f}(\mathbf{x}) + \mathbf{g}(\mathbf{x})u \quad (5.1)$$

$$\dot{w} = s(w) \quad (5.2)$$

The overdot indicates differentiation with respect to time. The first equation describes the plant with state \mathbf{x} and input u . The second equation describes the scalar exo-system. $\mathbf{f}(\mathbf{x})$ and $\mathbf{g}(\mathbf{x})$ are vector functions. An equation relating the error e_{pe} between the actual plant output $y = h(\mathbf{x})$ and the reference trajectory $y_d = q(w)$ can be represented as

$$e_{pe} = h(\mathbf{x}) - q(w) \quad (5.3)$$

It is desired to design the controller such that the error $e_{pe} \rightarrow 0$ as $t \rightarrow \infty$. Finally we assume that $(\mathbf{x}, w) = (0, 0)$ is an equilibrium of the system.

The problem of designing a state feedback controller for the plant involves determining a control law of the form

$$u = \alpha(\mathbf{x}, w) \quad (5.4)$$

such that

- The closed-loop system has an asymptotically stable equilibrium at $\mathbf{x} = 0$ when the exo-system is disconnected, i.e., when $w = 0$.

- For all initial conditions $\mathbf{x}(0), w(0)$ sufficiently close to the origin, $e_{pe}(t) \rightarrow 0$ as $t \rightarrow \infty$.

The method proposed by Isidori and Byrnes[47] for constructing the solution to the regulator problem is based on the following assumptions.

1. $w = 0$ is a stable equilibrium of the exo-system. This restricts the choice of the exo-system, to only those systems whose linear approximation at $w = 0$ has all eigenvalues on the imaginary axis. Selecting a stable exo-system ensures that $w \rightarrow 0$ as $t \rightarrow \infty$.
2. The pair $\mathbf{f}(\mathbf{x}), \mathbf{g}(\mathbf{x})$ has a stabilizable linear approximation at $\mathbf{x} = 0$, i.e., if the linearization of the nonlinear system (5.1), (5.2) is given by

$$\begin{aligned}\dot{\mathbf{x}} &= \mathbf{A}\mathbf{x} + \mathbf{B}u \\ \dot{w} &= Sw\end{aligned}$$

where $\mathbf{A} = \frac{\partial \mathbf{f}}{\partial \mathbf{x}}|_{\mathbf{x}=0}$, $\mathbf{B} = \mathbf{g}(0)$ and $S = \frac{\partial s}{\partial w}$. There exists a matrix \mathbf{K} such that all the eigenvalues of the matrix $\mathbf{A} + \mathbf{BK}$ have negative real parts.

Assumption 1 above implies that the composite system, consisting of the given system and the exo-system, has atleast one eigenvalue on the imaginary axis. Under these conditions, the composite system has a center manifold at $(0, 0)$, given by the graph of the mapping $\mathbf{x} = \pi(w)$. Isidori and Byrnes[47] prove that the regulator problem can be solved, if and only if there exists a mapping $\mathbf{x} = \pi(w)$ with $\pi(0) = 0$ and $\pi'(0) = 0$, satisfying the conditions

$$\frac{\partial \pi}{\partial w} s(w) = \mathbf{f}(\pi(w)) + \mathbf{g}(\pi(w))\alpha(\pi(w), w) \quad (5.5)$$

$$h(\pi(w)) + q(w) = 0 \quad (5.6)$$

Computing the functions $\pi(w)$ involves solving the above partial differential equation. It is not possible to obtain an exact solution in many cases. An approximation of the solution can be obtained by seeking the solution in the form of a power series[66]

$$\pi(w) = c_1 w^2 + c_2 w^3 + c_3 w^4 + \dots$$

The polynomial coefficients are determined by equating terms of the same order on the left and right hand sides.

Existence of the mapping $\mathbf{x} = \pi(w)$ is a direct consequence of the existence of a center manifold for the composite system. The feedback control law is then determined such that trajectories starting on this center manifold remain in it for all time, i.e., this center manifold is rendered invariant. Thus our objective is to find the feedback law such that the output e_{pe} of the composite system is zero at each point on the center manifold.

The solution of the state-feedback regulator problem (SFRP) is given by a feedback law of the form

$$\alpha(\mathbf{x}, w) = \bar{c}(w) + K(\mathbf{x} - \pi(w)) \quad (5.7)$$

It can be shown that $\bar{c}(w) = \alpha(\pi(w), w)$ [47]. The second part of the control law is required, to bring the trajectories beginning away from the center manifold, on to it. Once this has been achieved, the first part of the feedback law ensures that the plant tracks the reference signal exactly.

5.3 Results and Discussion

We now illustrate the applicability of the method on the Rossler system. Figure 4.2 shows a schematic diagram of the feedback control problem. System 1 is a model whose output y_d generates the desired (reference) behavior of the process. System 2 represents the actual process having an output y . We assume that the model represents the process exactly. The only difference between the two systems, is in the initial conditions of the state variables \mathbf{x}_m and \mathbf{x}_p respectively. The process cannot follow the desired trajectory in the absence of feedback, because of the chaotic nature of evolution of the system. It is desired to match (synchronize) the evolution of the controlled process output along its desired trajectory as time $t \rightarrow \infty$ using state feedback. Additionally, we require stability of the closed-loop system when the control loop is implemented.

At the moment, the control problem mentioned above is in a different form compared to the regulator problem (Fig. 5.2) discussed in the previous section. Therefore, in comparison with the previous chapter, we adopt a slightly different approach for regulating the chaotic output of the Rossler system. We work with a model obtained by

taking the error between the corresponding process states \mathbf{x}_p and the reference systems states \mathbf{x}_m . The model in this form will be referred to as the plant. The variables in the model of the plant are the state errors $\mathbf{e} = \mathbf{x}_m - \mathbf{x}_p$. In the absence of any control action, the error model has an unstable zero solution, consistent with the chaotic nature of evolution of the original system. Our objective will be to control this nonlinear system (the plant), in order to have its output y_p track a time-varying reference signal y_e generated by the exo-system. The exo-system is selected such that it has a stable zero solution. When the control action is successful, the states \mathbf{e} of the plant go to zero. This causes the actual states \mathbf{x}_p of the process to track their respective desired trajectories \mathbf{x}_m .

The Rossler system is represented by the following set of equations

$$\dot{X} = -Y - Z \quad (5.8)$$

$$\dot{Y} = X + aY \quad (5.9)$$

$$\dot{Z} = b + Z(X - c) \quad (5.10)$$

Here a , b and c are constant parameters. Throughout this work, we assume $a = b = 0.20$ and $c = 9.0$. As explained in the previous chapter, we represent the reference system (system 1) and the process system (system 2) with the following set of equations

$$\dot{X}_1 = -Y_1 - Z_1 \quad (5.11) \quad \dot{X}_2 = -Y_2 - Z_2 + u \quad (5.14)$$

$$\dot{Y}_1 = X_1 + aY_1 \quad (5.12) \quad \dot{Y}_2 = X_2 + aY_2 \quad (5.15)$$

$$\dot{Z}_1 = b + Z_1(X_1 - c) \quad (5.13) \quad \dot{Z}_2 = b + Z_2(X_2 - c) \quad (5.16)$$

We illustrate the case where the controlled output is a function of a single state. We consider X_2 to be the process output and u represents the manipulated input. As explained earlier in this section, implementation of the technique described in the previous section is facilitated by recasting the equations (5.11)-(5.16) in error form. These result in equations with state variables are the errors between the corresponding states of the reference system (system 1) and the process (system 2). We define the following set of variables

$$e_1 = X_1 - X_2, \quad e_2 = Y_1 - Y_2, \quad e_3 = Z_1 - Z_2$$

The state equations of the plant in the error form are given by

$$\dot{e}_1 = -e_2 - e_3 - u \quad (5.17)$$

$$\dot{e}_2 = e_1 + ae_2 \quad (5.18)$$

$$\dot{e}_3 = e_3(X_1 - c) + e_1(Z_1 - e_3) \quad (5.19)$$

This dynamical system representing the nonlinear plant has an equilibrium point at $(0, 0)$. The dynamics of the exo-system are assumed to be governed by the following equation

$$\dot{w} = \bar{a}w^3, \quad \bar{a} < 0 \quad (5.20)$$

The plant output (in error form) and the reference output are given by (Equation (5.3))

$$h(\mathbf{x}) = e_1 \quad (5.21)$$

$$q(w) = -w^2 \quad (5.22)$$

The control objective now is to track the time varying reference signal from the exo-system such that the error $e_{pe} = (e_1 - w^2) \rightarrow 0$ as $t \rightarrow \infty$. The exo-system has been selected such that it has a stable zero solution and the objective is to apply suitable control action in order to stabilize the zero solution of the plant. This would then ensure that the process tracks the reference trajectory.

The linearized form of the composite system comprising of the plant and the exo-system has one zero eigenvalue. Hence this system has a center manifold, which is the graph of the mapping $\mathbf{e} = \pi(w)$. The functions $\pi(w)$ are evaluated by employing the center manifold theorem. These functions are obtained by solving the partial differential equations (5.5). Computing the functions $\pi(w)$ involves solving the partial differential equations. Instead we approximate the solution assuming the solution to be of the form

$$\pi(w) = c_1w^2 + c_2w^3 + c_3w^4 + c_4w^5$$

Setting the error of the composite system equal to zero, we obtain the first component of $\pi(w)$ to be $e_1 = \pi_1(w) = w^2$. The other two components of $\pi(w)$ are obtained by solving the partial differential equations as explained in the previous section. The coefficients of the polynomial approximation are given by

$$e_2 = \pi_2(w) : \quad c_1 = \frac{-1}{a} \quad c_2 = 0$$

$$c_3 = \frac{2\bar{a}c_1}{a} \quad c_4 = 0$$

$$e_3 = \pi_3(w) : \quad c_1 = \frac{-Z_1}{X_1 - c} \quad c_2 = 0$$

$$c_3 = \frac{c_1 + 2\bar{a}c_1}{X_1 - c} \quad c_4 = 0$$

The feedback control law which solves the regulator problem is now given by

$$u = \alpha(x, w) = \bar{c}(w) + k_1(e_1 - w^2) + k_2(e_2 - \pi_2(w)) + k_3(e_3 - \pi_3(w)) \quad (5.23)$$

$$\bar{c}(w) = -2w\dot{w} - \pi_2(w) - \pi_3(w) \quad (5.24)$$

We integrated the system (5.11)-(5.16) using the above control law. Results of the simulations are shown in Figs. 5.3(a)-(e). Fig. 5.3(a) and 5.3(b) show the variation in the error components $e_1 = X_1 - X_2$, $e_2 = Y_1 - Y_2$ and $e_3 = Z_1 - Z_2$ with time respectively. Evolution of the differences $(e_1 - w^2)$, $(e_2 - \pi_2(w))$ and $(e_3 - \pi_3(w))$ with time is shown in Fig. 5.3(c) and 5.3(d) respectively. It can be seen that the evolution of the error between the system states corresponds to the evolution of the exo-system, thus rendering the center manifold invariant. The evolution of the control variable u is shown in Fig. 5.3(e).

In the previous chapter our objective was to design a controller for controlling the process output along a desired chaotic trajectory. As we saw in that chapter, tracking was successful only when the zero dynamics of the system were asymptotically stable. The controller design discussed in this chapter is based on a more stringent requirement. Here, It is desired to design the controller for tracking the reference output, but with the additional requirement of an asymptotically stable linearized form of the closed-loop system. This is reflected in the form of the control law, which consisted of two distinct

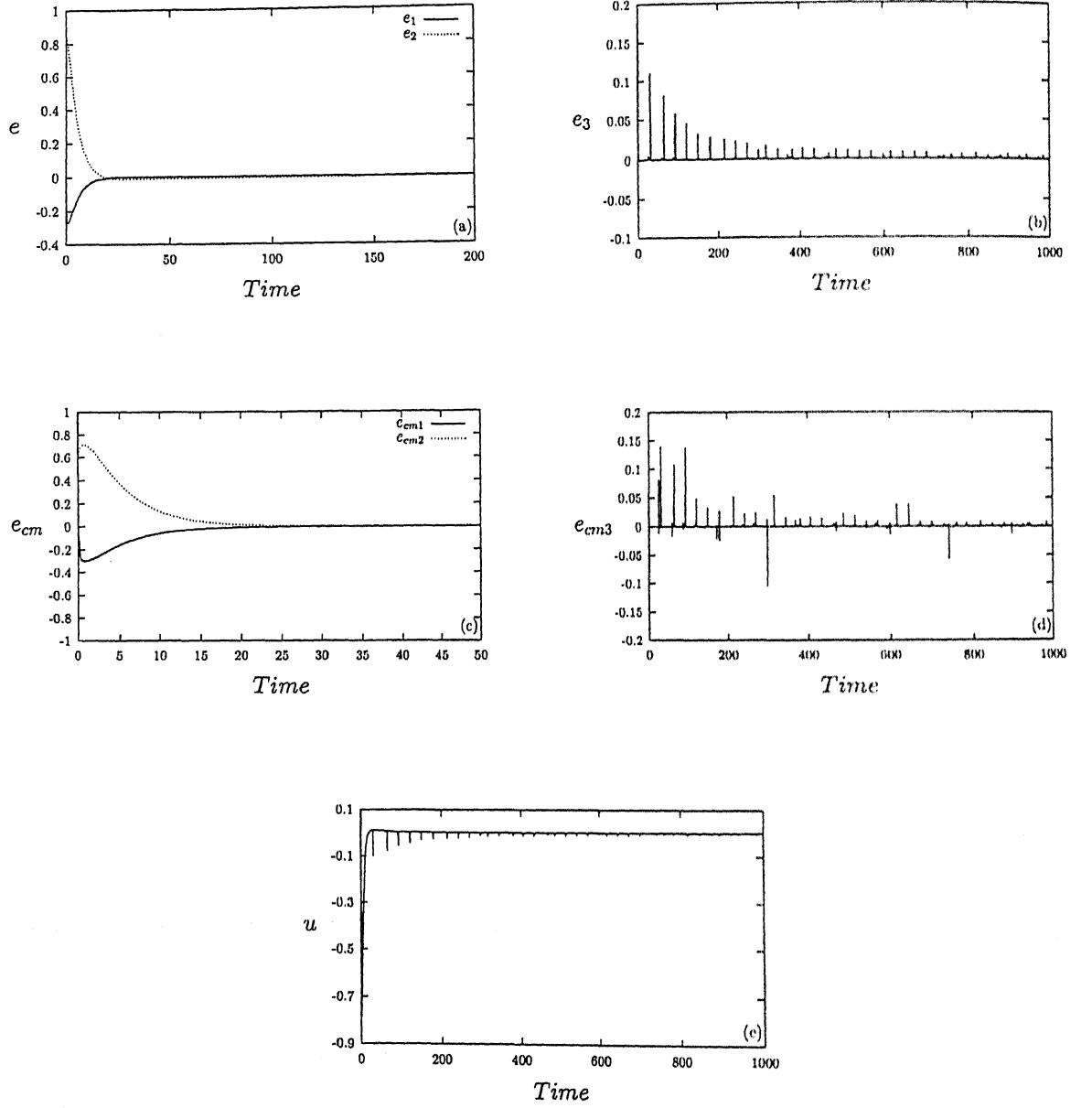


Figure 5.3: Evolution of the errors and the manipulated variable with time. (a): $e_1 = (X_1 - X_2)$ and $e_2 = (Y_1 - Y_2)$; (b): $e_3 = (Z_1 - Z_2)$; (c): $e_{cm1} = (e_1 - \pi_1(w))$ and $e_{cm2} = (e_2 - \pi_2(w))$; (d): $e_{cm3} = (e_3 - \pi_3(w))$; (e) u . $\bar{a} = -1$, $k_1 = 12$, $k_2 = 4$ and $k_3 = -1$ in (5.24).

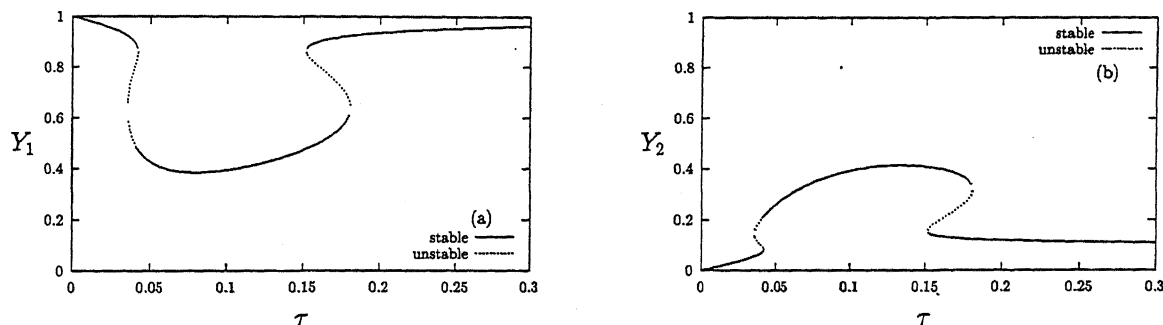
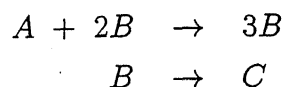


Figure 5.4: Steady-state bifurcation diagram depicting the dependence of the steady-states of (a) Y_1 and (b) Y_2 on τ .

parts (Equations (5.7) and (5.23)). The first part of the control law ensured tracking of the reference signal, while the second part ensures stability of the the linearized form of the closed-loop system.

5.4 An Autocatalytic Reaction in a CSTR

We now consider the cubic autocatalysis reaction with decay[8]



in an isothermal CSTR. The dimensionless mass balance equations for the species A and B respectively are given by

$$\dot{Y}_1 = \tau(1 - Y_1) - Y_1 Y_2^2 \quad (5.25)$$

$$\dot{Y}_2 = \tau(\beta - Y_2) + Y_1 Y_2^2 - k Y_2 \quad (5.26)$$

The overdot indicates differentiation with respect to time. The dimensionless parameters are defined as follows: τ is a dimensionless characteristic time of the system, β is the dimensionless feed concentration of species B and k is a dimensionless reaction rate constant. In this study, we fix $\beta = 0.10$ and $k = 0.080$. The dependence of the steady-states of Y_1 and Y_2 on τ is shown in Fig. 5.4.

There are two regions of τ where multiple steady-states occur. However, the region of interest to us, is the region where operating the reactor at two values of τ (the control input), gives the same steady-state value of the controlled output (Y_1 or Y_2). In this section our objective will be to design a nonlinear controller to stabilize the system at its desired steady-state. As mentioned in the first section of this chapter, several differential-geometry control techniques are of limited usefulness in such situations where the system can be non-minimum phase for the given choice of the controlled output.

For ease of application of the method described in section 5.2, we rewrite the above equations in deviation form, by defining new variables X and Y as follows

$$X = X_s - Y_1, \quad Y = Y_s - Y_2$$

Here, X_s and Y_s represent the desired steady states of the system. In the new coordinates, the model equations (5.25) and (5.26) are given by

$$\dot{X} = -\tau(1 + X - X_s) - (X_s - X)(Y_s - Y)^2 \quad (5.27)$$

$$\dot{Y} = -\tau(\beta + Y - Y_s) - (X_s - X)(Y_s - Y)^2 + k(Y_s - Y) \quad (5.28)$$

We again select the exo-system as

$$\dot{w} = \bar{a}w^3, \quad \bar{a} = -10.0 \quad (5.29)$$

It is desired to control the system (5.27)-(5.28) at its steady state $X = Y = 0$. The parameter τ is the control parameter. In the first case, we consider X to be the controlled output. Therefore, we have (Equation 5.3)

$$h(\mathbf{x}) = X, \quad q(w) = -w^2$$

Setting the error of the composite system equal to zero, we obtain the first component of $\pi(w)$ to be $X = \pi_1(w) = w^2$. The other component of $\pi(w)$ is obtained by solving the partial differential equations as explained in the previous section. We choose

$$Y = \pi_2(w) = c_1w^2 + c_2w^3 + c_3w^4 + c_4w^5$$

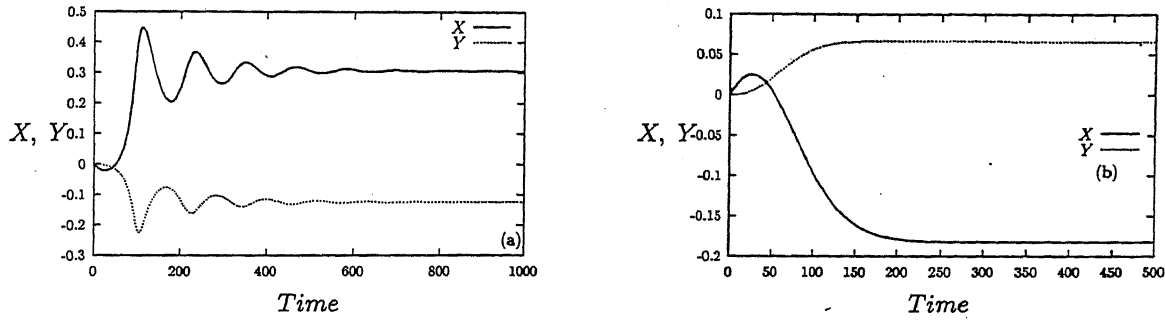


Figure 5.5: Response of the system states X and Y to a (a) +10% change and (b) -10% change in the input τ .

The coefficients in the above polynomial can be calculated to be

$$c_1 = \frac{Y_s^2(\beta - Y_s + 1 - X_s) - X_s Y_s^2 + k Y_s}{X_s Y_s^2 - 2X_s Y_s(\beta - Y_s + 1 - X_s) + k(1 - X_s)}$$

$$c_3 = \frac{-2c_1 Y_s(\beta - Y_s + 1 - X_s) - X_s c_1^2(\beta - Y_s + 1 - X_s) + Y_s^2 + c_1 Y_s^2 + 2X_s Y_s c_1 + 2X_s Y_s c_1^2 - k c_1 - 2\bar{a} c_1(1 - X_s) + 2\bar{a}(\beta - Y_s)}{X_s Y_s^2 + k(1 - X_s) - 2X_s Y_s(\beta - Y_s + 1 - X_s)}$$

$$\text{and } c_2 = 0, \quad c_4 = 0$$

The feedback control law for regulating the plant output is now given by

$$\tau = \alpha(\mathbf{x}, w) = \bar{c}(w) + k_1(X - w^2) + k_2(Y - \pi_2(w)) \quad (5.30)$$

$$\bar{c}(w) = \frac{-2\bar{a}w^4 + (X_s - w^2)(Y_s - \pi_2(w))^2}{(1 + w^2 - X_s)} \quad (5.31)$$

We study the controllability characteristics of this system for $\tau = 0.038$. The system exhibits input multiplicity for this value of τ . We consider the set-point to be the middle steady-state in Fig. 5.4. This corresponds to the steady-state values of $X_s = 0.7576$ and $Y_s = 0.1103$. The response of the system to a $\pm 10\%$ change in the input τ is shown in Fig 5.5.

We compare the results obtained using our output regulation method with those obtained using the input-output linearization procedure of Kravaris and Chung[67]. This technique aims at synthesising a feedback controller such that the input-output map is linearized. The linearization is obtained by seeking a transformed input $v =$

$v(\mathbf{x}, u)$ such that the dependence of plant output y on v is linear, i.e., the input-output relationship can be represented by a linear differential equation of the form

$$\sum_{j=0}^m \beta_j \frac{d^j y}{dt^j} = v \quad (5.32)$$

The conditions for the existence of such a map are discussed by Kravaris and Chung[67]. These developments are based on the techniques discussed in chapter 4.

Such a map which linearizes the relationship between the plant output y and the transformed input v is obtained by (i) multiplying the $(r+1)$ equations (4.5) by β_j , $j = 0, 1, \dots, r$ and (ii) summing the $(r+1)$ equations thus obtained. The transformed input v which linearizes the input-output map is given by

$$v = \beta_0 h(\mathbf{x}) + \beta_1 L_{\mathbf{f}} h(\mathbf{x}) + \dots + \beta_r L_{\mathbf{f}}^r h(\mathbf{x}) + \beta_r L_{\mathbf{g}} L_{\mathbf{f}}^{r-1} h(\mathbf{x}) u \quad (5.33)$$

The dynamics of the $v - y$ system are determined once the constants β_j , $j = 0, 1, \dots, r$, in (5.32) are specified. The transformed input v can be taken to be from an external PI controller which forces the output y to track the desired response y_d . Hence

$$v = K_e \left[(y_d - y) + \frac{1}{\tau_e} \int_0^t (y_d - y) \right] \quad (5.34)$$

Using (5.33) and (5.34), we can obtain the actual nonlinear feedback control law

$$u = \frac{K_e \left[(y_d - y) + \frac{1}{\tau_e} \int_0^t (y_d - y) \right] - \sum_{j=0}^r \beta_j L_{\mathbf{f}}^j h(\mathbf{x})}{\beta_r L_{\mathbf{g}} L_{\mathbf{f}}^{r-1} h(\mathbf{x})} \quad (5.35)$$

The input-output linearizing differential equation (5.32) above, is of order r . In most cases $r \leq n$, and this equation therefore, accounts only for part of the closed-loop dynamics of the process. Control of the system is successful only when the dynamics of the remaining $(n - r)$ states representing the internal dynamics of the system are stable. As discussed in the previous chapter, stability of the internal dynamics is given by the stability of the zero dynamics. Consequently, this technique can be successfully used only for minimum-phase systems.

In the case of the autocatalytic system, our objective is to regulate the system at its steady-state, i.e., at $y_d = 0$. The system is of relative order $r = 1$, since we consider

Output	Case	K_e	τ_e	β_0
X	+20%	5.0	0.25	-100.0
X	-20%	0.80	1.60	-2.0
Y	+20%	5.00	0.50	-10.0
Y	-20%	10.0	2.50	-2.50

Table 5.1: Parameter values. $\beta_1 = 1$, for all cases.

τ to be the manipulated input. For this case, the linearized input-output map is of the form

$$\beta_1 \frac{dy}{dt} = v + \beta_0 y \quad (5.36)$$

The parameters β_0 and β_1 are selected such that the eigenvalues of the system (5.36) are in the left-half plane. Specifying these constants and the parameters K_e and τ_e in (5.34) completely determines the dynamics of the linear $v - y$ system. The actual nonlinear feedback control law is obtained by solving (5.36) and (5.27) or (5.28) for τ . We have used this technique to track changes in the set-point of the system. Table 5.1 gives the values of the parameters used in the simulation studies.

The output regulation technique can be considered to be a general form of the input-output linearization procedure. This is because in the latter, the external system (Equation (5.2)) and the reference output $q(w)$ (Equation (5.3)) are of the form

$$\begin{aligned} \beta_1 \dot{w} &= \beta_0 w + v \\ q(w) &= w \end{aligned}$$

As mentioned earlier, Kravaris and Chung consider v to be an external input controlled by a PI controller. This input can be chosen to be equal to zero. Comparing the above equations with (5.29) and (5.3) respectively, it can be seen that defining the external system to be linear, results in a linear relationship between the input and the output. A disadvantage of this scheme is that it is useful only for the control of minimum-phase systems. Selecting the external system to be nonlinear and such that its linearization has all eigenvalues on the imaginary axis, enables us to employ the center manifold theorem in the design of the controller. Application of this result

Plant output	Case	Magnitude	k_1	k_2
X	SP	+20%	1.0	10.80
X	SP	-20%	1.0	6.0
X	UMD	+15% in β	0.10	6.0
X	UMD	-5% in β	1.0	10.0
X	MD	+15% in β	0.40	5.0
Y	SP	+20%	1.0	0.20
Y	SP	-20%	4.0	0.80
Y	UMD	+20% in β	5.0	0.20
Y	UMD	-5% in β	6.0	0.50
Y	MD	+20% in β	8.0	0.20
Y	MD	-5% in β	6.0	0.50

Table 5.2: Parameter values used in the output regulation technique. SP: Change in set-point; UMD: Unmeasured disturbance; MD: Measured disturbance.

enables us to successfully apply the control technique for the trajectory tracking of non-minimum phase systems.

The response of the system using the input-output linearization procedure of Kravaris and Chung[67], for a $\pm 20\%$ change in the setpoint, is shown in Fig. 5.6. The system is non-minimum phase for the choice of the controlled output. It can be seen from the figures that the system has stabilized at the steady-state corresponding to a non-zero value of Y . In both cases, the manipulated input has stabilized at a value close to 0.17. The response of the system for a $\pm 20\%$ change in the setpoint using the output regulation technique is shown in Fig. 5.7. The values of the parameters k_1 and k_2 used in the simulations are listed in Table 5.1. Applying this control can cause the input τ to be negative. We overcome this by resetting $\tau = 0.38$, whenever $\tau \leq 0$. It is seen from the figures that this resetting affects the evolution of X more than it affects Y .

The response of the system to unmeasured and measured disturbances in β is shown Fig. 5.8 and Fig. 5.9 respectively. In chapter 4, we presented the definition of the relative order of the system with respect to the input. The relative order of

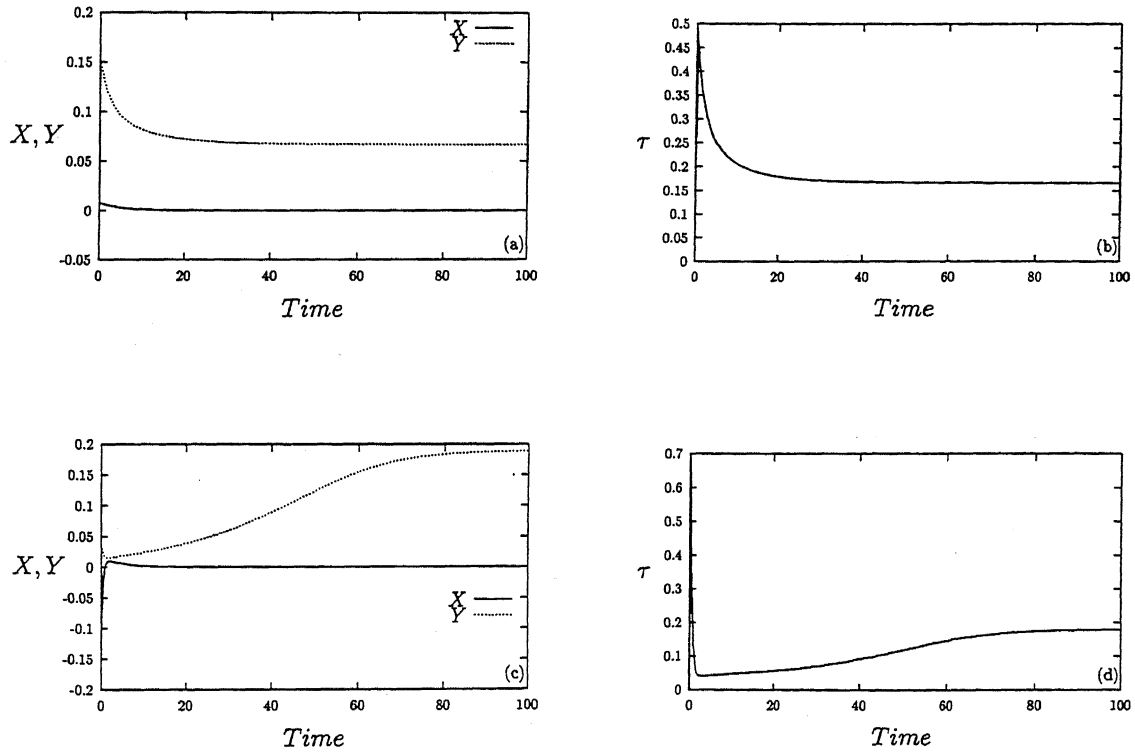


Figure 5.6: Response of the system states ((a), (c)) and the input ((b), (d)) to a +20% change ((a), (b)) and -20% change ((c), (d)) in the set-point using the input-output linearization technique.

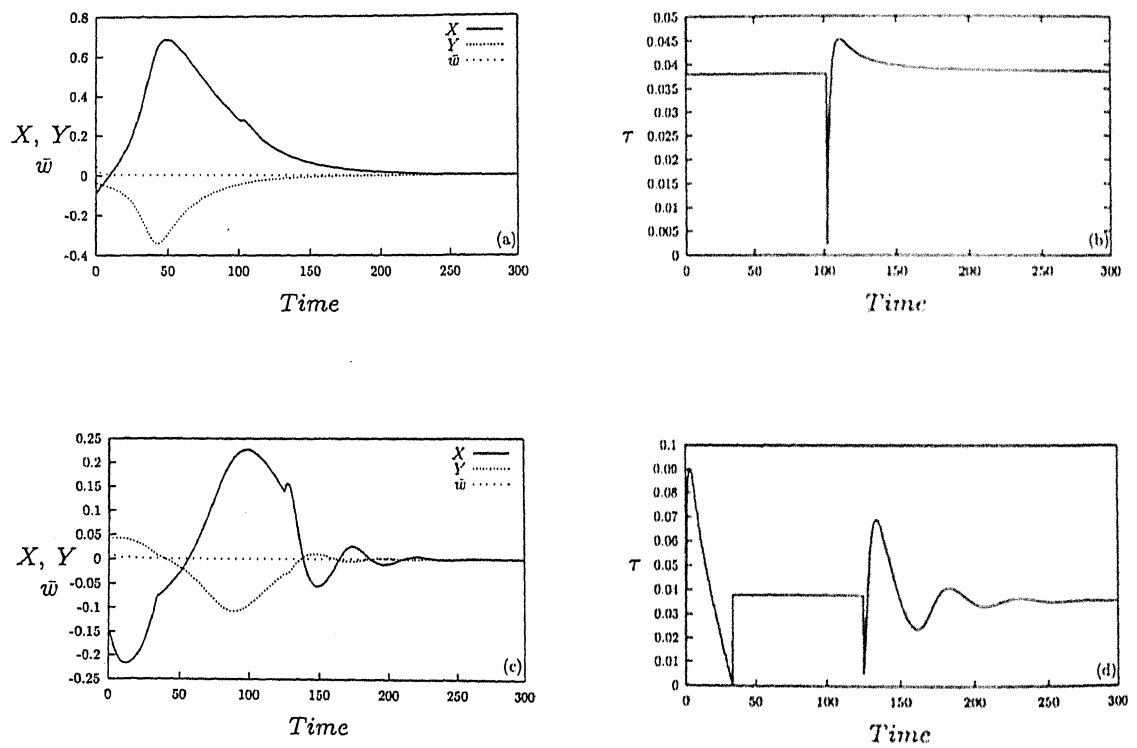


Figure 5.7: Response of the system states ((a), (c)) and the input ((b), (d)) to a +20% change ((a), (b)) and -20% change ((c), (d)) in the set-point using the output regulation technique. $\bar{w} = w^2$.

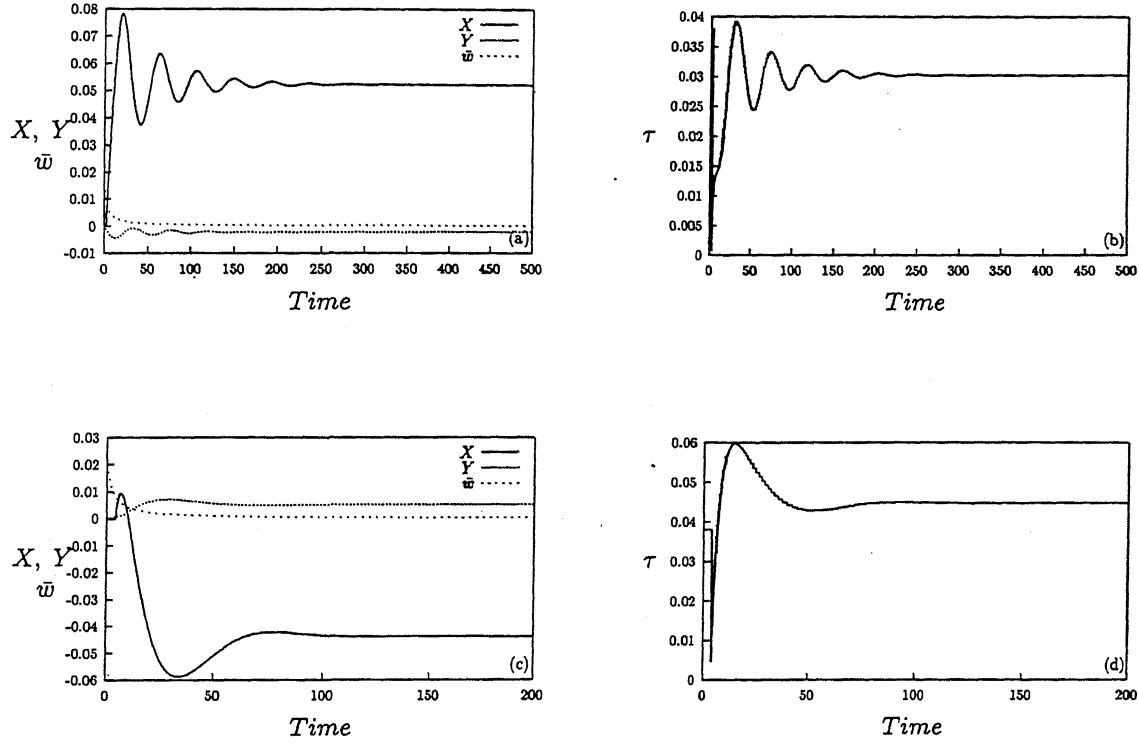


Figure 5.8: Response of the system states ((a), (c)) and the input ((b), (d)) to unmeasured disturbances of +15% ((a), (b)) and -5% ((c), (d)) in β . $\bar{w} = w^2$.

the system with respect to the disturbance can be defined along similar lines. For the case under consideration, the system is of relative order one with respect to the input and of relative order two with respect to the disturbance. Somewhat surprisingly, it is observed that the disturbance affects X more than it affects Y . The disturbance results in an off-set in the steady-state response of the system. It was observed that the off-set increased rapidly on increasing the magnitude of the disturbance.

We next consider the case when Y is the controlled output. Therefore, we have (Equation 5.3)

$$h(\mathbf{x}) = Y, \quad q(w) = -w^2$$

Setting the error of the composite system equal to zero, we obtain the first component of $\pi(w)$ to be $Y = \pi_1(w) = w^2$. The other component of $\pi(w)$ is obtained by solving

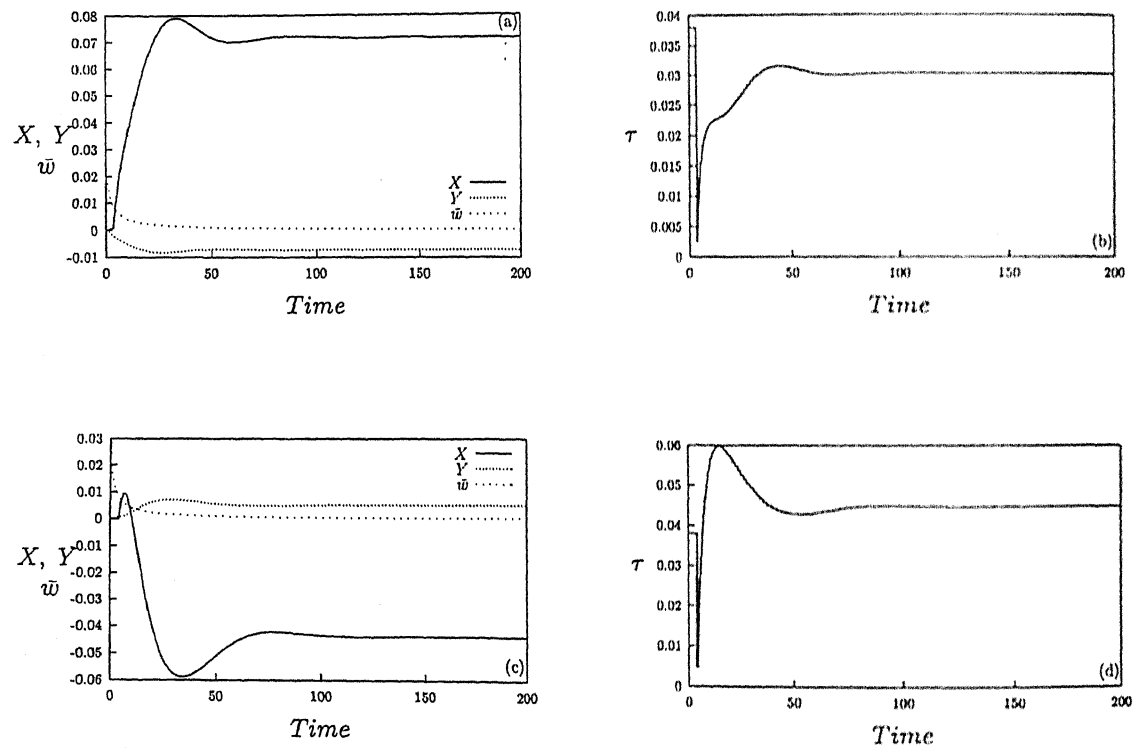


Figure 5.9: Response of the system states ((a), (c)) and the input ((b), (d)) to measured disturbances of +15% ((a), (b)) and -5% ((c), (d)) in β . $\bar{w} = w^2$.

the partial differential equations as explained in the previous section. We choose

$$X = \pi_2(w) = c_1 w^2 + c_2 w^3 + c_3 w^4 + c_4 w^5$$

The coefficients in the above polynomial can be calculated to be

$$\begin{aligned} c_1 &= \frac{-2X_s Y_s (1-X_s) + k(1-X_s) + X_s Y_s^2 - 2X_s Y_s (\beta - Y_s)}{Y_s^2 (1-X_s) - X_s Y_s^2 + k Y_s + Y_s^2 (\beta - Y_s)} \\ c_3 &= \frac{-2c_1 \bar{a}(\beta - Y_s) + 2\bar{a}(1-X_s) + k c_1 - Y_s Y_s c_1^2 + 2Y_s c_1 (1-X_s) + X_s (1-X_s)}{Y_s^2 (1-X_s) - X_s Y_s^2 + k Y_s + Y_s^2 (\beta - Y_s)} - \\ &\quad \frac{2X_s Y_s c_1 + 2Y_s c_1 (\beta - Y_s) - Y_s^2 c_1 + X_s (\beta - Y_s) - 2X_s Y_s}{Y_s^2 (1-X_s) - X_s Y_s^2 + k Y_s + Y_s^2 (\beta - Y_s)} \end{aligned}$$

$$\text{and } c_2 = 0, \quad c_4 = 0$$

The feedback control law for regulating the plant output is now given by

$$\tau = \alpha(\mathbf{x}, w) = \bar{c}(w) + (k_1(Y - w^2)) + (k_2(X - \pi_2(w))) \quad (5.37)$$

$$\bar{c}(w) = \frac{-2\bar{a}w^4 - (X_s - \pi_2(w))(Y_s - w^2)^2 + k(Y_s - w^2)}{(\beta - Y_s + w^2)} \quad (5.38)$$

We again study the controllability characteristics of this system for $\tau = 0.038$. The response of the system using the input-output linearization procedure of Kravaris and Chung[67], for a $\pm 20\%$ change in the setpoint, is shown in Fig. 5.10. The results indicate that the system can be non-minimum phase (for the $+20\%$ change in the setpoint) for this choice of the controlled output. The response of the system for a $\pm 20\%$ change in the set-point using the output regulation technique is shown in Fig. 5.11. The values of the parameters k_1 and k_2 used in the simulations are listed in Table 5.1.

The response of the system to unmeasured and measured disturbances in β is shown Fig. 5.12 and Fig. 5.13 respectively. For this case of the controlled output of the plant (Y), the system is of relative order one both with respect to the input as well as the disturbance. The disturbance results in an off-set in the steady-state response of the system. The results are similar to those obtained with the case when X was the controlled output.

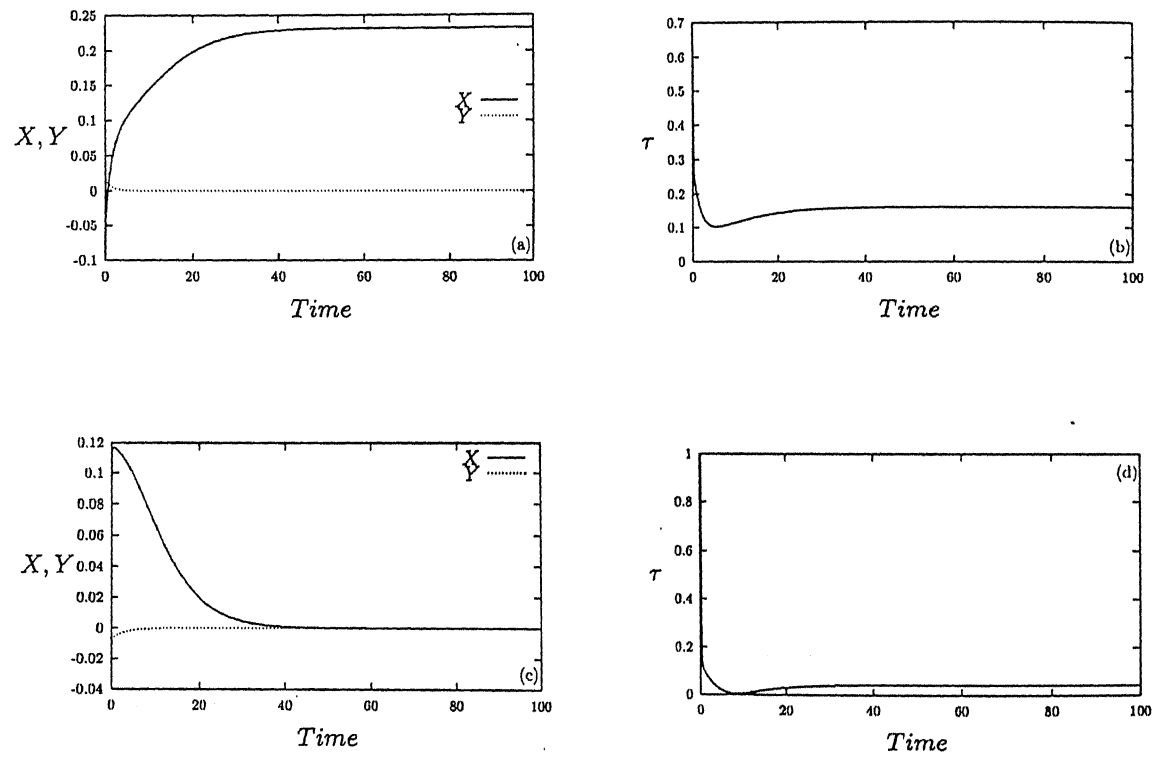


Figure 5.10: Response of the system states ((a), (c)) and the input ((b), (d)) to a +20% change ((a), (b)) and -20% change ((c), (d)) in the set-point using the input-output linearization technique.

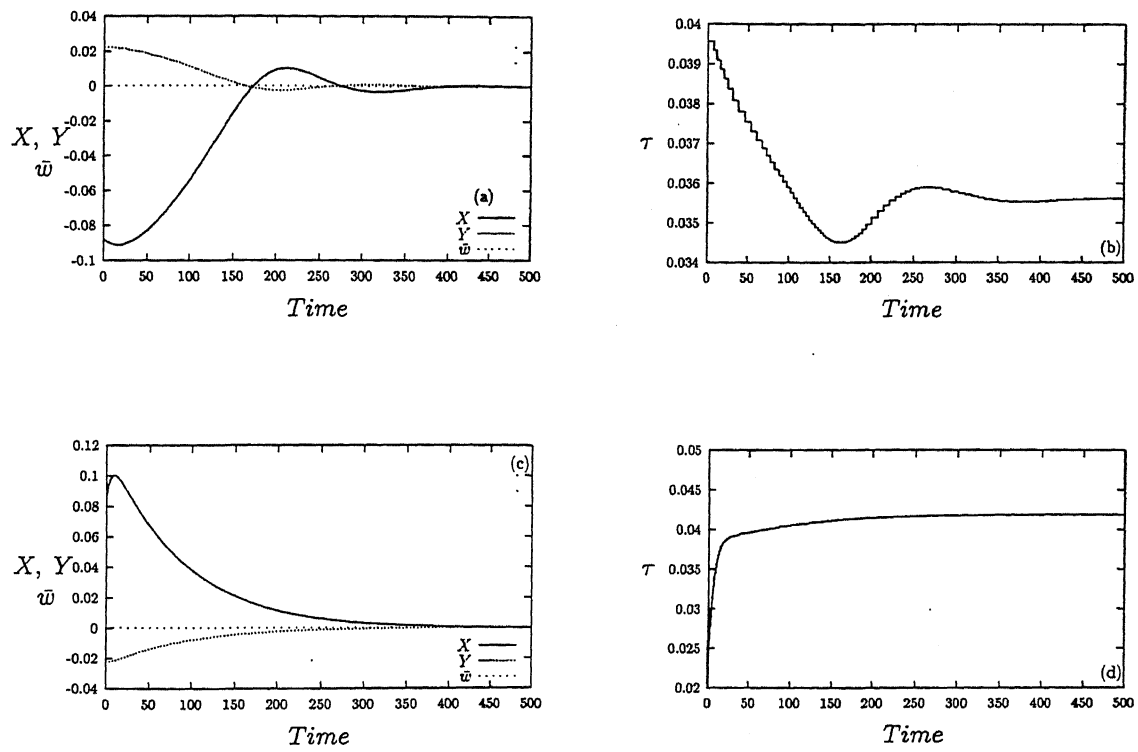


Figure 5.11: Response of the system states ((a), (c)) and the input ((b), (d)) to a +20% change ((a), (b)) and -20% change ((c), (d)) in the set-point using the output regulation technique. $\bar{w} = w^2$.

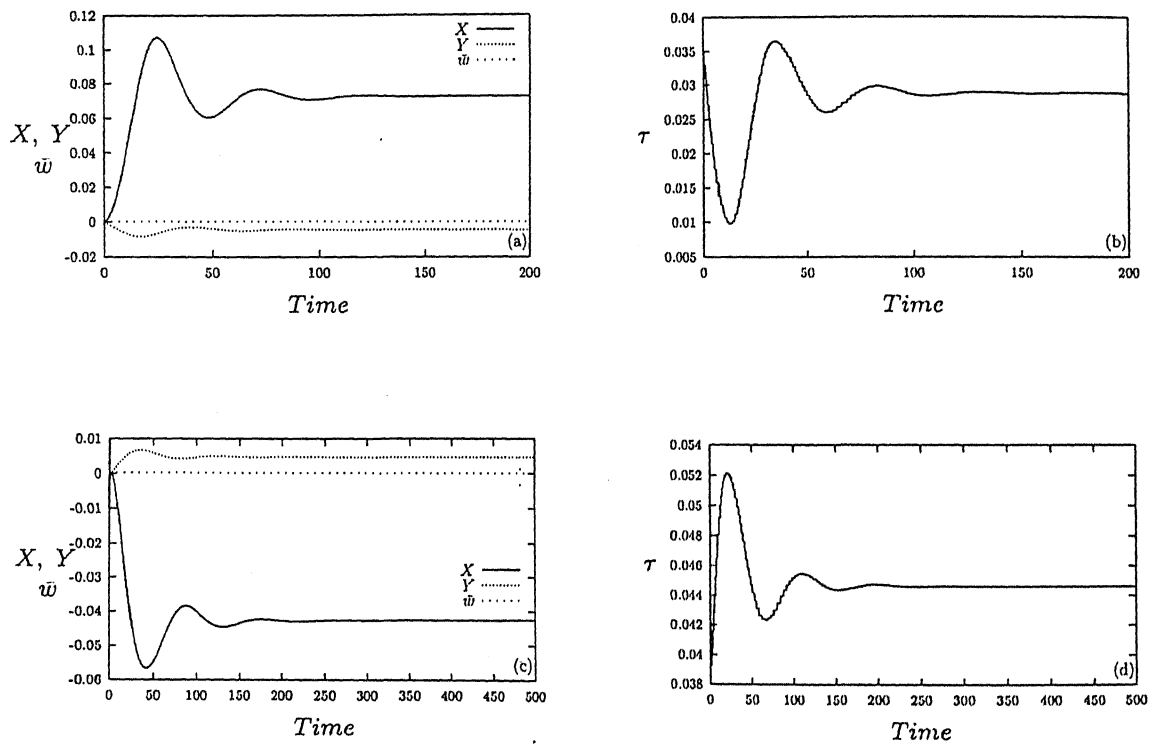


Figure 5.12: Response of the system states ((a), (c)) and the input ((b), (d)) to unmeasured disturbances of +15% ((a), (b)) and -5% ((c), (d)) in β . $\bar{w} = w^2$.

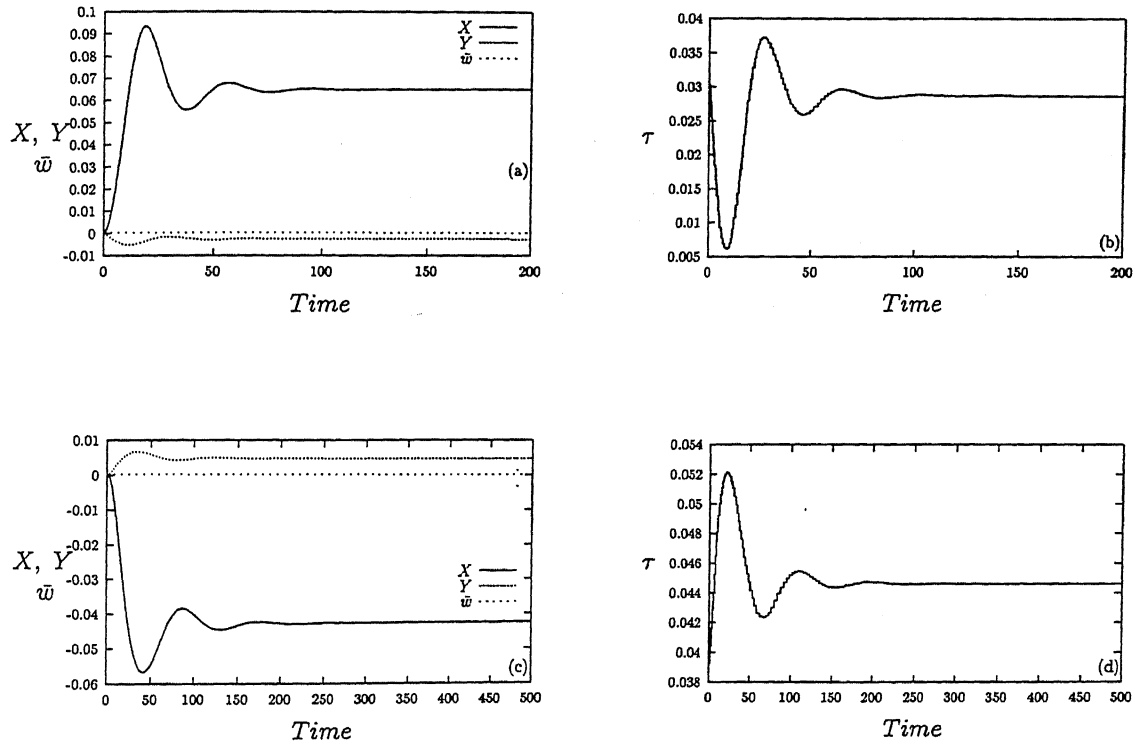


Figure 5.13: Response of the system states ((a), (c)) and the input ((b), (d)) to measured disturbances of +15% ((a), (b)) and -5% ((c), (d)) in β . $\bar{w} = w^2$.

5.5 Conclusions

It is well known that not all chaotic systems can be synchronized with the presently available methods of synchronization. The Rossler system is an example of such a system. We have employed recent results from nonlinear control theory and presented a method for the synchronization of such systems.

The method has been applied to develop a control technique for an isothermal reactor system exhibiting input multiplicity. The results obtained using the output regulation technique have been compared with those obtained using the input-output linearization procedure.

A limitation of the method appears to be its inability to handle models containing exponential nonlinearities. This is because applying the center manifold theorem to models containing these nonlinearities requires that we approximate the exponential term with the first few terms of its Taylor series expansion. This can lead to a drastic reduction in the performance of the controller.

Bibliography

- [1] Liljenroth, F. G., Starting and stability phenomena of Ammonia oxidation and similar reactions. *Chem. Met. Eng.* **19**, 287, 1918.
- [2] Van Heerden, C., Autothermic processes. *Ind. Eng. Chem.* **45**, 1242-1253, 1953.
- [3] Bilous, O. and Amundson, N. R., Chemical reactor stability and sensitivity. *AIChE J.* **1**, 513-521, 1955.
- [4] Poore, A. B., A model equation arising from chemical reactor theory. *Arch. Rat. Mech. Anal.* **52**, 358-388, 1973.
- [5] Uppal, A., Ray, W. H. and Poore, A. B., On the dynamic behavior of continuous stirred tank reactors. *Chem. Eng. Sci.* **29**, 967-985, 1974.
- [6] Uppal, A., Ray, W. H. and Poore, A. B., The classification of the dynamic behaviour of continuous stirred tank reactors - influence of reactor residence time. *Chem. Eng. Sci.* **31**, 205-214, 1976.
- [7] Gray, P. and Scott, S. K., Autocatalytic reactions in the isothermal CSTR - isolas and other forms of multiplicity. *Chem. Eng. Sci.* **38**, 29-43, 1983.
- [8] Gray, P. and Scott, S. K., *Chemical Oscillations and Instabilities - Nonlinear Chemical Kinetics*. Clarendon Press, Oxford, 1990.
- [9] Jorgensen, D. V. and Aris, R., On the dynamics of a stirred tank with consecutive reactions. *Chem. Eng. Sci.* **38**, 45-53, 1983.
- [10] Scott, S. K., *Chemical Chaos*. Oxford University Press, Oxford, 1991.

- [11] Sincic, D. and Bailey, J. E., Pathological dynamic behaviour of forced periodic chemical processes. *Chem. Eng. Sci.* **32**, 281-286, 1977.
- [12] Kevrekidis, I. G., Schmidt, L. D. and Aris, R., Some common features of periodically forced reacting systems. *Chem. Eng. Sci.* **41**, 1263-1276, 1986.
- [13] Kevrekidis, I. G., Aris, R. and Schmidt, L. D., The stirred tank forced. *Chem. Eng. Sci.* **41**, 1549-1560, 1986.
- [14] McKarnin, M. A., Schmidt, L. D. and Aris, R., Response of nonlinear oscillators to forced oscillations: Three chemical reaction case studies. *Chem. Eng. Sci.* **43**, 2833-2844, 1988.
- [15] Cordonier, G. A., Schmidt, L. D. and Aris, R., Forced oscillations of chemical reactors with multiple steady states. *Chem. Eng. Sci.* **45**, 1659-1675, 1990.
- [16] Mankin, J. C. and Hudson, J. L., Oscillatory and chaotic behaviour of a forced exothermic chemical reaction. *Chem. Eng. Sci.* **39**, 1807-1814, 1984.
- [17] Douglas, J. M. and Rippin, D. W. T., Unsteady state process operation. *Chem. Engg. Sci.* **21**, 305-315, 1966.
- [18] Codell, R. B. and Engel, A. J., A theoretical study of a controlled cycled stirred tank reactor. *AIChE. J.* **17**, 220-225, 1971.
- [19] Ausikaitis, J. and Engel, A. J., Steady-state multiplicity and stability in an adiabatic controlled cycled stirred tank reactor. *AIChE. J.* **20**, 256-263, 1974.
- [20] Lin, K. F. and Wu, L. L., Performance of an adiabatic controlled cycled stirred tank reactor. *Chem. Eng. Sci.* **36**, 435-444, 1981.
- [21] Kubickova, Z., Kubicek, M. and Marek, M., Fed batch operation of stirred reactors. *Chem. Eng. Sci.* **42**, 327-333, 1987.
- [22] Balakotaiah, V. and Luss, D., Structure of the steady-state solutions of lumped-parameter chemically reacting systems. *Chem. Eng. Sci.* **37**, 1611-1623, 1982.

- [23] Balakotaiah, V. and Luss, D., Multiplicity features of reacting systems - Dependence of the steady states of a CSTR on the residence time. *Chem. Eng. Sci.* **38**, 1709-1721, 1983.
- [24] Balakotaiah, V. and Luss, D., Global multiplicity features of multi-reaction lumped parameter systems. *Chem. Eng. Sci.* **39**, 865-881, 1984.
- [25] Morud, J. and Skogestad, S., Effects of recycle on dynamics and control of chemical processing plants. *Comp. Chem. Engg.* **18**, Suppl., S529-S534, 1994.
- [26] Morud, J. and Skogestad, S., Dynamic behaviour of integrated plants. *J. Proc. Cont.* **6**, 145-156, 1996.
- [27] Taylor, M. A. and Kevrekidis, I. G., Couple, double, toil and trouble: A computer assisted study of two coupled CSTR's. *Chem. Eng. Sci.* **48**, 2129-2149, 1993.
- [28] Luyben, W. L., Dynamics and control of recycle systems. 2. Comparison of different process designs. *Ind. Eng. Chem. Res.* **32**, 476-486, 1993.
- [29] Luyben, W. L., Dynamics and control of recycle systems. 3. Alternative process designs in a ternary system. *Ind. Eng. Chem. Res.* **32**, 1142-1153, 1993.
- [30] Tyreus, B. D. and Luyben, W. L., Dynamics and control of recycle systems. 4. Ternary systems with one or two recycle streams. *Ind. Eng. Chem. Res.* **32**, 1154-1162, 1993.
- [31] Luyben, W. L., Snowball effects in reactor/separator processes with recycle. *Ind. Eng. Chem. Res.* **33**, 299-305, 1994.
- [32] Luyben, M. L. and Luyben, W. L., Design and control of a complex process involving two reaction steps, three distillation columns and two recycle streams. *Ind. Eng. Chem. Res.* **34**, 3885-3898, 1995.
- [33] Luyben, M. L. Tyreus, B. D. and Luyben, W. L., Analysis of control structures for reaction/separation/recycle processes with second-order reactions. *Ind. Eng. Chem. Res.* **35**, 758-771, 1996.

- [34] Lyman, P. R. and Luyben, W. L., Production rate changes in a ternary two-recycle process. *Ind. Eng. Chem. Res.* **35**, 2198-2203, 1996.
- [35] Golubitsky, M. and Schaeffer, D., *Singularities and Groups in Bifurcation Theory*. Vol. 1, Springer-Verlag, New York, 1985.
- [36] Henson, M. A. and Seborg, D. E., Critique of exact linearization strategies for process control. *J. Proc. Cont.* **1**, 122-139, 1991.
- [37] Pecora, L. M. and Carroll, T. L., Synchronization in chaotic systems. *Phys. Rev. Lett.* **64**, 821-824, 1990.
- [38] Pecora, L. M. and Carroll, T. L., Driving systems with chaotic signals. *Phys. Rev.* **A44**, 2374-2383, 1991.
- [39] Rulkov, N. F., Suschik, M. M., Tsimring, L. S. and Abarbanel, H. D. I., Generalized synchronization of chaos in directionally chaotic systems. *Phys. Rev.* **E51**, 980-994, 1995.
- [40] Kocarev, L. and Parlitz, U., Generalized synchronization, predictability, and equivalence of unidirectionally coupled dynamical systems. *Phys. Rev. Lett.* **76**, 1816-1819, 1996 and references therein.
- [41] Kocarev, L. and Parlitz, U., General approach for chaotic synchronization with applications to communication. *Phys. Rev. Lett.* **74**, 5028-5031, 1995 and references therein.
- [42] Parlitz, U., Kocarev, L., Stojanowski, T. and Preckel, H., Encoding messages using chaotic synchronization. *Phys. Rev.* **E53**, 4351, 1996.
- [43] Koppel, L. B., Input multiplicities in nonlinear, multivariable control systems. *AIChE J.* **28**, 935-945, 1982.
- [44] Koppel, L. B., Input multiplicities in process control. *Chem. Engg. Edu.* , 58-63 and continued on 89-92, Spring 1983.
- [45] Balakotaiah, V. and Luss, D., Input-multiplicity in lumped-parameter systems. *Chem. Eng. Commun.* **39**, 309-322, 1985.

- [46] Isidori, A., *Nonlinear Control Systems*. Springer-Verlag, New York, 1989.
- [47] Isidori, A. and Byrnes, C. I., Output regulation of nonlinear systems. *IEEE Trans. Auto. Cont.* **35**, 131-140, 1990.
- [48] Kubicek, M. and Marek, M., *Computational Methods in Bifurcation Theory and Dissipative Structures*. Springer-Verlag, Berlin, 1983.
- [49] Swinney, H. L., Observation of order and chaos in nonlinear systems. *Physica* **7D**, 3-15, 1983.
- [50] Grebogi, C., Ott, E. and Yorke, J. A., Crises, sudden changes in chaotic attractors and transient chaos. *Physica* **7D**, 181-200, 1983.
- [51] Sommerer, J. C. and Grebogi, C., Determination of crisis parameter values by direct observation of manifold tangencies. *Int. J. Bif. Theory and Chaos* **2**, 383-396, 1992.
- [52] Manneville, P. and Pomeau, Y., Different ways to turbulence in dissipative dynamical systems. *Physica* **1D**, 219-226, 1980.
- [53] Pomeau, Y. and Manneville, P., Intermittent transition to turbulence in dissipative dynamical systems. *Commun. Math. Phys.* **74**, 189-197, 1980.
- [54] Gaspard, P. and Wang, W. J., Homoclinic orbits and mixed-mode oscillations in far-from-equilibrium systems. *J. Stat. Phys.* **48**, 151-199, 1987.
- [55] May, R. M., Simple models with very complicated dynamics. *Nature* **261**, 456-467, 1976.
- [56] Wolf, A., Swift, J. B., Swinney, H. L. and Vastano, J. A., Determining Lyapunov exponents from a time series. *Physica* **16D**, 285-317, 1985.
- [57] Turner, G. S., Roux, J. C., McCormick, W. D. and Swinney, H. L., Alternating periodic and chaotic regimes in a chemical reaction- experiment and theory. *Phys. Lett.* **85A**, 9-12, 1981.

- [58] Kennedy, M. P. and Chua, L. O., Van der Pol and chaos. *IEEE-CAS* **33**, 974-980, 1986.
- [59] Pei, L. Q., Guo, F., Wu, S. X. and Chua, L. O., Experimental confirmation of the period adding route to chaos in a nonlinear circuit. *IEEE-CAS* **33**, 438-442, 1986.
- [60] Van der Pol, B. and Van der Mark, J., Frequency demultiplication. *Nature* **120**, 363-364, 1927.
- [61] Hlavacek, V., Kubicek, M. and Jelinek, J., Modeling of chemical reactors-XVIII Stability and oscillatory behaviour in a CSTR. *Chem. Eng. Sci.* **32**, 1441-1461, 1977.
- [62] Kravaris, C. and Kantor, J. C., Geometric methods for nonlinear process control. I. Background. *Ind. Eng. Chem. Res.* **29**, 2295-2310, 1990 and references therein.
- [63] Kravaris, C. and Kantor, J. C., Geometric methods for nonlinear process control. II. Controller synthesis. *Ind. Eng. Chem. Res.* **29**, 2310-2323, 1990 and references therein.
- [64] Slotine, J. J. E. and Li, W., *Applied Nonlinear Control*. Prentice-Hall, Englewood Cliffs, New Jersey, 1991.
- [65] Chen, G. and Dong, X., From chaos to order - Perspectives and methodologies in controlling chaotic nonlinear dynamical systems. *Int. J. Bif. Chaos* **3**, 1363-1409, 1993.
- [66] Carr, J., *Applications of Centre Manifold Theory*. Springer-Verlag, New York, 1981.
- [67] Kravaris, C. and Chung, C. B., Nonlinear state feedback synthesis by global input-output linearization. *AIChE. J.* **33**, 592-603, 1987.

Appendix A

Singularity Theory

The steady states of lumped-parameter nonlinear systems are determined by solving systems of nonlinear algebraic equations. These systems are often characterized by a large number of parameters. In such cases it can be very difficult to determine the behavior of the system by an exhaustive study. In many situations of practical interest, two important issues which need to be addressed are

- What is the number of possible steady-states the system can possess and
- How are the steady-states influenced by changes in one or more of the system parameters?

Application of singularity theory enables us to answer these questions in an elegant and comprehensive manner.

In this Appendix, we summarise the features of singularity theory[35], with emphasis on the applicability of the technique to the coupled reactor-separator system.

We begin by assuming that at steady-state, the model of the system under consideration can be represented by a single nonlinear algebraic equation in one of the state variables x

$$f(x, \lambda, p) = 0 \tag{A.1}$$

Here x represents the dependent (state) variable, λ represents the control parameter and p is the parameter set containing all other parameters. We are interested in studying the dependence of x on λ .

The multiplicity features of the system depend on the choice of the parameters in the parameter set p . These are represented as bifurcation diagrams. A bifurcation diagram describes the steady-state dependence of the state variable x on the control parameter λ . This control parameter is known as the bifurcation parameter. The bifurcation diagrams are plotted by fixing all the other parameters p . In this discussion, a bifurcation point is defined as a point in parameter space, where there is a change in the number of solutions.

The multiplicity features can change only when critical surfaces in the parameter space p are crossed. Singularity theory enables us to identify these surfaces and to classify the parameter space into regions having different multiplicity features. The bifurcation diagrams in each region of the parameter space are therefore qualitatively different.

A detailed presentation of the mathematical theory is given in Golubitsky and Schaeffer[35]. Balakotiah and Luss[22–24] have applied the theory to analyse the steady-state multiplicity features of several lumped-parameter systems.

The first step in the application of singularity theory consists of identifying the **normal form** of the system. This is the simplest polynomial $g(y, \mu) = 0$, depending on a parameter μ , to which the system $f(x, \lambda)$ is equivalent. The notion of equivalence is defined by conditions for the two solution sets of the equations $f = 0$ and $g = 0$ to be qualitatively similar. These conditions reduce to computing the values of some of the parameters from the parameter set p , at which the system $f = 0$ has an identical qualitative behavior as the polynomial $g = 0$ at the origin. Singularity theory provides a list of the calculations which must be performed to recognize a given equation $f(x, \lambda)$ to be of a given qualitative type. The point in parameter space at which the system is equivalent to the simple polynomial $g(y, \mu)$ is the **singular point** of the system. If the function f satisfies the conditions of equivalence at the singular point in parameter space p , then we expect the solution sets of the system $f = 0$ to be similar to the solution sets of the polynomial $g = 0$ in the neighborhood of this point. This follows since f will have the same Taylor series expansion at the singular point as the polynomial g has about the origin. A list of normal forms is tabulated in Golubitsky and Schaeffer[35].

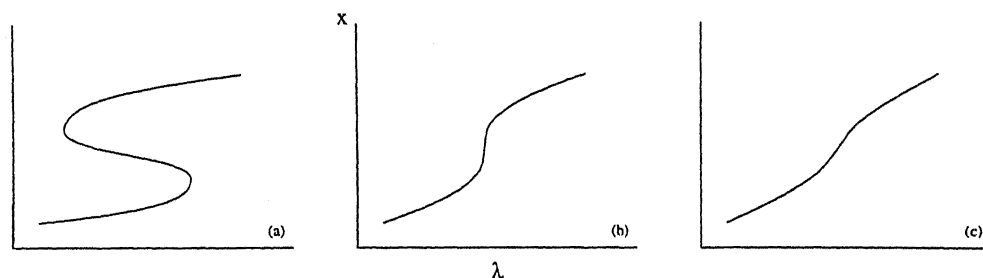


Figure A.1; Bifurcation diagrams showing the change in the multiplicity features (a) before crossing the hysteresis variety; (b) on the hysteresis variety and (c) after crossing the hysteresis variety.

parameters in p are kept constant. The hysteresis variety can thus be represented as a curve in a two-parameter plot. For parameter values on the hysteresis variety, the bifurcation diagram shows a point of inflexion or a point with a vertical tangent. Across the variety, two new solutions appear or disappear (depending on the direction of crossing). Fig. A.1 shows a schematic of the bifurcation diagram on the hysteresis variety and on either side of it.

- **Isola Variety:** This critical surface is generated by solving

$$f = \frac{\partial f}{\partial x} = \frac{\partial^2 f}{\partial \lambda} = 0 \quad (\text{A.3})$$

These equations are solved for x , λ and a parameter from the parameter set p , while keeping the others constant. Crossing the isola variety can either result in an isola bifurcation or a simple bifurcation. In the case of an isola bifurcation, an isolated branch of solutions either appear or disappear as the isola variety is crossed. In the case of a simple bifurcation, two solution branches merge and then separate. These are shown in Fig. A.2.

When there are no constraints acting on the state variable x , multiplicity features of the system can change only when the hysteresis or the isola varieties are crossed. However, as we have seen in the third chapter, steady-state behavior of the reactor-separator system can be influenced by the presence of constraints on the conversion z . To recall,

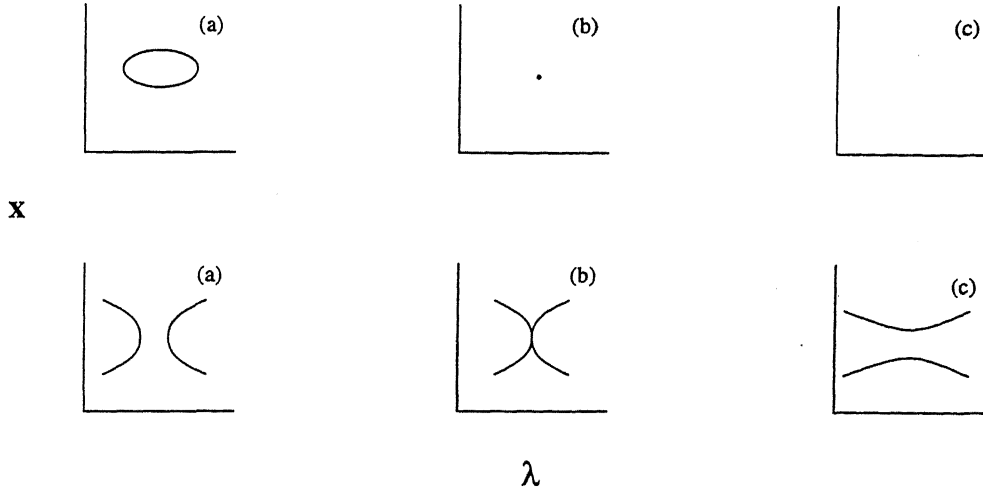


Figure A.2: Bifurcation diagrams showing the change in the multiplicity features (a) before crossing the isola variety; (b) on the isola variety and (c) after crossing the isola variety. Figures in the first and second rows are for the isola bifurcation and the simple bifurcation respectively.

feasible steady-state operation of the system is possible only when $y_e < z < x_e$. Such constraints on the state variable appear as feasibility boundaries in the bifurcation diagrams. New types of multiplicity features arise depending on the manner in which these boundaries are crossed. Singularity theory can also be employed to account for these new kinds of multiplicity features in a systematic way. Special parameter sets have been defined to account for the presence of the feasibility boundaries[24, 35]. These enable us to demarcate the locus of the feasibility boundaries in a suitable parameter space. We now summarise these special parameter sets. We have retained the notation used in section 3.3 of the third chapter.

- **Boundary limit set (BLS):** The parameter set corresponding to which a turning point of the steady-state branch in the bifurcation diagram lies on the feasibility boundary forms the BLS. This set is given by the solution to the set of equations

$$G = G_z = 0 \quad \text{at} \quad z = x_e \quad \text{or} \quad z = y_e \quad (\text{A.4})$$

- **Boundary tangent set (BTS):** For parameter values belonging to this set, the steady-state branch in the bifurcation diagram is tangential to the feasibility boundary. This is obtained by solving

$$G = G_\tau = 0 \quad \text{at} \quad z = x_e \quad \text{or} \quad z = y_e \quad (\text{A.5})$$

- **Double cross set (DCS):** This is given by the values of $x_e - y_e$ for which two branches of the bifurcation diagram cross the feasibility boundaries simultaneously. This is obtained by the solution to the set of equations

$$G(z = x_e) = G(z = y_e) = 0 \quad (\text{A.6})$$

In chapter 3, these equations have been solved for τ and β_0 for fixed values of all the other parameters. Fig. A.3 shows the different types of bifurcation diagrams resulting due to the presence of these feasibility boundaries.

In section 3.4 of the third chapter, we have considered z to be the bifurcation parameter for the case of isothermal-isobaric flash and when F and F_0 are the specified variables. In this case, the feasibility boundaries (BLS) appear on the bifurcation parameter z . Schematic representation of the bifurcation diagrams are shown in Fig. A.4.

Multiplicity features for the case of isothermal and isobaric separation when (M_R, F) are the specified variables (section 3.3.2), can change when another critical surface is crossed in the parameter space. This is the limit and cross set (LCS). Fig. A.5 shows the different types of bifurcation diagrams when this set is crossed. This set is obtained by solving the following sets of equations

$$G(z = y_e) = 0, \quad G = G_z = 0 \quad (\text{A.7})$$

In section 3.1 of chapter 3, these equations have been solved for z , τ and β_0 for fixed values of all the other parameters.

In section 3.3 of the third chapter, we have applied singularity theory to determine

- all the possible local bifurcation diagrams and
- classifying a suitable parameter space into regions having different multiplicity features

for different sets of specifications of the reactor-separator system.

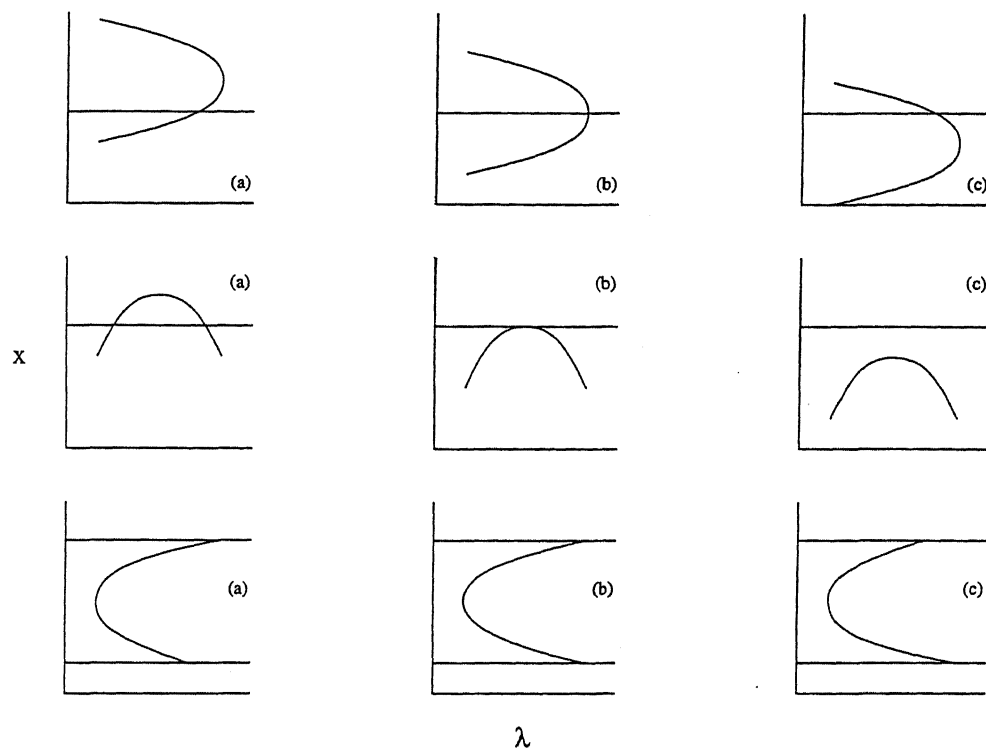


Figure A.3: Bifurcation diagrams showing the change in the multiplicity features in the presence of feasibility boundaries. (a) before crossing the boundary sets; (b) on the boundary sets and (c) after crossing the boundary sets. Figures in the first, second and third rows are for the BLS, the BTS and the DCS respectively.

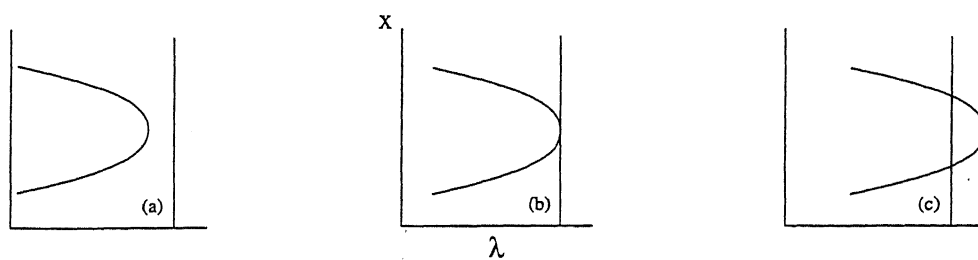


Figure A.4: Bifurcation diagrams showing the change in the multiplicity features for the case of (T_F, P) and (F, F_0) flash. (a) before crossing the BLS; (b) on the BLS and (c) after crossing the BLS.

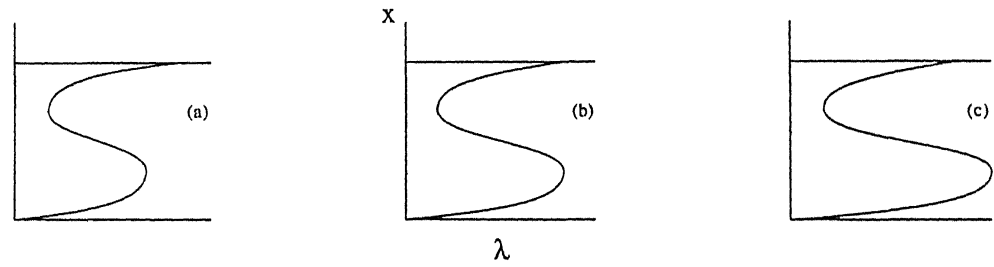


Figure A.5: Bifurcation diagrams showing the change in the multiplicity features for the case of (T_F, P) and (M_R, F) flash. (a) before crossing the LCS; (b) on the LCS and (c) after crossing the LCS.



125675

Date Slip

This book is to be returned on the
date last stamped.

A

125675

3-0 188 1999

16-7-99

CHE



A125675